# Chemical characteristics of R chondrites: Implications for nebular and parent body processes

**Applicant: Rahat Khan**

**Supervisor: Mitsuru Ebihara**

**Dissertation for a Ph. D. Degree**

**Graduate School of Science and Engineering**
**Tokyo Metropolitan University**

**2015**

# 首都大学東京　博士（理学）学位論文（論文博士）

論 文 名　Rコンドライトの化学的特徴：母天体形成前後の諸過程との関連（英文）

著　者　ラハット カーン

審査担当者

主　査　　海老原 充

委　員　　竹川 暢之

委　員　　大谷 栄治

委　員　　三澤 啓司

上記の論文を合格と判定する

平成　　年　　月　　日

首都大学東京大学院理工学研究科教授会

研究科長

**DISSERTATION FOR A DEGREE OFDOCTOR OF PHILOSOPHY IN SCIENCE**

**TOKYO METROPOLITAN UNIVERSITY**

**TITLE : Chemical characteristics of R chondrites: Implications for nebular and parent body processes**

**AUTHOR : Rahat Khan**

**EXAMINED BY**

**Examiner in chief**

**Examiner**

**Examiner**

**Examiner**

**QUALIFIED BY THE GRADUATE SCHOOL OF SCIENCE AND ENGINEERING TOKYO METROPOLITAN UNIVERSITY**

**Dean**

**Date**

# Contents

# Acknowledgments

I would like to express my humble gratitude to my supervisor Prof. Mitsuru Ebihara for his invaluable guidance, advice and encouragement for this research. Without his philosophical directions this research could not be conclusive. I am very much thankful to Assistant Prof. Dr. Naoki Shirai for his continuous training on analytical techniques and invaluable advises regarding the cosmochemistry as well as the Japanese life. Associate Prof. Dr. Yasuji Oura is gratefully acknowledged for his kind helps during the tenure of my PhD work.

I thank Dr. Akira Yamaguchi of the National Institute of Polar Research (NIPR, Japan) and the curator of Johnson Space Center, NASA (USA) for kindly providing me the meteoritic samples. I am grateful to Dr. Shun Sekimoto of Kyoto University Research Reactor Institute for helping me to irradiate my samples. I am also thankful to Mr. Kazuya Kumagai for his technical assistance for the ICP-AES experiment.

I am grateful to many people who have helped me over the years, particularly the members of Cosmochemistry laboratory of Tokyo Metropolitan University. This work is partially supported by Asian Human Resources Fund defrayed by the Tokyo metropolitan government, Japan.

# Abstract

To study the compositional trends associated with their systematic variation with petrologic grade and their fractionation, 41 elements (Na, Mg, Al, P, Ca, Sc, V, Cr, Mn, Fe, Co, Ni, Zn, As, Se, Br, Cd, In, Sb, La, Ce, Pr, Nd, Sm, Eu, Gd, Tb, Dy, Ho, Er, Tm, Yb, Lu, Os, Ir, Au Tl, Pb, Bi, Th and U) have been determined in 15 R chondrites (PRE 95411, ALH 85151, Y 793575, Y 983270, A 881988, MIL 07440, LAP 03639, Y 983720, Y 983097, LAP 04840, MIL 11207, Y 980702, Y 980703, LAP 02238, PCA 91002), covering all petrologic types. For the determination of volatile elements (Zn, Pb, Tl, In and Cd), very precise isotope dilution technique coupled with ICP-MS was used followed by solvent extraction and anion exchange column chromatography. Bi was determined by using $^{208}Pb/^{209}Bi$ ratio. Detailed abundances of rare earth elements (REEs), Th and U were determined by ICP-MS using internal calibration method. $^{149}$Samarium spike was used for recovery calculation. In ICP-MS experiments, necessary isobaric and oxide interferences were corrected. Phosphorus was determined by ICP-AES using Be as internal standard. Other elemental abundances were determined by instrumental neutron activation analysis using a research reactor of Kyoto University Research Reactor Institute (KURRI) and the gamma-counting facilities of KURRI and TMU. Accuracy and precision of all analytical data have been ensured by analyzing the Smithsonian Allende powder repeatedly and comparing their abundances with the literature values.

CI-normalized volatile elements abundances (Pb, Bi, Tl, In and Cd) in R chondrites are decreasing with the increasing degree of metamorphism, excluding for the highly weathered MIL 11207.8 and Y 793575.44. Lead abundances in R chondrites vary from 0.33×CI to 0.64×CI. With a similar trend, Bi (0.15-0.63×CI), In (0.15-0.56×CI), Tl (0.02-0.79×CI) and Cd (0.03-0.81×CI) also change among the petrologic suite of R chondrites of this study. Distinguishing the petrologic type 3 from petrologic type 4 is difficult – only Tl can do so. Similarly, distinguishing the petrologic type 4 from 5/6 is also difficult – only Bi can separate these petrologic types. But petrologic type 3 and 5/6 can be easily distinguished by the CI-normalized volatile elements abundances. For unequilibrated chondrites, CI-normalized Bi, Tl, In and Cd abundances in R chondrites are within the range of ordinary chondrites. But in higher metamorphic grade, CI normalized Bi, Tl, In and Cd abundances in R chondrites are generally higher than those of H, L and LL chondrites with a few exceptions. The higher abundances of volatile elements in

equilibrated R chondrites are more prominent for Bi, In and Cd. For Tl, the trend of higher volatile elements abundances in R chondrites is also noticeable (especially for petrologic type 6), but somehow less conspicuous than Bi, In and Cd. For the systematic variation of volatile elements in R chondrites, a plausible explanation can be given; - high temperature early condensates were more depleted in volatile elements whereas low temperature later condensates were comparatively enriched with the volatile elements. If nebular condensation and accretion occurred simultaneously, the high temperature condensates were placed in the inner portion of the parent body followed by the low temperature condensates sequentially at the outer portion of the parent body. If R chondrite parent body possesses the onion-shell model, then the metamorphic heating caused the higher degree of recrystallization at the inner portion compared with that of outer portion. Impact can be responsible to convert the onion-shell parent body to rubble-pile type parent body where the different petrologic types are randomly distributed over the parent body.

CI-normalized detailed abundances of REEs in R chondrites shows a faint enrichment of heavy REEs compared with those of light REEs. REEs abundances vary from 1.2×CI to 1.5×CI. Nebular process can be responsible for such small HREE-LREE fractionation in R chondrites. To explain the nebular process in R chondrites, an analogically well explained fractionated pattern of REEs, Th and U abundances in Allende meteorite can be considered. In Allende, HREEs are depleted compared with LREEs. According to condensation calculation, high temperature early condensates (e.g., perovskite, hibonite, corundum etc.) enriched with refractory HREEs could have been removed from the nebular gas, making the remaining gas enriched with less refractory LREEs. It is likely that the Allende parent body must have formed from such later condensates of the remaining gas. In R chondrites, the inclination of CI-normalized REE pattern is opposite to the Allende pattern (except positive Tm anomaly). A simple interpretation is that R chondrites formed in the nebula where early condensates were relatively abundant. Unlike the REE fractionation pattern, Th-U fractionation patterns are the same both in R chondrites and in Allende. In the seven replicate measurements of Allende powder, Th/U ratio is 4.10 ± 0.20 whereas in R chondrites, Th/U ratio is 3.81 ± 0.13. A subtle positive Ce anomaly (5.4 ± 1.5 %) is observed in CI-normalized REE abundance pattern of R chondrites. Phosphorus abundances in R chondrites are very close to cosmic abundance (0.9-1.1×CI). Phosphorus abundances show anti-correlation with La, Ce, Er and Yb.

In our INAA study, CI, Cr-normalized lithophile abundance pattern in R chondrites are almost flat and are comparable with those of ordinary chondrites. Mean CI-normalized Na and Mn abundances are 1.32 ± 0.07 and 1.21 ± 0.04, respectively, which are comparable with those of ordinary chondrites but much higher than those of carbonaceous and enstatite chondrites. However, CI, Cr-normalized siderophile abundance pattern in R chondrites are intermediate between H and L chondrites. A mean iron content in R chondrites is 24.6 ± 0.7 (%, 1σ, n=15, this study) whereas the mean iron contents in H, L and LL are 27.1 ± 0.7 (%, 1σ, n=22), 21.6 ± 0.5 (%, 1σ, n=20) and 18.4 ± 0.4 (%, 1σ, n=16), respectively. Bulk Ir contents in R chondrites also show the same trend as iron. CI-normalized Ni/Co ratios (~0.9) in R chondrites are comparable with those of ordinary chondrites. Moderately volatile elements, Zn and Se in R chondrites are more abundant than those in ordinary chondrites. Both of them share the same nebular condensation temperature, but they are fractionated. Enstatite chondrites are the most reduced chondritic meteorites whose Se abundances are comparable with those in R chondrite. But Zn abundances in R chondrite are remarkably higher than those in EL chondrite and comparable with CM chondrite abundances. Higher stability of ZnO in oxidized condition can be a plausible explanation for this Zn enrichment.

This study characterizes the R chondrites depending on their bulk chemical compositions. And the bulk chemical composition is implemented to reveal the nebular and the parent body processes.

# Chapter-1

## Introduction

## 1.1 Meteorites

Our solar system formed ~4.6 billion years ago from the collapse of a dense core inside an interstellar molecular cloud (Trieloff et al., 2003). The subsequent formation of solid bodies took place rapidly. The first stages of planetary accretion in the early solar system produced small bodies, or `planetesimals`, of rock and ice. Most of these first-born were swallowed up by the present-day planets as they grew, but some survived as asteroids, orbiting between Mars and Jupiter where no large planet formed to consume them. These asteroids suffer continuing collisions, and rocks from their interiors may find their way to the earth as meteorite (wood, 2003). The period of <10 milllion years over which planetesimals were assembled can be investigated through the study of meteorites (Allègre et al., 1995).

## 1.2 Classification of meteorites

### 1.2.1 Primary characteristics: Chemical composition

Meteorites are broadly classified into two classes – Chondrites and Nonchondrites. Chondrites are more pristine in character whereas nonchondrites are less pristine and differentiated. Using bulk chemical compositions, chondrites are divided into clans and subdivided into groups, identified by a letter or combination of letters. Chondrites are of three clans – Carbonaceous, Ordinary and Enstatite chondrites. Carbonaceous chondrites consist of well-established eight chondritic groups – CI (Ivuna –like), CM (Mighei-like), CO (Ornans-like), CV (Vigarano-like), CB (Bencubbin-like), CR (Renazzo-like), CH (ALH A 85005-like) and CK (Karoonda-like). Depending on the metal and iron abundances, ordinary chondrites are of three groups – H (high metal), L (low metal) and LL (low metal and low iron) whereas enstatite chondrites possess only two groups – EH (high metal) and EL (low metal). Enstatite chondrites are strongly reduced, with virtually all the iron in them occurring as metal. Beside these groups, there are two other chondritic groups – one is K (Kakangari-like) chondrite and another is R chondrite (Krot et al., 2005).

### 1.2.2 Secondary characteristics: Petrologic types

Chondrites are divided into various petrologic types based on the degree to which they have been thermally metamorphosed or altered. According to Van Schmus and Wood (1967) classification, CI chondrites were considered to be the most primitive meteorites, because their compositions provide the best match to solar elemental abundances. CI

chondrites are classified as petrologic type 1, some other carbonaceous chondrites are type 2, relatively unmetamorphosed ordinary and enstatite chondrites are petrologic type 3, and petrologic types 4, 5 and 6 indicate progressively higher degree of thermal metamorphism. Type 7 have sometimes been recognized although it is unclear whether this type reflects the effects of shock as well as thermal metamorphism. Van Schmus and Wood (1967) provided mineralogical and textural criteria to recognize each petrologic type. McSween (1979) demonstrated that petrologic types 1 and 2 were the reflection of the increasing degree of aqueous alteration, while types 3-6 continued to be interpreted as increasing degree of thermal metamorphism (Fig. 1.1). Thus, the most primitive chondrites are actually petrologic type 3. Sears et al. (1980) subdivided type 3 chondrites into types 3.0 to 3.9, based on their thermoluminescence (TL) characteristics. Table 1.1 shows criteria for classifying chondrites according to petrologic type (Weisberg et al., 2006).

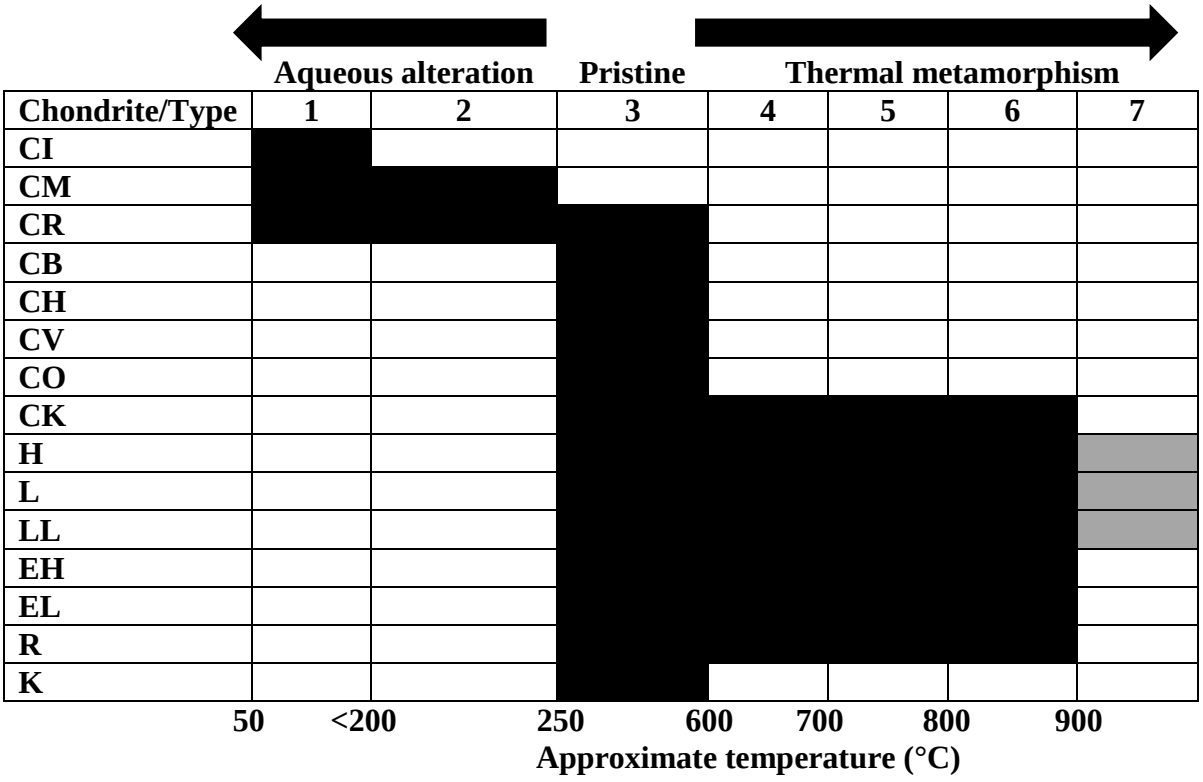


**Fig. 1.1** Classification system for chondrites. A meteorite is classified by identifying its chemical group and petrologic type. Approximate temperatures for metamorphism or alteration are shown at the bottom (McSween and Huss, 2010).

**Table 1.1** Criteria for classifying chondrites according to petrologic type (Weisberg et al., 2006).

| Criteria / Petrologic type | **1** | **2** | **3** | **4** | **5** | **6** | **7** |
|---|---|---|---|---|---|---|---|
| Homogeneity of olivine composition | - | > 5% mean deviation | | ≤5% | Homogeneous | | |
| Structurally state of low-Ca pyroxene | - | Predominantly monoclinic | | >20% monoclinic | ≤20% monoclinic | Orthorhombic | |
| Feldspar | - | Minor primary grains | | Secondary <2 μm grains | Secondary 2-50 μm grains | Secondary >50 μm grains | |
| Chondrule glass | Altered or absent | Mostly altered, some preserved | Clear, isotropic | Devitrified | Absent | | |
| Metal: Maximum Ni (Wt%) | - | <20%; taenite minor or absent | >20%; Kamacite and taenite in exsolution relationship | | | | |
| Sulfides: Mean Ni (Wt%) | - | > 0.5% | <0.5% | | | | |
| Matrix | Fine grained opaque | Mostly fine-grained opaque | Opaque to transparent | Transparent, recrystallized | | | |
| Chondrule-Matrix integration | No chondrules | Sharp chondrule boundaries | | Some chondrule can be discerned, fewer sharp edges | Chondrules poorly delineated | Primary textures destroyed | |
| Carbon (Wt%) | 3-5 | 0.8-2.6 | 0.2-1 | <0.2 | | | |
| Water (Wt%) | 18-22 | 2-16 | 0.3-3 | <1.5 | | | |

### 1.2.3 Other classification parameters: shock and weathering

Another important secondary process affecting many chondrites is shock metamorphism. Stöffler et al. (1991) quantified the shock effects observed in olivine and plagioclase, and used these for a shock classification of ordinary chondrite. Scott et al. (1992) extended this shock classification to carbonaceous chondrites and Rubin et al. (1997) developed a scheme for enstatite by including shock effects in othopyroxene. The classification recognizes shock stages S1 to S6, representing increasing degree of shock pressure, finally culminating in completely melted rocks. Many shocked chondrites are breccias, formed from fragments of rocks that have been cemented together to form new rocks. A chondritic breccia in which all the fragments are of the same chemical group (but usually different petrologic types) is called monomict. A breccia containing fragments of different meteorite groups is called polymict.

Terrestrial weathering has significantly altered the chemistry of some meteorites. Weathering leaches out certain mobile elements and introduces others, as well as oxidizes metals to form rust. Based on surface rustiness and the presence or absence of surficial deposits of evaporate minerals, Antarctic meteorites are categorized (Table 1.2a based on Cassidy, 1980). Depending on oxidation effects of metallic Fe-Ni and troilite visible in polished thin section, ordinary chondrites belong to different weathering scale (Table 1.2b; Wlotzka, 1993a). But for metal-poor CK and R chondrites, Rubin (2005) proposed weathering index which is shown in Table 1.2c.

**Table 1.2a** Weathering categories for Antarctic meteorites.

| Weathering categories | Description | Remarks |
|---|---|---|
| A | Minor rustiness | Rust haloes on metal particles and rust stains along fractures are minor. |
| B | Moderate rustiness | Large rust haloes occur on metal particles and rust stains on internal fractures are extensive. |
| C | Severe rustiness | Metal particles have been mostly stained by rust throughout. |
| e | Evaporite minerals | Evaporite minerals visible to naked eye. |

**Table 1.2b** Weathering Scale for ordinary chondrites.

| Weathering Scale | Description |
|---|---|
| W0 | No visible oxidation of metal or sulfide. A limonitic staining may be noticeable in transmitted light. |
| W1 | Minor oxide rims around metal and troilite; minor oxide veins. |
| W2 | Moderate oxidation of metals, about 20-60% being affected |
| W3 | Heavy oxidation of metal and troilite, 60-95% being replaced |
| W4 | Complete (>95%) oxidation of metal and troilite |
| W5 | Beginning alteration of mafic silicates, mainly along cracks. |
| W6 | Massive replacement of silicates by clay minerals and oxides |

**Table 1.2c** Weathering index for CK and R chondrites.

| Weathering index | Description | Remarks |
|---|---|---|
| Wi-0 | Unweathered | <5 vol% of silicates stained brown |
| Wi-1 | Slightly weathered | 5-25 vol% of silicates stained brown |
| Wi-2 | Moderately weathered | 25-50 vol% of silicates stained brown |
| Wi-3 | Significantly weathered | 50-75 vol% of silicates stained brown |
| Wi-4 | Highly weathered | 75-95 vol% of silicates stained brown |
| Wi-5 | Severely weathered | >95 vol% of silicates stained brown |
| Wi-6 | Extremely weathered | Nearly complete brown staining of silicates. Significant replacement of mafic silicates by phyllosilicates. |

### 1.3 R chondrites

R chondrites have been recognized as a new, well-established chondritic group differing from carbonaceous, ordinary and enstatite chondrites since 1994 (Rubin and Kallemeyn, 1994; Schulze et al., 1994 and Bischoff et al., 1994). This group is named after the Rumuruti meteorite, the first and so far the only R chondrite fall (Schulze et al., 1994). The Rumuruti meteoritic shower fell in Rift valley, Kenya on 1934 (Wlotzka, 1993).

Previously, R chondrites were known as Carlisle Lakes-like chondrites and denoted as a `grouplet` by Rubin and Kallemeyn (1989) who analyzed three samples (Carlisle Lakes, ALH 58151 and Y 75302) of such kind. They used the term `grouplet` instead of `group`, as Wasson (1985) recommended that a meteoritic group should be required to have five or more members. Carlisle Lakes was found in Australia by 1977 and was classified as a new subclass of ordinary chondrites having high oxidation state (Binns and Pooley, 1979) while ALH 85151 and Y 75302 were discovered from Antarctica. Weisberg et al., 1991 found the highest $\Delta^{17}O$ value (up to 2.91) for the aforesaid meteorites and distinguished them from the other chondritic groups. After this, Acfer 217 (Bland et al., 1992), Y 793575 (Yanai, 1992), PCA 91002 (Marlow and Mason, 1992), Y 82002 (Nakamura et al., 1993) were also identified as Carlisle Lakes-type chondrites. Furthermore, clasts with strong affinities to Carlisle Lakes-type chondrites were discovered along with ordinary chondrite clasts in the Weatherford chondrite breccia (Prinz et al., 1993). The large number of these chemically and mineralogically related meteorites justifies the definition of a new group of chondrites (Rubin and Kallemeyn, 1994; and 1994 and Bischoff et al., 1994) which was R chondrite.

## 1.4 R chondrite constituents

### 1.4.1 Chondrules

Condrule abundance in R chondrites (>40%) is much lower than those in ordinary chondrites and enstatite chondrites (60-80%) while in CI chondrites chondrule abundance is less than 5% (Scott and Krot, 2005). All of the major chondrule types (Gooding and Keil, 1981) have been identified in R chondrites: porphyritic olivine (PO, type-I and II), porphyritic pyroxene (PP), porphyritic olivine-pyroxene (POP), barred olivine (BO), radial pyroxene (RP), cryptocrystalline (C) and granular olivine-pyroxene (GOP) (Kallemeyn et al., 1996). The average chondrule diameter in R chondrite is 400 μm which is intermediate between H (300 μm) and L (500 μm) chondrites (Scott and Krot, 2005). Bischoff et al., 1994 found a mean chondrule diameter of 410 μm for Acfer 217. Similar mean chondrule diameter was found for Carlisle Lakes (460 μm), ALH 85151 (410 μm), Y 75303 (420 μm), Rumuruti (365 μm) and PCA 91002 (310 μm) (Rubin and Kallemeyn, 1989, 1994; Schulze et al., 1994 and Kallemeyn et al., 1996). Isa et al., 2014 pointed out that a chondrule size of 400-500 μm is typical for R chondrites.

#### 1.4.1.1 Al-rich chondrules

Rout and Bischoff (2008) and Rout et al., (2010) have studied 20 R chondrites of different petrologic types and reported 19 Al-rich chondrules of variable sizes (upto 550 μm) and mineralogical compositions. The dominant mineral phases in these Al-rich chondrules are plagioclase, fassaite, spinel, diopside and olivine while the accessory minerals are ilmenite and sulfides. Al-rich chondrules are also well established group of chondrules in ordinary chondrites, enstatitie chondrites and carbonaceous chondrites (e.g., Bischoff A. and Keil K, 1983, 1984; Bischoff et al., 1985; MacPherson and Huss, 2005).

### 1.4.2 Matrix

Based on a study of Carlisle Lakes, ALH 85151, Y 75302, Y 793575, Y 82002, Acfer 217, PCA 91002 and PCA 91241 Rubin and Kallemeyn (1993) determined R chondrite matrix abundances of 42 ± 11 vol% besides chondrules, larger mineral and lithic fragments. Matrix abundance in R chondrites is much higher than the ordinary (10-15%) and enstatite (<0.1-10) chondrites while the highest matrix abundance is observed in CI (95%) chondrites (Scott and Krot, 2005). Bischoff (2000) reported a chondrule-matrix ratio of ~1:1 in type 3 clast from R chondrite breccias.

### 1.4.3 Ca, Al-rich inclusions

In 20 R chondrites of different petrologic types, Rout and Bischoff (2008) found 101 Ca, Al-rich inclusions (CAIs). The sizes of these inclusions in R chondrites are very small. The largest CAI is 600 μm in size whereas most are <200 μm. According to the size of CAIs in different chondrite groups, the following sequence can be given: CV > CM ≈ CO > CR > RC ≥ CH > OC > EC. The abundance of CAIs in R chondrites is very low (<0.1%). According to the abundance of CAIs, chondrites can be arranged in the following way: CC > RC > OC > EC. The dominant phases in CAIs of type 3 lithologies in R chondrites are spinel ($MgAl_2O_4$), fassaite ($Ca(Mg,Fe,Al)(Si,Al)_2O_6$), nepheline ($Na_3KAl_4Si_4O_{16}$), sodalite ($Na_8(Al_6Si_6O_{24})Cl_2$) and diopside ($MgCaSi_2O_6$) and the accessory phases are hibonite ($(Ca,Ce)(Al,Ti,Mg)_{12}O_{19}$), anorthite ($CaAl_2Si_2O_3$), olivine ($(Mg,Fe)_2SiO_4$), ilmenite ($FeTiO_3$) and perovskite ($CaTiO_3$). Perovskite is only found in CAIs in lithologies of lower petrologic type while in higher metamorphic grade, only ilmenite is observed. CaO in perovskite is replaced by FeO to form ilmenite during

secondary alteration. In several cases, grains have cores of perovskite and rims of ilmenite. Similar observations were made for perovskite-ilmenite assemblage in CAIs from ordinary chondrites (Bischoff and Keil, 1983, 1984).

## 1.5 Mineralogy of R chondrite

### 1.5.1 Olivine

R chondrites are olivine-rich rocks with an olivine abundance of typically 65-78% (e.g. Schulze et al., 1994; Kallemeyne et al., 1996) while in ordinary chondrites olivine abundance ranges from 40-60% (Weisberg et al., 1991). A typical olivine composition in R chondrites is $Fa_{37-41}$ (e.g., Rubin and Kallemeyn, 1989, 1994; Weisberg et al., 1991; Bischoff et al., 1994; Kallemeyn et al., 1996; Isa et al., 2014) which is much higher than that of ordinary chondrites ($Fa_{18-30}$) (Rubin, 1990; Weisberg et al., 1991). Kallemeyn et al. (1996) reported the olivine/low-Ca pyroxene ratio ranges from 6.7 in Carlisle Lakes to ~140 in Rumuruti (and to ≥ 1500 in Y 793575). Ordinary chondrites contain much lower normative olivine/low-Ca pyroxene ratio: e.g., ~1.5 and ~2.1 in H and L chondrites, respectively (Dodd, 1981 cited by Kallemeyn et al., 1996).

### 1.5.2 Pyroxene

In equilibrated R chondrites, Ca-pyroxene by far the dominating mineral whereas in unequilibrated chondrites low-Ca and Ca-pyroxene occur roughly in similar proportions (Bischoff et al., 2011). The average modal abundances of low-Ca pyroxene and Ca-pyroxene in R chondrites are 4.3% and 5.8%, respectively (Kallemeyn et al., 1996). Ca-pyroxene in R chondrites is moderately higher than that in ordinary chondrite (4-5%) but low Ca-pyroxene is much lower than that in ordinary chondrites (H: ~29%, L: ~25%, LL: ~18%; Van Schmus, 1969).

### 1.5.3 Plagioclase

Modal abundances of plagioclase (5.5-13.0%, mean: 9.6%) in R chondrites are similar to those in ordinary chondrite (~10%) (Kallemeyn et al., 1996). In R chondrites, plagioclase are mostly albites or oligoclases (e.g., Rubin and Kallemey, 1989; Bischoff et al., 1994).

### 1.5.4 Sulfides

Isa et al., (2014) demonstrated that most of the sulfide grains in equilibrated R chondrites are pentlandite ($(Fe,Ni)_9S_8$) and Pyrrhotite ($Fe_{1-x}S$). Monosulfide solid solution ($Fe_{1-x}S – Ni_{1-x}S$) is also present in equilibrated R chondrites as well as in R chondrite clasts in Bencubbin and Murchison. Troilite (FeS) abundance in ordinary chondrites is much higher than that in R chondrites (Weisberg et al., 1991).

### 1.5.5 Oxides

The most abundant oxides are Cr-spinels with high $TiO_2$ and $Fe_3O_4$ (Bland et al., 1992; Schulze et al., 1994; Bischoff et al., 1994). Remarkably high $TiO_4$-concentrations were published for spinels in Rumuruti (~6 wt%; Schulze et al., 1994), Carlisle Lakes and ALH 85151 (6.4 and 5.6 wt%, respectively; Rubin and Kallemeyn, 1989). Magnetite (Rubin and Kallemeyn, 1994), Ilmenite (Schulze et al., 1994, Bischoff et al., 1994) and Perovskite (Rout and Bischoff, 2008) were also reported as oxide phase in R chondrites.

### 1.5.6 Phosphates

Phosphates have been reported from several chondrites (e.g., Weisberg et al., 1991; Bischoff et al., 1994; Schulze et al., 1994; Rubin and Kallemeyn, 1994; McCanta et al., 2008; Endo et al., 2010). They probably occur as a minor phase (<1 vol%) in R chondrites. A large Cl-apatite-rich aggregate of ~500 μm × 180 μm was found in Acfer 217 (Bischoff et al., 1994). Beside chlorapatite in Rumuruti and Acfer 217, mirrillite was reported from Rumuruti (Schulze et al., 1994) and Rubin and Kallemeny (1994) determined an abundance of 0.3 vol% of chlorapatite and 0.2 vol% of mirrillite in PCA 91002. LAP 04840 contains little apatite (~0.6 vol%) as scattered euhedral and anhedral crystals with a chemically high proportion of OH relative to Cl and F (McCanta et al., 2008). Modal abundance of phosphate in R chondrites is moderately lower than those in ordinary chondrites (~0.7%, Van Schmus, 1969).

### 1.5.7 Metal phase

Kallemeyn et al., (1996) reported that metallic Fe-Ni is extremely rare to absent in most of R chondrites. They analyzed Carlisle Lakes, ALH 85151, PCA91002, Y 75302, Y 793575, Y 82002, Acfer 217 and Rumuruti and found metal phase only in Rumuruti

(0.005%) and in ALH 85151 (0.9%) where metal phase is Ni rich (awaruite, $Ni_{2-3}Fe$). In ordinary chondrites metal phase is much higher than those in R chondrites (Weisberg et al., 1991). Kamacite and Taenite are the dominating metal phases in ordinary chondrites whereas they are completely absent in R chondrites (Van Schmus, 1969; Weisberg et al., 1991; Kallemeyn et al., 1996; Isa et al., 2014).

### 1.6 Textural characteristics of R chondrites

Most of the R chondrites are breccias and many are regolith breccias with solar wind implanted gases (Weber and Schultz, 1995). For instance, Acfer 217, Rumuruti, Dar al Gani 013 contain unequilibrated type 3 fragments and clasts metamorphosed to various degrees (Bischoff et al., 1994; Schulze et al., 1994; Jäckel et al., 1996; Kallemeyn et al., 1996). Impact melt (in Dar al Gani 013; Jäckel et al., 1996) and dark clast (in Rumuruti; Schulze et al., 1994) were also reported for R chondrites.

### 1.7 Shock effects

Most of the R chondrites are very weakly (S2) or weakly shocked (S3) (Bischoff et al., 2011), using the shock classification scale for ordinary chondrites (Stöffler et al., 1991). Shock stage of NWA 053, NWA 753, NWA 755, NWA 4419, Dar al Gani 417, Ouzina, Sahara 99248 were reported as S2 (Bischoff et al., 2001; Weber and Schultz, 2001; Caporali et al., 2009) whereas Carlisle Lakes and Hammadah al Hamra 119 appear unbrecciated and have been classified as S3 chondrites (Dixon et al., 2003). The brecciated Rumuruti chondrite is only very weakly shocked (S2), but a vain in one of the clasts indicates that different fragments have experienced different degrees of shock metamorphism at different times in the evolution of the breccia (Schulze et al., 1994; Dixon et al., 2003). Acfer 217 is very weakly shocked (S2), although some fragments have experienced higher degrees of shock (Bland et al., 1992; Bischoff et al., 1994). Similar observations were made for ALH 85151 and PCA 91002 (Rubin and Kallemeyn, 1989, 1994). Nevertheless, the complex breccia Dar al Gani 013 was classified as S1 chondrite (Jäckel et al., 1996). Fragments in ALH 85151 and Rumuruti exhibit significant silicate darkening due to the dispersion of fine-grained sulfide and chromite (Kallemeyn et al., 1996). However, shock veins appear to be quite rare in R chondrites (Bischoff et al., 2011). So far, only a few have been reported in different lithologies from R chondrites, e.g., Rumuruti, Y 82002 and PCA 91002 (Schulze et al., 1994; Rubin and Kallemeny, 1994).

### 1.8 R chondrite chronology

Dixon et al., (2003) determined the $^{39}$Ar-$^{40}$Ar ages for the whole-rock of Carlisle Lakes, Rumuruti, Acfer 2017 and PCA 91002 which were breccias except for Carlisle Lakes. Noticing a complicated age spectra due to the diffusive loss of radiogenic $^{40}$Ar to various extent, they reported the peak $^{39}$Ar-$^{40}$Ar ages: ≥4.35 Ga (Carlisle Lakes), ~4.47±0.02 Ga (Rumuruti), 4.30±0.07 Ga (Acfer 217) and ≥4.37 Ga (PCA 91002). R chondrites have relatively old $^{39}$Ar-$^{40}$Ar ages that overlap those of the oldest L and LL chondrites (Dixon et al., 2003 and references therein). Dixon et al. (2003) interpreted that during parent body metamorphism, the clasts were heated to different temperatures at different depths in the body. At ~4.47 Ga ago, an impact caused mixing of material from different depth and resetting the $^{39}$Ar-$^{40}$Ar ages. Rapid subsequent cooling under a rather thin regolith layer could have prevented further metamorphism of the clasts. Later impacts (~4.37 Ga ago) probably reset at least partially some of the samples. Buikin et al. (2006) and Trieloff et al. (2007) studied different lithologies from Rumuruti breccia and found that the coarse grained type 5/6 lithology has the best defined age plateau of 4.53 ± 0.01 Ga.

### 1.9 Oxygen isotopic composition

Kallemeyn et al. (1996) reported the whole-rock $\Delta^{17}$O values (~2.9) for Rumuruti, ALH 85151 and PCA 91002, which were the highest of any known meteorites. Similar finding was also observed by Weisberg et al. (1991). Bischoff et al. (2011) reviewed the previous literature (e.g., Schulze et al., 1994; Bischoff et al., 1994; McCanta et al., 2008) data and calculated a mean $\Delta^{17}$O value (2.71±0.31) for R chondrites. Rubin (2011) demonstrated that the $\Delta^{17}$O values increase in the inner solar system with increasing of heliocentric distance from enstatite chondrites (0.0‰) to H, L and LL ordinary chondrites (0.7‰, 1.1‰ and 1.3‰, respectively) to R chondrites (2.9‰). The values peak around the R-chondrite location and then become increasingly negative among carbonaceous chondrites with increasing of distance from the Sun: CR (-1.0‰), CV-CK (-4.2‰ to -4.6‰), CO-CM (-4.7‰ to -5.2‰) and CI (-6.5‰). Furthermore, Greenwood et al. (2000) measured oxygen isotopic compositions of magnetite and olivine in thin sections of PCA 91241 and PCA 91002, and discussed about a generic linkage between R chondrites and ordinary chondrites. In their study, $\Delta^{17}$O values for magnetite and olivine are ranging from +2.5‰ to +4.3‰ and -1.2‰ to +2.9‰, respectively. Fig. 1.2 (McSween and Huss, 2010)

demonstrated the oxygen isotopic composition of bulk R chondrites in comparison to the other chondritic groups.

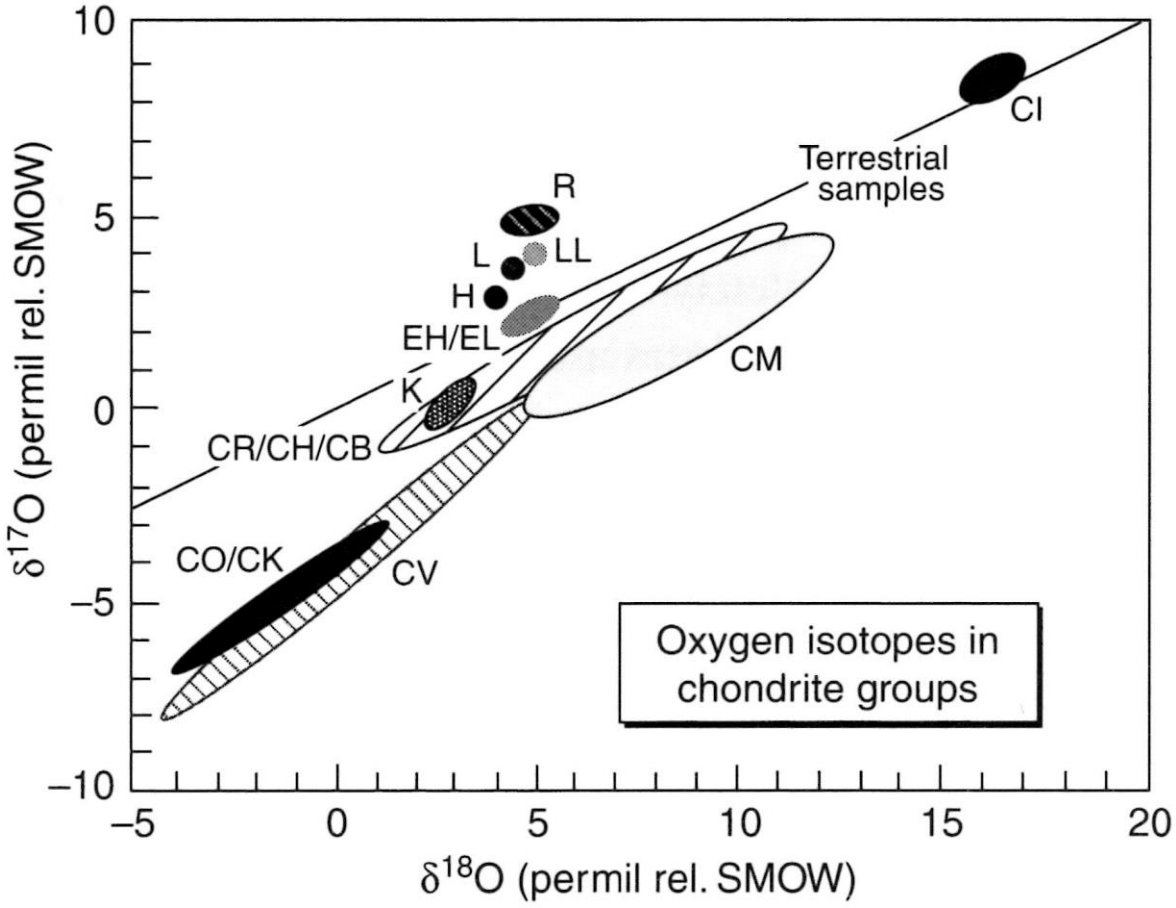


**Fig. 1.2** Oxygen isotopic compositions for bulk chondrites, after Clayton (2004). By convention, $^{17}O/^{16}O$ and $^{18}O/^{16}O$ ratios are plotted as deviations from the composition of standard mean ocean water (SMOW) in unit of parts per thousand (permil). The δ values are calculated as follows: $\delta^{17}O = [((^{17}O/^{16}O)_{sample}/(^{17}O/^{16}O)_{SMOW}) - 1] \times 1000$, and similarly for $\delta^{18}O$ (McSween and Huss, 2010; with the permission of Cambridge University Press).

## 1.10 Bulk chemical composition

The bulk chemical compositions of R chondrites are mostly done by using instrumental neutron activation analysis (e.g., Rubin and Kallemeyn, 1989, 1994; Bischoff et al., 1994, Schulze et al., 1994; Kallemeyn et al., 1996; Palme et al., 1996; Isa et al., 2014). The general bulk chemical characteristics of R chondrites are as follows:

(a) In bulk chemical composition, R chondrites have some affinity to ordinary chondrites (Palme et al., 1996; Kallemeyn et al., 1996, Greenwood et al., 2000; Isa et al., 2014).

(b) The average CI, Mg-normalized lithophile element abundances are ~0.95×CI, which is lower than those for the carbonaceous chondrites (≥1.0×CI; Kallemyn and Wasson, 1981) and slightly higher than those for ordinary chondrites (~0.9×CI) (Kallemeyn et al., 1996).

(c) Total Fe content in R chondrites (~24wt%) (Rubin and Kallemeyn, 1989, 1994; Bischoff et al., 1994, Schulze et al., 1994; Kallemeyn et al., 1996; Palme et al., 1996; Ozaki et al., 1998; Isa et al., 2014) is intermediate between those of H (27.1wt%) and L (21.6wt%) chondrites (Kallemeyn et al., 1989).

(d) The absence of significant depletions in Mn and Na in R chondrites and ordinary chondrites is an important feature to distinguish these groups from carbonaceous chondrites (Palme et al., 1996).

(e) Mean R chondrite abundances of refractory siderophiles (Os, Ir), common siderophiles (Ni, Co, Fe) and Au are intermediate between those in L chondrites and H chondrites (Isa et al., 2014).

(f) The abundances of Zn and Se are much higher than those of ordinary chondrites (Kallemeyn et al., 1996, Palme et al., 1996, Isa et al., 2014).

(g) Anomalous abundances of Au, Ni and Co in some R chondrites are probably due to terrestrial weathering (Kallemeyn et al., 1996; Bischoff et al., 1996; Palme et al., 1996).

## 1.11 Motivation of this work

Other than instrumental neutron activation analysis (INAA), some other analytical techniques were also applied for determining the bulk chemical composition of R chondrites, e.g., RNAA (Xiao and Lipschutz, 1992), XRF (Dreibus et al., 1995; Palme et al., 1996), PGA (Ozaki et al., 1998), ICP-MS (Acken et al., 2011), MS-ID (Nakamura et al.,

1999), etc. Bulk chemical compositions of most of the R chondrites have been analyzed by neutron activation analysis techniques. However, the bulk chemical data-base for R chondrites is still not so rich like carbonaceous, ordinary and enstatite chondrites. But to understand the nebular origin and the parent body processes, a greater set of bulk chemical composition data is an essential tool.

Nakamura et al., (1999) used isotope dilution technique (MS-ID) for determining rare earth elements in five Antarctic R chondrites. Isotope dilution technique provides a very precise data for the rare earth elements, but it is unable to determine the mono-isotopic Pr, Tb, Ho and Tm. Boynton, 1978 demonstrated that detailed REE abundance pattern as well as Th and U should be determined for explaining the nebular and parent body processes. Palme et al. (1996) applied XRF for bulk chemical analysis of only three R chondrites (Rumuruti, Acfer 217 and Dar al Gani 013), especially phosphorus. Phosphorus abundance is important for explaining the REE, Th and U abundance (Goreva and Burnett, 2001). Boynton (1975) and Davis and Grossman (1979) demonstrated the REE fractionation in solar nebula in terms of fractional condensation. So, the detail abundances of REEs, Th and U along with the P abundance are important to ascertain the nebular processes of chondrites. But, for R chondrites, detail abundances of REEs, Th and U are not available.

Using RNAA, Xiao and Lipschutz (1992) analyzed one R chondrite (ALH 58151) for volatile elements. Volatile elemental abundances are important tool for explaining the nebular and/or parent body processes (Takhashi et al., 1978). Volatile elements are strongly depleted in chondritic meteorites compared with those of solar composition (CI meteorite). For explaining the volatile composition in chondrites, two-component model has been proposed by Anders and coworkers (e.g., Anders, 1964; Larimer and Anders, 1967). According to this model, the volatile elemental abundance pattern in chondrites was established during accretion from solar nebula. In a regime of falling temperatures, volatile elements would condense in succession on the fine grind dust (fraction A), but not on the coarse-grained chondrules-plus-metal (fraction B). The composition of fraction A would thus vary with temperature, while that of fraction B remains essentially fixed. Meteorites last to accrete would therefore be richest in volatiles. This model can approximately explain the systematic variation of volatile elements in type II (CM chondrites, 0.55×CI) and type III (CV and CO chondrites, 0.32×CI) carbonaceous chondrites relative to the type I (CI chondrites) carbonaceous chondrites (Larimer and Anders, 1967). Tandon and Wasson

(1967) reported a systematic variation of indium in a petrologic suite of L-group chondrites and, to explain this variation, they proposed three-component model (Tandon and Wasson, 1968). According to this model, elemental abundances were established during accretion, as in the two-component model. However, strongly depleted elements were brought in mainly by a third component (fraction C), strongly enriched in all volatile elements. Along with the two and three-component models, another condensation model was proposed known as multi-component model (Blander and Abdel-Gawad, 1969). In this model, condensation and accretion proceed simultaneously (as in two-component model), with the condensation efficiency on components A and B being governed by surface area, and the volatile content of the fine-grained dust increases with falling temperatures. However, some of the dust (along with chondrules) continually agglomerates to `chunks`, and thereafter ceases to take up volatiles on further cooling. Thus a large number of sub-components ($A_1$, $A_2$, $A_3$ … $A_n$) are produced, each having a composition reflecting its agglomeration temperature. The volatile content of a given meteorite thus reflects the proportions of components $A_1$ to $A_n$, rather than the accretion temperature of the meteorite itself. In all condensation models, condensation and accretion proceed simultaneously.

Metamorphism model was also proposed for explaining the volatile depletions (Wood, 1967; Dodd, 1969). In this model, all ordinary chondrites initially had the composition and mineralogy of petrologic type 3. The depletion pattern was established during metamorphism, with the most intensely metamorphosed meteorites losing the greatest proportion of volatiles. Later on, by a series of paper Lipschutz and co-workers (e. g., Ikramuddin and Lipschutz, 1975; Ikramuddin et al., 1976, 1977) presented their heating experiment and supported the metamorphism model along with the condensation model. That is, volatile elements are important for discussing the nebular and/or parent body process(es). Previously, Anders, Wasson, Lipschutz and their coworkers reported volatile elemental abundances in different chondritic meteorites (e.g., Keays et al., 1971; Takahashi et al., 1978; Tandon and Wasson, 1967, 1968; Kaczaral et al., 1989; Wang and Lipschutz, 2007) using radiochemical neutron activation analysis. But for R chondrites, no volatile elemental data are available (except for ALH 85151 by Xiao and Lipschutz, 1992) for discussing their nebular and/or parent body process (es). So this study will focused on the most thermally labile trace elements - particularly Zn, Pb, Bi, In, Tl and Cd, since these are the most sensitive to genetic processes accompanied by significant heating (e.g., metamorphic heating and/or shock heating) (Lipschutz, 1997 and Wasson, 2005).

## 1.12 Objective of this study

This work will characterize R chondrites chemically from a comprehensive study of bulk chemical composition by INAA, ICP-MS, ICP-AES and MS-ID experiments, in a significant number of R chondrites of all petrologic types. The major goals of this work are as follows:

(a) Using instrumental neutron activation analysis, 24 elements (Na, Mg, Al, Ca, Sc, V, Cr, Mn, Fe, Co, Ni, Zn, As, Se, Br, Sb, La, Sm, Eu, Yb, Lu, Os Ir and Au) will be analyzed for chemical characterization of R chondrites. These elemental abundances will be used for taxonomic study and for explaining the nebular oxidation process.

(b) ICP-MS and ICP-AES experiments will provide the detailed REEs, Th and U, and P abundances, respectively. This study will explain the REEs, Th and U fractionations in R chondrites.

(c) A precise volatile elemental (Zn, Cd, In, Tl, Pb and Bi) abundances will be presented from MS-ID experiment to explain the nebular and/or parent body process (es).

# Chapter-2

## Experimental

## 2.1 Sample information

R chondrite is one of the rare classes of chondritic group that comprises only about 0.1% of the chondritic fall on Earth (Grady, 2000). But the recent discoveries of meteorites from Antarctica mainly by National institute of polar science (NIPR), Tokyo and US Antarctic search for meteorites program (ANSMET) provide the all petrologic specimen of R chondrites and allow us a systematic study of this group. According to the meteoritical society database, 152 chondrites are classified as R chondrite (upto July, 2014). To study the nebular and/or parent body processes of R chondrites, it is essential to consider all the petrologic grade samples.

In this study 15 antarctic R chondrites (Table 2.1) have been analyzed. Seven of them were obtained from National institute of polar research, Tokyo (Y-793575.44, A-881988.68, Y-983270.56, Y-983720.81, Y-983097.81, Y-980702.61, Y-980703.71) and others were obtained from NASA, Johnson space center (PRE 95411.21, ALH 85151.41, MIL 07440.8, LAP 03639.33, LAP 04840.12, MIL 11207.8, LAP 02238.13, PCA 91002.64). Among these samples PRE 95411, LAP 03639 and LAP 04840 were analyzed by Isa et al. (2014), ALH 85151 by Rubin & Kallemeyn (1989) and PCA 91002 & Y 793575 by Kallemeyn et al. (1996) using instrumental neutron activation analysis. All specimens were interior chips and were free from fusion crust. For systematic study we have chosen the samples to cover all types of petrologic grade (R3 to R6). Rubin and Huber (2005) demonstrated the weathering index for the R chondrites and showed the loss of some elements, presumably by leaching. This study generally avoided requesting R chondrites exhibiting such weathering but did include one sample of C class. Weathering index for Y-980702 and Y 980703 were not assigned. The available weathering indexes (wi) from Rubin and Huber (2005) are also mentioned in Table 2.1. The total masses of the individual R chondrites were ranged from 0.6g to 0.8g, except that for ALH 85151 (0.434g). Each of the samples was separately ground by a clean agate mortar to make homogeneous powder.

In all experiments, Smithsonian Allende (USNM 3529, split/position: 22/6) powder was used as a control sample.

**Table 2.1** Ancillary data for meteorites in this study

| Meteorite | Abbreviation | Position | Class[a] | Weathering[a] | Fayalite (mol%) | Ferrosilite (mol%) | Sample ground (mg) | Sources[c] |
|---|---|---|---|---|---|---|---|---|
| Mount Prestrud 95411 | PRE 95411 | 21 | R3 | A/B | 1-41[d], 40[e] | 15-29 [d] | 829 | JSC |
| Allan Hills 85151 | ALH 85151 | 41 | R3.6 | B(wi2)[b] | 0.1-41[f] | 6-30[f] | 434 | JSC |
| Yamato 793575 | Y 793575 | 44 | R3.8 | (wi4) [b] | | | 633 | NIPR |
| Asuka 881988 | A 881988 | 68 | R4 | (wi3) [b] | 35[e] | | 619 | NIPR |
| Yamato 983270 | Y 983270 | 56 | R4 | A | 38.4-40.1[g] | | 623 | NIPR |
| Miller Range 07440 | MIL 07440 | 8 | R4 | Be | 38[h] | 10[h] | 792 | JSC |
| LaPaz Icefield 03639 | LAP 03639 | 33 | R4 | A/B | 19-38[i] | 13-29[i] | 821 | JSC |
| Yamato 983720 | Y 983720 | 81 | R4 | A | 39.6, (12.8-46.9)[g] | | 616 | NIPR |
| Yamato 983097 | Y 983097 | 81 | R5 | A | 35.0, (34.2-37.0)[g] | 29.3 | 632 | NIPR |
| Yamato 980702 | Y 980702 | 61 | R6 | ? | 38[e] | | 666 | NIPR |
| Yamato 980703 | Y 980703 | 71 | R6 | ? | 39.1, (38.4-40.2)[j] | | 645 | NIPR |
| LaPaz Icefield 04840 | LAP 04840 | 12 | R6 | A/B | 38 [i] | 30[i] | 870 | JSC |
| Miller Range 11207 | MIL 11207 | 8 | R6 | Ce | 39-41[k] | 20[k] | 854 | JSC |
| LaPaz Icefield 02238 | LAP 02238 | 13 | R | B(wi4) [b] | 39[e], (27-46)[l] | 18-36 [l] | 760 | JSC |
| Pecora Escarpment 91002 | PCA 91002 | 64 | R3.8-6 | A/B(wi1)[b] | 1-44[f] | 1-28[f] | 829 | JSC |

[a]Antarctic Meteoritic Newsletters, [b]Rubin and Huber (2005), [c]JSC: Johnson Space Center, NASA, USA, [c]NIPR: National Institute of Polar Research, Tokyo, Japan, [d]Grossman (1998), [e]Isa et al. (2014), [f]Grossman (1994), [g]Yamaguchi et al. (2012), [h]Righter (2011), [i]Connolly Jr. et al. (2007), [j]Kojima et al. (2009), [k]Righter (2012), [l]Russell et al. (2004).

## 2.2 Experimental techniques

For a systematic study of bulk chemical composition, three different analytical techniques were used,

a) Instrumental neutron activation analysis (INAA),
b) Inductively coupled plasma atomic emission spectrometry (ICP-AES), and
c) Inductively coupled plasma mass spectrometry (ICP-MS).

In ICP-MS experiment, both internal calibration method and isotope dilution technique have been applied.

## 2.3 Instrumental neutron activation analysis

### 2.3.1 Sample preparation

About 40 mg of each powdered sample (Table 2.2) was taken into a 1cm × 1cm polyethylene bag and sealed. These bags were then doubly packed by another layer of polyethylene and sealed. At the same time, JB-1 (geological standard) and Allende were also prepared as standard and control samples, respectively. For correcting the $^{28}Si(n,p)^{28}Al$, $^{27}Al(n,p)^{27}Mg$ and $^{27}Al(n, \alpha)^{24}Na$ effect in determining the Al, Mg and Na, Al, MgO and Si chemical reagents were prepared for short irradiation. For long irradiation, Se, Sb, Os, Ir and Au chemical standards were prepared from reagents.

**Table 2.2** Sample weight for INAA experiment.

| | R chondrites | Sample weight (g) |
|---|---|---|
| 1. | PRE 95411 | 0.04320 |
| 2. | ALH 85151 | 0.03976 |
| 3. | Y 793575 | 0.03978 |
| 4. | A 881988 | 0.03862 |
| 5. | Y 983270 | 0.04472 |
| 6. | MIL 07440 | 0.03951 |
| 7. | LAP 03639 | 0.04302 |
| 8. | Y 983720 | 0.04116 |
| 9. | Y 983097 | 0.04172 |
| 10. | Y 980702 | 0.04118 |
| 11. | Y 980703 | 0.04188 |
| 12. | LAP 04840 | 0.04057 |
| 13. | MIL 11207 | 0.04306 |
| 14. | LAP 02238 | 0.04151 |
| 15. | PCA 91002 | 0.04291 |

### 2.3.2 Sample irradiation and counting

To determine the short-lived elements, samples, standard, Allende and chemical reagents were irradiated separately at Kyoto University Research Reactor at 1MW for 10 seconds. After ~5 minutes cooling, the outer bag of the irradiated sample was changed with a new one and counting was taken in a HPGe detector using 300 seconds as live time. For long Irradiation, the samples were irradiated simultaneously at 1MW for 4hours. After six days of cooling and changing the outer bag, the first counting was taken for 3 hours as live time in HPGe detector at Radioisotope Research Center, Tokyo metropolitan university. Three weeks later, counting was again taken for 12 hours to determine the long-lived radionuclides. Twenty four elements were determined in R chondrites from different irradiations and counting stages (Table 2.3).

**Table 2.3** Elements analyzed at different irradiation and counting stage.

| | Decay time | Counting time | Elements determined |
|---|---|---|---|
| Short irradiation | 5 min | 300 s | Na, Mg, Al, Ca, V and Mn |
| Long irradiation (first counting) | 6 days | 3 hr. | Na, Sc, Cr, Fe, Co, As, Br, Sb, Au, La, Sm, Yb and Lu |
| Long irradiation (second counting) | 3 weeks | 12 hr. | Cr, Fe, Co, Ni, Ir, Os, Se, Eu and Zn |

### 2.3.3 Accuracy and precision

For all elements, JB1 (a geological reference sample issued by Geological Survey of Japan) was used as standard except that for Os, Ir, Au and Se. For these elements, chemical reagents were used as standard. Data reductions were done by using information noted in Table 2.4. In the possible cases, we used more than one gamma-energy (in keV) for elemental abundance calculations. Elemental abundances obtained by using different gamma-energy are in good agreement with each other.

To ensure the data quality, the Allende Smithsonian powder was used as a control sample. To do so, three replicates of Allende powder (~40 mg) were irradiated under identical conditions at Kyoto University Research Reactor (KURR). These samples were irradiated in two segments giving approximately six months of interval (June – December, 2012). Results are shown in Table 2.5 with 1σ uncertainty (n=3). The maximum deviation from the mean is about 6% for Br and lower for the other elements analyzed. Relative standard deviations of the replicate measurements are lower than the % of uncertainty

generated from counting statistics. In Fig. 2.1 Allende data of this study is normalized to that of literature data (Kallemeyn & Wasson, 1981 and Kallemeyn et. al., 1989). For all elements, our data are consistent with the literature data, except for La, Sm and Ir. Lanthanum and Sm data are about 8% higher while Ir is ~10% lower compared with those of Kallemeyn & Wasson (1981) and Kallemeyn et. al. (1989). But, our La, Sm & Ir data are in good agreement with those of Wasson et. al. (2013). Furthermore, La & Sm were also determined by ICP-MS and the data of La & Sm obtained both from INAA and ICP-MS are consistent within the limit of uncertainty.

**Table 2.4** Nuclear reactions, half-life and energy considered for corresponding elemental determination.

| Elements | Reaction | Half-life | Energy (keV) |
|---|---|---|---|
| Na | $^{23}Na(n,\Upsilon)^{24}Na$ | 14.7 h | 1368, 2754 |
| Mg | $^{26}Mg(n,\Upsilon)^{27}Mg$ | 9.46 m | 1014.4 |
| Al | $^{27}Al(n,\Upsilon)^{28}Al$ | 2.24 m | 1778.9 |
| Ca | $^{48}Ca(n,\Upsilon)^{49}Ca$ | 8.72 m | 3084.4 |
| Sc | $^{45}Sc(n,\Upsilon)^{46}Sc$ | 83.8 d | 889 |
| V | $^{51}V(n,\Upsilon)^{52}V$ | 3.75 m | 1434.1 |
| Cr | $^{50}Cr(n,\Upsilon)^{51}Cr$ | 27.7 d | 320.2 |
| Mn | $^{55}Mn(n,\Upsilon)^{56}Mn$ | 2.58 h | 1810.7 |
| Fe | $^{58}Fe(n,\Upsilon)^{59}Fe$ | 44.5 d | 1099, 1292 |
| Co | $^{59}Co(n,\Upsilon)^{60}Co$ | 5.27 y | 1173, 1332 |
| Ni | $^{58}Ni(n,p)^{58}Co$ | 70.9 d | 811 |
| Zn | $^{64}Zn(n,\Upsilon)^{65}Zn$ | 244 d | 1115.5 |
| As | $^{75}As(n,\Upsilon)^{76}As$ | 26.3 h | 559 |
| Se | $^{74}Se(n,\Upsilon)^{75}Se$ | 121d | 264.5 |
| Br | $^{81}Br(n,\Upsilon)^{82}Br$ | 35.3 h | 554, 777 |
| Sb | $^{121}Sb(n,\Upsilon)^{122}Sb$ | 2.75 d | 564 |
| La | $^{139}La(n,\Upsilon)^{140}La$ | 1.68 d | 1596 |
| Sm | $^{152}Sm(n,\Upsilon)^{153}Sm$ | 46.7 h | 103.1 |
| Eu | $^{151}Eu(n,\Upsilon)^{152}Eu$ | 13.3 y | 1408 |
| Yb | $^{174}Yb(n,\Upsilon)^{175}Yb$ | 4.19 d | 396 |
| Lu | $^{176}Lu(n,\Upsilon)^{177}Lu$ | 6.71 d | 208 |
| Os | $^{190}Os(n,\Upsilon)^{191}Os$ | 15.4 d | 129.6 |
| Ir | $^{190}Ir(n,\Upsilon)^{191}Ir$ | 73.8 d | 468, 604, 308, 296 |
| Au | $^{197}Au(n,\Upsilon)^{198}Au$ | 2.69 d | 411.8 |

**Table 2.5** Major and trace element abundances obtained by INAA for Allende (uncertainties are due to counting statistics, 1σ).

| | | June, 2012 | December, 2012 | | Average | SD | RSD | Literature data | | |
|---|---|---|---|---|---|---|---|---|---|---|
| | | 1 | 2 | 3 | (n=3) | (1σ) | (%) | *a* | *b* | *c* |
| Na | ppm | 3270 ± 20 | 3390 ± 20 | 3340 ± 20 | 3330 | 60 | 1.8 | 3290 | 3290 | 3360 |
| Mg | % | 15.3 ± 1.6 | 14.7 ± 1.2 | 14.9 ± 1.2 | 15.0 | 0.3 | 2.1 | 14.8 | 14.9 | |
| Al | % | 1.71 ± 0.02 | 1.74 ± 0.02 | 1.68 ± 0.02 | 1.71 | 0.03 | 1.8 | 1.76 | 1.77 | |
| Ca | % | 1.66 ± 0.21 | 1.79 ± 0.16 | 1.81 ± 0.18 | 1.75 | 0.08 | 4.7 | 1.88 | 1.84 | 1.78 |
| Sc | ppm | 11.32 ± 0.02 | 11.09 ± 0.03 | 11.23 ± 0.03 | 11.21 | 0.12 | 1.1 | 11.23 | 11.27 | 10.9 |
| V | ppm | 92.8 ± 3.1 | 95.7 ± 4.2 | 96.1 ± 3.8 | 94.9 | 1.8 | 1.9 | 99.5 | 98.2 | |
| Cr | ppm | 3600 ± 20 | 3570 ± 20 | 3630 ± 20 | 3600 | 30 | 0.9 | 3630 | 3640 | 3650 |
| Mn | ppm | 1470 ± 50 | 1490 ± 60 | 1430 ± 60 | 1460 | 30 | 2.1 | 1450 | 1450 | 1460 |
| Fe | % | 23.4 ± 0.1 | 23.8 ± 0.1 | 23.8 ± 0.1 | 23.7 | 0.2 | 1.0 | 23.7 | 23.7 | 23.7 |
| Co | ppm | 661 ± 3 | 669 ± 4 | 655 ± 4 | 662 | 7 | 1.1 | 662 | 661 | 666 |
| Ni | % | 1.42 ± 0.04 | 1.37 ± 0.03 | 1.41 ± 0.03 | 1.40 | 0.03 | 1.9 | 1.33 | 1.36 | 1.36 |
| Zn | ppm | 114 ± 10 | 109 ± 10 | 118 ± 11 | 114 | 5 | 4.0 | 119 | 116 | 117 |
| As | ppm | 1.51 ± 0.30 | 1.49 ± 0.20 | 1.56 ± 0.20 | 1.52 | 0.04 | 2.4 | 1.56 | 1.57 | 1.59 |
| Se | ppm | 8.19 ± 0.34 | 8.29 ± 0.28 | 8.05 ± 0.30 | 8.18 | 0.12 | 1.5 | 8.23 | 8.17 | 8.27 |
| Br | ppb | 1.50 ± 0.38 | 1.68 ± 0.42 | 1.53 ± 0.46 | 1.57 | 0.10 | 6.1 | 1.55 | 1.58 | 1.62 |
| Sb | ppb | 84 ± 16 | 87 ± 19 | 81 ± 17 | 84 | 3 | 3.6 | 83 | 82 | 85 |
| La | ppb | 537 ± 29 | 520 ± 21 | 532 ± 30 | 530 | 9 | 1.7 | 490 | 498 | 499 |
| Sm | ppb | 335 ± 8 | 319 ± 7 | 327 ± 7 | 327 | 8 | 2.5 | 299 | 304 | 308 |
| Eu | ppb | 115 ± 15 | 111 ± 14 | 117 ± 16 | 114 | 3 | 2.7 | 113 | 114 | 115 |
| Yb | ppb | 320 ± 60 | 330 ± 50 | 320 ± 40 | 320 | 10 | 3.1 | 320 | 330 | 320 |
| Lu | ppb | 44 ± 9 | 48 ± 8 | 46 ± 8 | 46 | 2 | 4.3 | 46 | 48 | 45 |
| Os | ppb | 840 ± 90 | 790 ± 90 | 820 ± 90 | 820 | 30 | 3.1 | 828 | 833 | 812 |
| Ir | ppb | 702 ± 5 | 707 ± 5 | 713 ± 5 | 707 | 6 | 0.8 | 785 | 789 | 757 |
| Au | ppb | 141 ± 5 | 146 ± 4 | 143 ± 4 | 143 | 3 | 1.8 | 145 | 144 | 146 |

[a]Kallemeyn and Wasson (1981)
[b]Kallemeyn et. al. (1989)
[c]Wasson et. al. (2013)

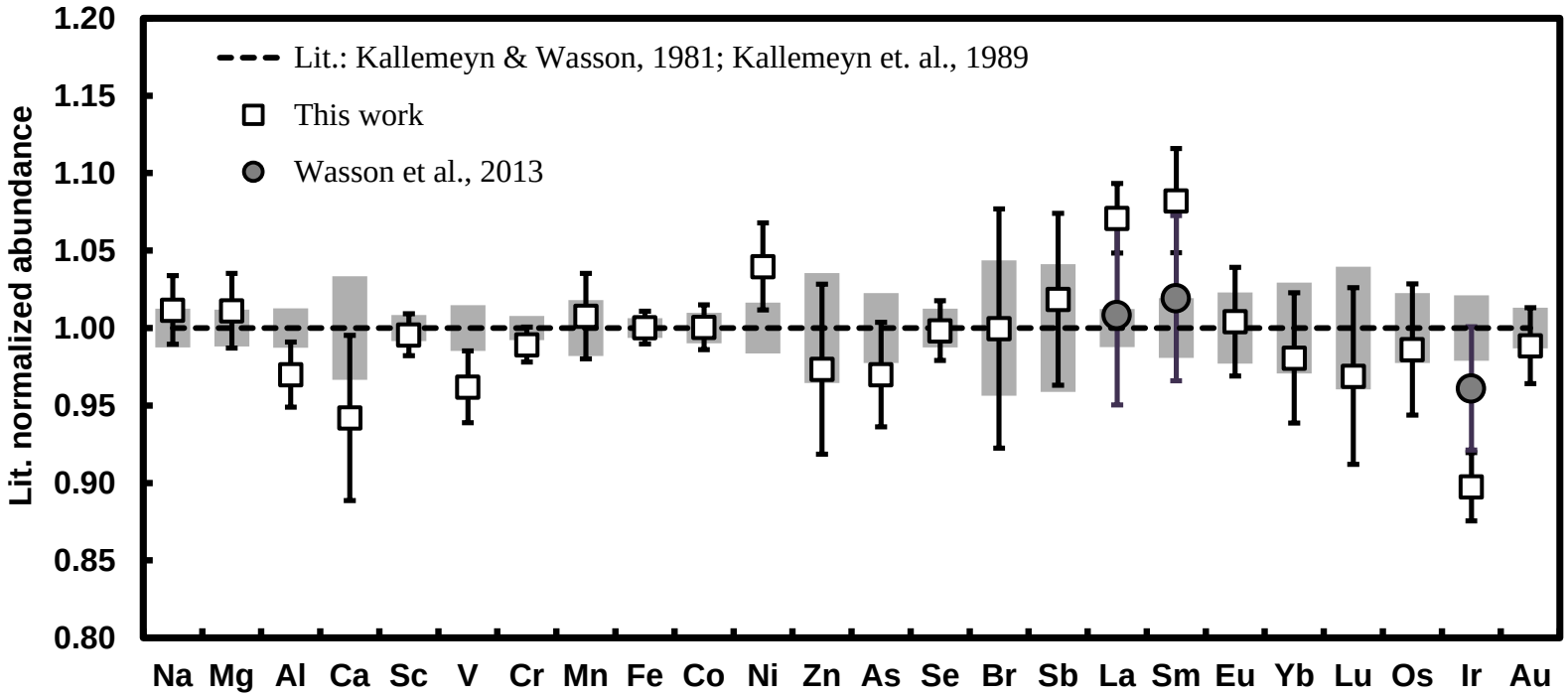


**Fig. 2.1** Literature (Kallemeyn & Wasson, 1981 and Kallemeyn et. al., 1989) normalized elemental abundances of Allende. Gray rectangles represent the uncertainty (1σ, n=17, standard deviation of all the tabulated values for Allende in Kallemeyn & Wasson, 1981 and Kallemeyn et. al., 1989), blank squares represent this work with 1σ uncertainty (n=3) and gray circles represent the data from Wasson et. al., 2013.

## 2.4 Inductively coupled plasma mass spectrometry

In this study, Plasma-Quad 3 spectrometer (Fisons Instruments, UK) and iCAP Q ICP-MS (Thermo SCIENTIFIC, USA) were used. Both of them are quadrupole spectrometers. For the determination of REEs, Th and U, internal calibration method was used but among the REEs, only Sm was determined by both internal calibration method as well as isotope dilution technique for recovery calculation. The volatile elements (Pb, Zn, Cd, In, Tl) were determined by isotope dilution technique and Bi was determined by using Pb/Bi ratio. Zinc, Cd, In and Tl were determined by iCAP Q ICP-MS after chemical (Tl only) and column (Zn, Cd and In) separation.

### 2.4.1 Internal calibration method for REEs, Th and U determination

#### 2.4.1.1 Sample preparation

Typically 20 mg (Table 2.6) of each powdered sample was dissolved in closed screw-top Teflon vessel (Thermo scientific) at about 150°C for 24 hours using 0.2 ml concentrated HF, 0.1 ml concentrated $HNO_3$ and 0.1 ml concentrated $HClO_4$. After evaporation to dryness of the acid mixture, approximately 0.1 ml concentrated $HClO_4$ was added and placed back on the hot plate with closed cap for over night. After drying up, approximately 0.1 ml concentrated HCl was added and the Teflon vessel was allowed to heat again for dryness. Addition of 0.1 ml HCl and drying up cycle was repeated twice to ensure the digestion of oxides and dissolution of fluoride. Then necessary amounts of 1M $HNO_3$ was added to the sample to prepare stock solutions having ~300 dilution factor (Fig. 2.2). No residual grains were observed in stock solutions.

#### 2.4.1.2 $^{149}$Samarium spike

A samarium spike enriched with $^{149}Sm$ ($^{149}Sm/^{147}Sm$ = 316.7) was also added during the sample digestion (Table 2.6 and Fig. 2.2). The Sm spike solution was calibrated using Spex (USA) standard solution of Sm by reverse isotope dilution method. Using Sm isotope dilution data, the percent of recovery during sample preparation was corrected (Table 2.6). In this experiment, for all samples, percent of recovery was more than 96%. Samarium is a middle rare earth element. Chemical characteristic of rare earth elements are almost similar, though the chemical properties of REEs can change from light to heavy rare earth elements slightly. So in this experiment, the mid-rare earth element, Sm is used for recovery calculation. To do so, Sm was determined in samples both by isotope dilution

techniques as well as by internal calibration method. Isotope dilution technique is only depending on the isotopic ratio and is independent of recovery percentages, whereas internal calibration method is dependent on percent of recovery. So by comparing the data obtained from isotope dilution technique and internal calibration method, percent of recovery can be accurately corrected to obtain the accurate result for the other rare earth elements.

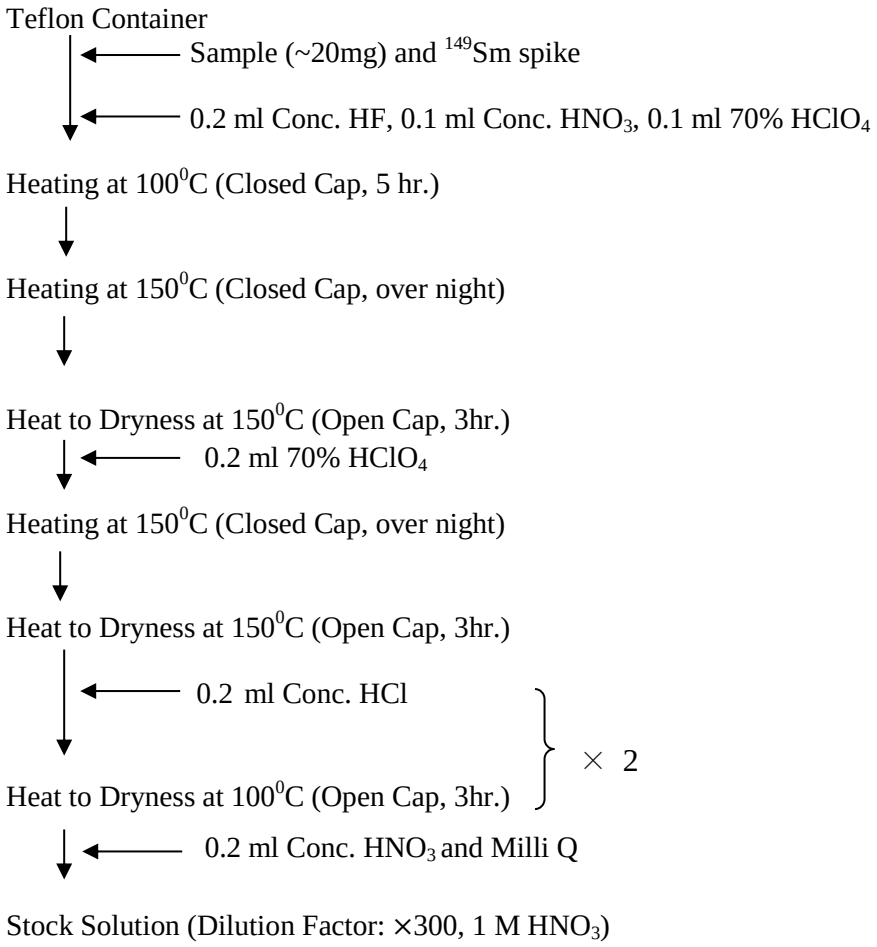


**Fig. 2.2** Acid Digestion procedure for REEs, Th and U determination.

### 2.4.1.3 Standards

For REEs, Th and U analyses, a custom multi-element standard stock solution from Spex, USA was used. To correct the signal drift in this study, In, Tl and Bi were used as internal standards. The linear interpolation correction between In and Tl was applied for REEs while only Bi was used for Th and U determinations.

**Table 2.6** Sample and $^{149}Sm$ Spike weight and the % of recovery in this study.

| Allende (22/6) | Sample [g] | $^{149}Sm$_Spike [g] | Recovery [%] |
|---|---|---|---|
| A1 | 0.02997 | 0.04910 | 99.2 |
| A2 | 0.02982 | 0.02758 | 97.8 |
| A3 | 0.03044 | 0.02713 | 96.7 |
| A4 | 0.02043 | 0.01839 | 99.3 |
| A5 | 0.02003 | 0.01846 | 99.2 |
| | | | |
| R-Chondrites | | | |
| PRE 95411.21 | 0.02026 | 0.01004 | 99.5 |
| ALH 85151.41 | 0.02009 | 0.00988 | 98.4 |
| Y 793575.44 | 0.02004 | 0.01012 | 98.4 |
| Y 983270.56 | 0.02000 | 0.01019 | 99.7 |
| A 881988.68 | 0.02031 | 0.01020 | 98.1 |
| MIL 07440.8 | 0.02049 | 0.01009 | 99.1 |
| LAP 03639.33 | 0.02009 | 0.01007 | 100 |
| Y 983720.81 | 0.02062 | 0.00998 | 99.6 |
| Y 983097.81 | 0.02066 | 0.01008 | 98.7 |
| LAP 04840.12 | 0.01956 | 0.01006 | 99.9 |
| MIL 11207.8 | 0.02027 | 0.01002 | 99.2 |
| Y 980702.61 | 0.01995 | 0.00995 | 98.6 |
| Y 980703.71 | 0.02005 | 0.01011 | 98.2 |
| LAP 02238.13 | 0.01951 | 0.01006 | 99.6 |
| PCA 91002.64 | 0.02002 | 0.01016 | 99.5 |

#### 2.4.1.4 Determination of REEs, Th and U

The concentrations of REEs, Th and U were determined by ICP-MS using a Plasma-Quad 3 spectrometer (Fisons Instruments, UK) following the procedure of Shinotsuka and Ebihara (1997) with small modification. The instrument was always optimized to obtain maximum count rates for In. Counts were taken for 5 voltage points on the peak top to provide a single mass peak intensity reading. Background corrections were made for the 5% $HNO_3$ carrier solution.

Four sets of interference correcting solutions, set-1 (only Ce), set-2 (Ba & Pr), set-3 (Sm, Tb & Gd) and set-4 (only Nd), were prepared for the correction of $^{135}Ba^{16}O^{+}$, $^{140}Ce^{16}O^{+}$, $^{140}Ce^{16}O^{1}H^{+}$, $^{141}Pr^{16}O^{+}$, $^{141}Pr^{16}O^{1}H^{+}$, $^{143}Nd^{16}O^{+}$, $^{147}Sm^{16}O^{+}$, $^{146}Nd^{16}O^{1}H^{+}$, $^{149}Sm^{16}O^{+}$, $^{156}Gd^{16}O^{+}$ and $^{159}Tb^{16}O^{+}$ species in measuring $^{151}Eu$, $^{156}Gd$, $^{157}Gd$, $^{158}Gd$, $^{159}Tb$, $^{163}Dy$, $^{165}Ho$, $^{172}Yb$ and $^{175}Lu$, respectively (Table 2.7). For REEs, Th and U determinations, about 1000 dilution factor was used.

**Table 2.7** Interference correction

| Nuclide | Interference from | [%] |
|---|---|---|
| $^{151}Eu$ | $^{135}Ba^{16}O^{+}$ | 0.32 |
| $^{156}Gd$ | $^{140}Ce^{16}O^{+}$ | 10.5 |
| $^{157}Gd$ | $^{140}Ce^{16}O^{1}H^{+}$, $^{141}Pr^{16}O^{+}$ | 2.74 |
| $^{158}Gd$ | $^{141}Pr^{16}O^{1}H^{+}$ | 0.05 |
| $^{159}Tb$ | $^{143}Nd^{16}O^{+}$ | 0.88 |
| $^{163}Dy$ | $^{147}Sm^{16}O^{+}$, $^{146}Nd^{16}O^{1}H^{+}$ | 0.09 |
| $^{165}Ho$ | $^{149}Sm^{16}O^{+}$ | 0.77 |
| $^{172}Yb$ | $^{156}Gd^{16}O^{+}$ | 0.38 |
| $^{175}Lu$ | $^{159}Tb^{16}O^{+}$ | 0.40 |

### 2.4.1.5 Accuracy and precision

Precision and accuracy of this study were checked by repeated analyses of Allende homogenized powders and comparing our data with literature data. In ICP-MS experiments five replicates of Smithsonian Allende samples have been analyzed from September to November 2013 in three segments. Results of ICP-MS experiments for Allende are shown in Table 2.8. Relative standard deviations (in %, 1σ, n=5) for all the elements are less than 2%, except those for U, Er & Tm. For U, relative standard deviation (RSD) is 4% while for Er & Tm RSDs are less than 3%. In Fig 2.3 we have compared our Allende data with the literature data (Pourmand et. al., 2012; Makishima & Nakamura, 2006; Shinotsuka et. al., 1995; Jarosewich et. al., 1987; Nakamura, 1974; Wakita & Schmitt, 1970; Tatsumoto et. al., 1973; Chai et. al., 2003; Dauphas & Pourmand, 2011) after normalizing those data to CI-mean value (Anders & Grevesse, 1989). All the Allende replicates are consistent with the literature data. In ICP-MS experiment, we monitored $^{139}La$, $^{140}Ce$, $^{141}Pr$, $^{143}Nd$, $^{146}Nd$, $^{147}Sm$, $^{149}Sm$, $^{151}Eu$, $^{153}Eu$, $^{156}Gd$, $^{157}Gd$, $^{158}Gd$, $^{159}Tb$, $^{163}Dy$, $^{165}Ho$, $^{167}Er$, $^{169}Tm$, $^{172}Yb$, $^{175}Lu$, $^{232}Th$ and $^{238}U$. Elemental abundances calculated by using different isotopes (e.g., $^{143}Nd$ & $^{146}Nd$) were in good agreement with each other. Interference from $^{135}Ba^{16}O^{+}$, $^{140}Ce^{16}O^{+}$, $^{140}Ce^{16}O^{1}H^{+}$, $^{141}Pr^{16}O^{+}$, $^{141}Pr^{16}O^{1}H^{+}$, $^{143}Nd^{16}O^{+}$, $^{147}Sm^{16}O^{+}$, $^{146}Nd^{16}O^{1}H^{+}$, $^{149}Sm^{16}O^{+}$, $^{156}Gd^{16}O^{+}$ and $^{159}Tb^{16}O^{+}$ in measuring $^{151}Eu$, $^{156}Gd$, $^{157}Gd$, $^{158}Gd$, $^{159}Tb$, $^{163}Dy$, $^{165}Ho$, $^{172}Yb$ and $^{175}Lu$, respectively, were corrected. Interference of $^{140}Ce^{16}O^{+}$ in measuring $^{156}Gd$ is ~11% and the combined interference of $^{140}Ce^{16}O^{1}H^{+}$ & $^{141}Pr^{16}O^{+}$ in measuring $^{157}Gd$ is ~3% while in all other cases, interference is less than 1%.

**Table 2.8** REE, Th and U abundances (in ppb) obtained by ICP-MS for the Allende powder and compared with literature values.

| | La | Ce | Pr | Nd | Sm | Eu | Gd | Tb | Dy | Ho | Er | Tm | Yb | Lu | Th | U |
|---|---|---|---|---|---|---|---|---|---|---|---|---|---|---|---|---|
| *This work* | | | | | | | | | | | | | | | | |
| A1 | 528 | 1334 | 200 | 1033 | 331 | 117 | 403 | 71.3 | 474 | 105 | 312 | 53.1 | 317 | 46.0 | 63.2 | 14.4 |
| A2 | 536 | 1323 | 204 | 1035 | 337 | 116 | 405 | 72.4 | 476 | 101 | 295 | 53.0 | 319 | 45.4 | 63.5 | 14.9 |
| A3 | 523 | 1316 | 201 | 1023 | 331 | 114 | 398 | 70.5 | 465 | 97.2 | 291 | 51.5 | 310 | 44.5 | 61.2 | 15.7 |
| A4 | 516 | 1352 | 205 | 1024 | 338 | 114 | 409 | 72.7 | 486 | 102 | 292 | 53.1 | 313 | 46.2 | 61.7 | 14.8 |
| A5 | 522 | 1317 | 198 | 1024 | 337 | 117 | 402 | 72.1 | 486 | 102 | 295 | 53.4 | 321 | 45.7 | 62.8 | 15.9 |
| *Mean* | *525* | *1328* | *202* | *1028* | *335* | *116* | *403* | *71.8* | *477* | *102* | *297* | *52.8* | *316* | *45.6* | *62.5* | *15.2* |
| *RSD*[a] | *1.4* | *1.1* | *1.5* | *0.5* | *1.0* | *1.0* | *1.0* | *1.2* | *1.8* | *2.7* | *3.0* | *1.4* | *1.4* | *1.5* | *1.6* | *4.0* |
| *Literature data* | | | | | | | | | | | | | | | | |
| TIMS (ID)[b] | 507 | 1325 | | 1004 | 330 | 113 | 414 | | 504 | | 303 | | 315 | 46.5 | 62.2 | 15.3 |
| ICP-MS[c] | 503 | 1260 | 197 | 997 | 318 | 108 | 394 | 69.0 | 466 | 95.0 | 288 | 49.6 | 311 | 45.6 | 61.0 | 15.4 |
| ICP-MS[d] | 534 | 1320 | 206 | 1060 | 338 | 111 | 411 | 73.5 | 491 | 106 | 284 | 51.8 | 317 | 45.1 | 55.1 | 15.4 |
| ICP-MS[e] | 547.7 | 1374 | 212.2 | 1087 | 345.6 | 118.3 | 446.8 | 80.7 | 544.3 | 108.8 | 316.5 | 55.1 | 328.3 | 46.0 | 58.64 | 15.54 |
| ICP-MS[f] | 516 | 1290 | 201 | 1020 | 329 | 114 | 417 | 76.2 | 508 | 107 | 310 | 55.9 | 325 | 45.9 | 59.4 | 15.2 |
| Compiled[g] | 520 | 1330 | 210 | 990 | 330 | 120 | 430 | 81 | 430 | 100 | 300 | | 290 | 51 | | |

[a]Relative standard deviation (1σ; %).
[b]ID: isotope dilution. Nakamura (1974) for REEs. Tatsumoto et al. (1973) for Th and U.
[c]Shinotsuka et al. (1995)
[d]Makishima and Nakamura (2006)
[e]Pourmand et al. (2012) for REEs. Dauphas and Pourmand (2011) for Th and U by ID-ICP-MS.
[f]Barrat et al. (2012)
[g]Mean values of Jarosewich et al. (1987). Two-digit numbers are listed as significant figures for REEs except Ce, for which a three-digit number is given.

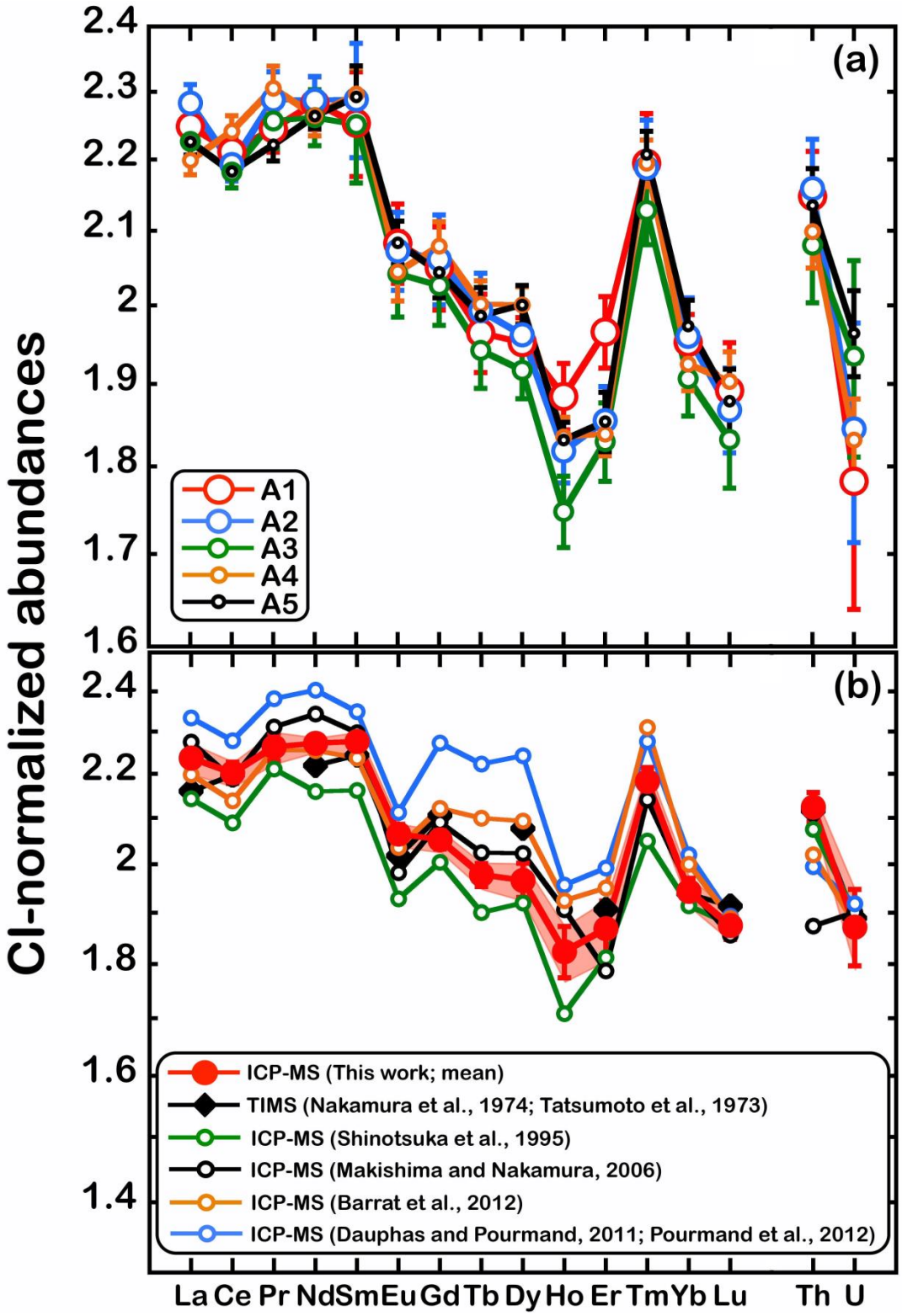


**Fig. 2.3** CI- (Anders & Grevesse, 1989) normalized REEs, Th and U abundance patterns in Allende (of this study) are shown at the top while in the bottom the average REEs, Th and U abundances (thick red line) with 1σ uncertainty (shadow) are compared with the literature values.

### 2.4.2 Isotope dilution techniques (Zn, Cd, In, Tl and Pb determination)

Isotope dilution (ID) is an analytical method suitable to obtain reliable data for elemental abundances. But, for monoisotopic elements (e.g., Bi, Pr, Tb, Ho, Tm) ID-technique cannot be applied. In ID experiment, spike is added to the sample. Spike possesses a different isotopic composition compared with that of sample. For instance, natural isotopic composition of In is $^{113}$In : $^{115}$In = 4.29 : 95.71(Berglund and Wieser, 2011) whereas spike isotopic composition of In is $^{113}$In : $^{115}$In = 93.41 : 6.59.

Quantitative determination of concentration is based on the measurement of isotopic ratio of elements in the sample-spike mixture (e.g., Watters et al., 2003). Measuring isotope ratios has the advantage that it is robust according to a variety of instrument operation settings. A changing sensitivity of the detector system with time and spikes that occur when large droplet of analyte get injected into the plasma both affect the total ion counts during one analysis. Since these parameters influence the measurements of different isotopes and elements (e.g., Pb and Bi) in nearly the same way, the reproducibility of count measurements can be improved when isotope and element ratio (e.g., Pb and Bi) are calculated (Willbold et al., 2003). Once the isotopic compositions of spike and sample attain the equilibrium, isotopic ratio in sample-spike mixture does not change significantly at different stages of analytical procedure (e. g., solvent extraction, column chromatography etc.). So, the use of ID technique can eliminate the recovery problem which is more common for external calibration technique (Van Heuzen et al. 1989).

Following the error propagation law, any statistical error in the isotope ratio measurement is increased by an ‘ error magnification factor ’. This factor depends on the measured isotopic ratio of the sample/spike mixture. Accordingly, an optimum value for the measured isotopic ratio ($R_{opt}$) has to be obtained to keep the error magnification factor as low as possible. So, before adding spike solution to a sample, an optimum sample/spike ratio must be obtained associated with the $R_{opt}$. $R_{opt}$ can be obtained from the following equation [1]-

$$R_{opt} = \sqrt{\frac{A_n A_s}{B_n B_s}} \qquad \text{.....[1]}$$

Where,

$A_n$, $B_n$ = Natural abundances of isotope A and B

$A_s$, $B_s$ = Spike abundances of isotope A and B

By using the optimum spike ratio $R_{opt}$ from equation [1], the amount of spike solution ($M_s$) added to a sample can be calculated by equation [2]-

$$M_s = \frac{\frac{XM_n}{Aw_n}(A_n - R_{opt}B_n)}{\frac{Y}{Aw_s}(B_sR_{opt} - A_s)} \quad \text{.....[2]}$$

Where,

| | | |
|---|---|---|
| X | = | Elemental concentration of sample (initially assumed) |
| Y | = | Elemental concentration of calibrated spike |
| $M_n$ | = | Weight of the sample |
| $Aw_n$ | = | Elemental atomic weight in sample |
| $Aw_s$ | = | Elemental atomic weight in spike |

Following equation [2], a specific amount of spike ($M_s$) is added to the sample. In this study, spike was added to the samples before dissolution procedure started. Then elemental abundances are calculated from the measured isotopic ratio ($R_m$) of sample-spike mixture by ICP-MS, following equation [3] –

$$R_m = \frac{Counts\ per\ second_{(isotope\ A)}}{Counts\ per\ second_{(isotope\ B)}} = \frac{\frac{A_nXM_n}{Aw_n} + \frac{A_sYM_s}{Aw_s}}{\frac{B_nXM_n}{Aw_n} + \frac{B_sYM_s}{Aw_s}} \quad \text{.....[3]}$$

$$\text{or,} \quad X = \frac{\frac{YM_s}{Aw_s}(A_s - R_mB_s)}{\frac{M_n}{Aw_n}(R_mB_n - A_n)} \quad \text{.....[4]}$$

The accuracy of the determined elemental concentration depends on the accuracy of the determined isotopic ratio (e. g., $^{113}$In : $^{115}$In) or elemental ratio (e. g., $^{208}$Pb : $^{209}$Bi). In ICP-MS measurement light ions are more deflected compared with those of heavy ions due to the mutual repulsion in the ion beam and caused the mass fractionation (MF) in determining the isotopic and (or) elemental ratios (Heumann et al., 1998). Thus, MF is an important factor for the accurate determination of isotopic ratios and their application to ID technique. Tentatively, the MF can be expressed as (Heumann et al., 1998),-

$$\text{MF}\ [amu^{-1}] = \left[\frac{R_{true}}{R_m} - 1\right] \times \frac{1}{\Delta m_{A,\ B}} \qquad \text{.....[4]}$$

Where $R_{true}$ is the true ratio of two isotopes A and B on one element obtained from tabulated isotopic composition of elements (Berglund and Wieser, 2011), $R_m$ is the measured isotopic ratio by ICP-MS and $\Delta m_{A,\ B}$ is the mass difference between both isotopes in amu. Generally, in-run mass fractionations are corrected by using normalizing isotopic ratios with constant natural abundances or certified isotopic abundances (e. g., Pb isotopic abundances). Mass fractionations of this study have been corrected by using Spex solution for Zn, Cd, In, Tl and Sm. But, for Pb, NIST SRM981 was used for correcting the mass fractionation. Natural isotopic abundances for Zn, Cd, In, Tl and Sm, were taken from Berglund and Wieser (2011) and for Pb isotopic abundances were taken from NIST certificate for SRM981. Isotopic abundances and the atomic weights used in this study are listed in Table 2.9 and 2.10.

**Table 2.9** Isotopic compositions of Pb in Pb standards, spike, Allende and JB2.

| | Isotopic abundances (%) | | | | Atomic weight |
|---|---|---|---|---|---|
| | $^{204}$Pb | $^{206}$Pb | $^{207}$Pb | $^{208}$Pb | |
| NIST SRM981[a] | 1.4255 | 24.1442 | 22.0833 | 52.3470 | 207.2393 |
| Spex[b] | 1.348 | 25.28 | 21.07 | 52.30 | 207.2256 |
| Spike[b] | 0.008 | 2.102 | 92.48 | 5.410 | 207.0328 |
| Allende[c] | 1.816 | 20.435 | 20.800 | 56.949 | 207.3107 |
| JB2[d] | 1.3664 | 25.065 | 21.2641 | 52.3045 | 207.2314 |

[a]NIST certificate (1973)
[b]Cosmochemistry laboratory, TMU data (2014)
[c]Tatsumoto et al. (1973)
[d]Baker et al. (2004)

**Table 2.10** Isotopic compositions of Zn, Cd, In and Tl in nature and in Spikes.

| | | Natural | | Spike | |
|---|---|---|---|---|---|
| | | Isotopic abundance (%)[a] | Atomic weight | Isotopic abundance (%) | Atomic weight |
| Zn | $^{64}$Zn | 49.1704 | 65.45065 | 1.43 | 66.97145 |
| | $^{66}$Zn | 27.731 | | 3.77 | |
| | $^{67}$Zn | 4.0401 | | 89.63 | |
| | $^{68}$Zn | 18.4483 | | 5.1 | |
| | $^{70}$Zn | 0.6106 | | 0.06 | |
| Cd | $^{106}$Cd | 1.25 | 112.508 | <0.01 | 111.0137 |
| | $^{108}$Cd | 0.89 | | <0.01 | |
| | $^{110}$Cd | 12.49 | | 0.34 | |
| | $^{111}$Cd | 12.80 | | 96.11 | |
| | $^{112}$Cd | 24.13 | | 2.02 | |
| | $^{113}$Cd | 12.22 | | 0.5 | |
| | $^{114}$Cd | 28.73 | | 0.91 | |
| | $^{116}$Cd | 7.49 | | 0.08 | |
| In | $^{113}$In | 4.29 | 114.9142 | 93.41 | 113.1318 |
| | $^{115}$In | 95.71 | | 6.59 | |
| Tl | $^{203}$Tl | 29.524 | 204.410 | 98.15 | 203.037 |
| | $^{205}$Tl | 70.476 | | 1.85 | |

[a]Berglund and Wieser (2011)

### 2.4.2.1 Sample preparation

R chondrites and Allende samples were weighed (~100 mg) and mixed together with the $^{67}$Zn, $^{113}$In, $^{111}$Cd, $^{203}$Tl and $^{207}$Pb spikes in a 10ml Savillex Teflon PFA screw cap container. $^{67}$Zn, $^{113}$In, $^{203}$Tl and $^{207}$Pb spikes were added as a composite spike whereas $^{111}$Cd spike was added separately. After adding 0.2ml con. $HNO_3$, 0.2ml con. $HClO_4$ and 0.4ml con. HF to the samples, the tightly capped containers were put on a hot plate for 24 hours for digestion. The samples were dried stepwise after Yokoyama et al. (1999) to decompose fluorides. To make sure that the fluorides were decomposed, 0.2ml of con. $HClO_4$ was further added and dried. After this, 0.2ml of 6M HCl was added and the digested sample was dried to decompose any remaining fluorides (Makishima et al., 2010). Addition of 6M HCl and drying up cycle was repeated three times. Then 10ml stock solution-1 was prepared in 3M $HNO_3$ having dilution factor of ~100. From this stock solution-1, Pb and Bi measurement solution was prepared (dilution factor: ~1000) in 1M $HNO_3$.

Stock solution-1 was dried. Addition of 6M HCl and drying up cycle was repeated three times. 6ml of 6M HCl and few drops of $H_2O_2$ (for the conversion of $Fe^{2+}$ to $Fe^{3+}$) were added to the digested residue and heat at 120°C with closed cap, overnight. This solution was cooled gently to prepare stock solution-2. Stock solution-2 will be used for solvent extraction (for Tl determination) and ion-exchange column chromatography (for Zn, In and Cd determination).

For solvent extraction, stock solution-2 and 10 ml of diisopropyl ether were put into a quick-fit separating funnel and shack for 15 minutes by a shaker. Organic phase (diisopropyl ether) was then separated from the aqueous phase. In the aqueous phase, again 10 ml of diisopropyl ether was added and after shacking, organic phase was separated. This solvent extraction processes were performed 3 to 4 times. Thallium is partitioned into the organic phase along with iron. This iron was then back extracted by successive addition and removal of 1M HBr. The organic phase was evaporated to dry out. The measurement solution for Tl was prepared in 1M $HNO_3$.

Aqueous phase was then dried out and the digested sample was redissolved in 3M HCl. This sample solution was loaded onto an anion-exchange resin (Dowex® 1 × 8, Cl form) column (column volume, C.V. = 2ml). The column was previously equilibrated with 3M HCl. 6C.V. of 3M HCl were eluted through the column for separating the matrix. Zinc and In were separated by eluting 18 C.V. of 0.06M HCl while Cd was separated by 1M $HNO_3$. All the measurement solutions were prepared in 1M $HNO_3$. Dilution factors for preparing the measurement solution are given in Table 2.11.

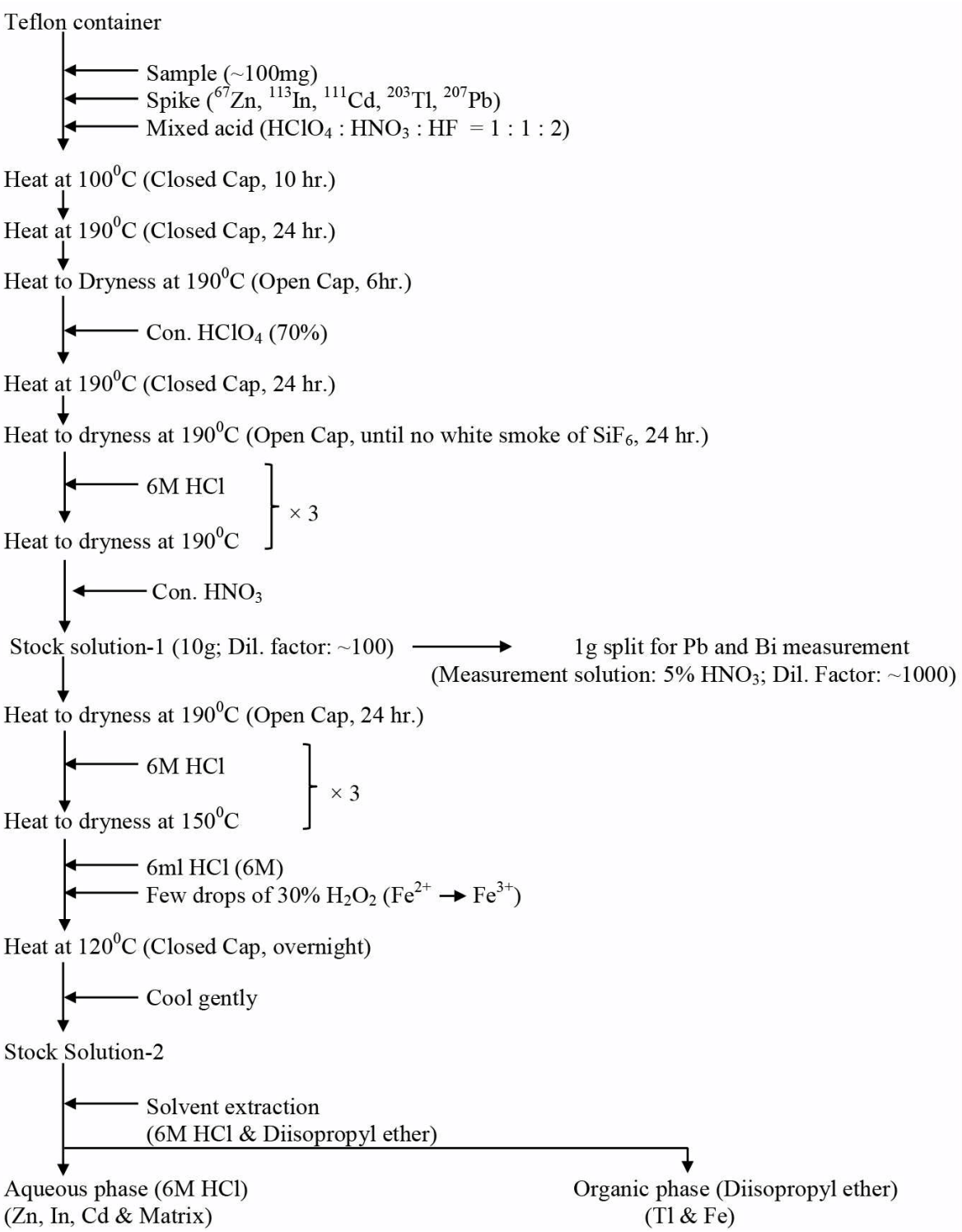
Teflon container
Sample (~100mg)
Spike ($^{67}Zn$, $^{113}In$, $^{111}Cd$, $^{203}Tl$, $^{207}Pb$)
Mixed acid ($HClO_4$ : $HNO_3$ : HF = 1 : 1 : 2)
Heat at 100$^0$C (Closed Cap, 10 hr.)
Heat at 190$^0$C (Closed Cap, 24 hr.)
Heat to Dryness at 190$^0$C (Open Cap, 6hr.)
Con. $HClO_4$ (70%)
Heat at 190$^0$C (Closed Cap, 24 hr.)
Heat to dryness at 190$^0$C (Open Cap, until no white smoke of $SiF_6$, 24 hr.)
6M HCl
× 3
Heat to dryness at 190$^0$C
Con. $HNO_3$
Stock solution-1 (10g; Dil. factor: ~100)
1g split for Pb and Bi measurement
(Measurement solution: 5% $HNO_3$; Dil. Factor: ~1000)
Heat to dryness at 190$^0$C (Open Cap, 24 hr.)
6M HCl
× 3
Heat to dryness at 150$^0$C
6ml HCl (6M)
Few drops of 30% $H_2O_2$ ($Fe^{2+}$ → $Fe^{3+}$)
Heat at 120$^0$C (Closed Cap, overnight)
Cool gently
Stock Solution-2
Solvent extraction
(6M HCl & Diisopropyl ether)
Aqueous phase (6M HCl)
(Zn, In, Cd & Matrix)
Organic phase (Diisopropyl ether)
(Tl & Fe)

*(Continue)*

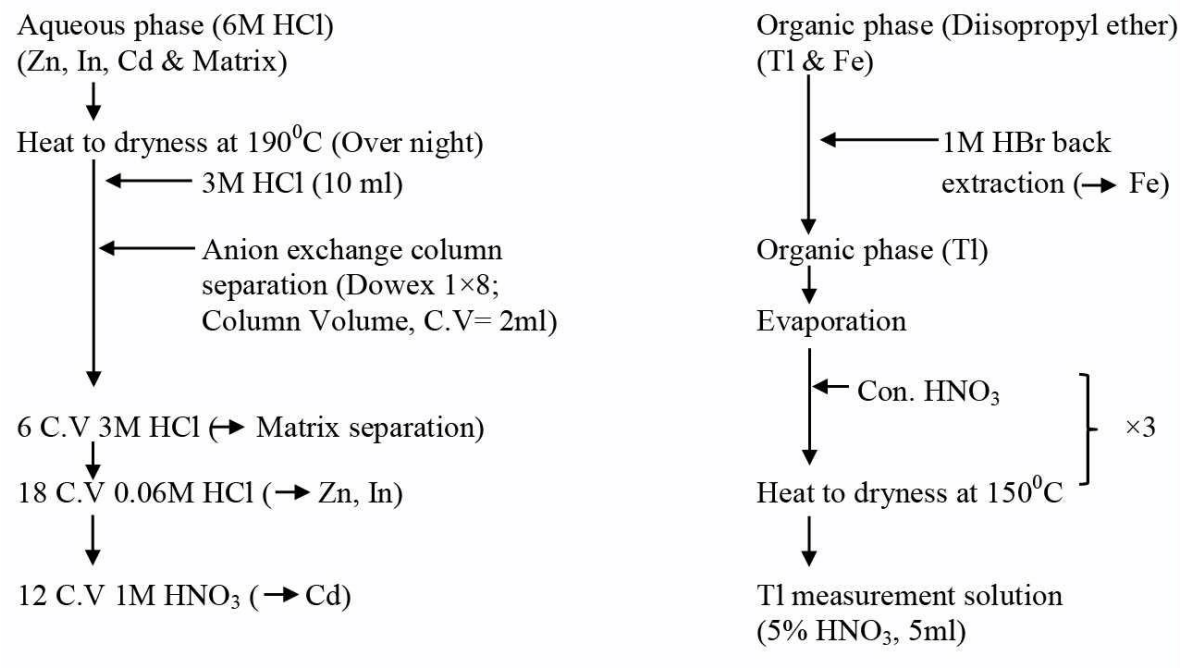


**Fig. 2.4** Procedure for the determination of Zn, Pb, Cd, Bi, Tl and In.

**Table 2.11** Dilution factors for preparing measurement solution.

| Measurement solution for | Dilution factor |
|---|---|
| Pb and Bi | 1000 |
| Zn | 10,000 |
| In | 50 |
| Cd | 100 |
| Tl | 25 |

### 2.4.2.2 Spikes

For isotope dilution analyses, $^{67}$Zn, $^{113}$In, $^{111}$Cd, $^{203}$Tl and $^{207}$Pb enriched isotopes were used. Before adding spike solution to a sample, an optimum isotopic ratio must be calculated in order to reduce the error magnification factor. To minimize the preparation time, composite spike for Zn, In, Tl and Pb was prepared whereas Cd spike was added separately. Cadmium spike was separated from the composite spike, because $^{113}$Cd has an isobaric interference on $^{113}$In. In the same way, two sets of spikes were also prepared for procedure blank. Calibration of spike was done by using standard stock solution from Spex, USA (by reverse isotope dilution method). Spikes concentrations are given in Table 2.12.

**Table 2.12** Calibration of composite spikes.

| | Composite Spike for R-chondrites_SI#24: | | |
|---|---|---|---|
| | n=3 | SD | RSD |
| Zn_ppm: | **110.2** | 0.5 | 0.5 |
| In_ppb: | **96.30** | 0.10 | 0.1 |
| Tl_ppb: | **161.3** | 0.6 | 0.4 |
| Pb_ppm: | **2.343** | 0.004 | 0.2 |

| | Composite Spike for Blank_SI#25: | | |
|---|---|---|---|
| | n=3 | SD | RSD |
| Zn_ppm: | **0.986** | 0.008 | 0.8 |
| In_ppb: | **2.49** | 0.01 | 0.4 |
| Tl_ppb: | **4.05** | 0.02 | 0.5 |
| Pb_ppb: | **18.85** | 0.04 | 0.2 |

| | Cd_spike for R chondrites: SI#17-2 | | |
|---|---|---|---|
| | n=3 | SD | RSD |
| Cd_ppb: | **611.0** | 1.1 | 0.2 |

| | Cd_spike for blank: SI#17-3 | | |
|---|---|---|---|
| | n=3 | SD | RSD |
| Cd_ppb: | **1.72** | 0.01 | 0.9 |

### 2.4.2.3 Sample information

Sample and Spike weights used in this experiment are shown in Table 2.13. Along with the Allende and R chondrites, seven sets of blank samples have also been prepared for blank correction.

**Table 2.13** Sample and spikes weight

| Name | Sample_[g] | Comp. Spike_[g] | Cd_Spike_[g] |
|---|---|---|---|
| Allende (22/6) | | | |
| A1 | 0.09950 | 0.07375 | 0.07634 |
| A2 | 0.10040 | 0.07418 | 0.07652 |
| A3 | 0.10411 | 0.07430 | 0.04030 |
| A4 | 0.09990 | 0.07434 | 0.04038 |
| | | | |
| R chondrites | | | |
| PRE 95411.21 (R3) | 0.10139 | 0.07398 | 0.07636 |
| ALH 85151.41 (R3.6) | 0.10106 | 0.07404 | 0.07631 |
| Y 793575.44 (R3.8) | 0.10212 | 0.07291 | 0.07518 |
| Y 983270.56 (R4) | 0.10236 | 0.07408 | 0.07641 |
| A 881988.68 (R4) | 0.10058 | 0.07406 | 0.07525 |
| MIL 07440.8 (R4) | 0.10262 | 0.07408 | 0.07637 |
| LAP 03639.33 (R4) | 0.10105 | 0.07418 | 0.07632 |
| Y 983720.81 (R4) | 0.10072 | 0.07390 | 0.07633 |
| Y 983097.81 (R4) | 0.10195 | 0.07479 | 0.04040 |
| LAP 04840.12 (R6) | 0.10320 | 0.07445 | 0.04048 |
| MIL 11207.8 (R6) | 0.10098 | 0.07440 | 0.03853 |
| Y 980702.61 (R6) | 0.10017 | 0.07449 | 0.04280 |
| Y 980703.71 (R6) | 0.10071 | 0.07464 | 0.04045 |
| LAP 02238.13 (R) | 0.10074 | 0.07461 | 0.04057 |
| PCA 91002.64 (R3.8-6) | 0.10052 | 0.07426 | 0.04067 |

#### 2.4.2.4 Determination of volatile elements (Zn, Pb, Bi, Tl, In and Cd)

Lead abundances in R chondrites as well as in Allende were determined by isotope dilution technique. Being a mono-isotopic element, Bi cannot be analyzed by using isotope dilution technique. Using $^{208}Pb/^{209}Bi$ ratio, Bi was determined with a comparable accuracy of isotope dilution technique. Zinc, Cd, In and Tl were determined by solvent extraction followed by column chromatography. Interference of $^{132}Ba^{2+}$, $^{134}Ba^{2+}$ and $^{136}Ba^{2+}$ were corrected for $^{66}Zn$, $^{67}Zn$ and $^{68}Zn$ isotopes, respectively. Isobaric interferences of $^{110}Pd$ and $^{112}Sn$ and the oxide interferences of $^{94}Zr^{16}O^{+}$, $^{94}Mo^{16}O^{+}$, $^{95}Mo^{16}O^{+}$, $^{96}Zr^{16}O^{+}$ and $^{96}Mo^{16}O^{+}$ were corrected for Cd determination. For In determination isobaric interference from $^{113}Cd$ was corrected.

#### 2.4.2.5 Accuracy and precision

Precision and accuracy of this study were checked by repeated analysis of Smithsonian Allende homogenized powder (USNM 3529, split/position: 22/6) and JB2 (basalt standard provided by Geological Survey of Japan) and comparing our data with the literature data. In this study four replicates of Smithsonian Allende sample have been analyzed for all volatile elements (Zn, Pb, Bi, Tl, In and Cd). But for Pb and Bi, additional three replicate measurements have been performed. Replicate measurements of JB2 (basalt standard provided by Geological Survey of Japan) were also performed for ensuring the data quality as well as for the method validation.

*Lead and Bismuth*

Lead and Bi abundances in Allende are shown in Table 2.12a. For the determination of Pb abundances, Pb isotopic composition of Allende (from Tatsumoto et al., 1973) is used. The precision of this study is around 3% (1σ). We monitored $^{204}Pb$, $^{206}Pb$, $^{207}Pb$ and $^{208}Pb$ and Pb abundances in Allende were calculated from $^{204}Pb/^{207}Pb$, $^{206}Pb/^{207}Pb$ and $^{208}Pb/^{207}Pb$ ratios which were found to be internally consistent. Accuracy of our experiment has been checked by comparing our data with those of literature data (Table 2.17 and 2.18). There is a range of Pb abundance data for Allende meteorite:

(1) Using external calibration method, Makishima and Nakamura (1997) determined Pb in four replicates of Smithsonian Allende powder. They used standard bracketing method for each solution where Spex solution was used as standard and only $^{208}Pb$ isotope

was monitored in their study. Their determined Pb abundance is 1.69 ± 0.16 ppm (RSD: 9.1%, n = 4).

(2) Makishima and Nakamura (2006) analyzed Pb abundance in Smithsonian Allende powder using Spex standard. They used $^{149}$Sm as internal standard and monitored only $^{208}$Pb. Their determined Pb abundances are 1.08 and 1.09 ppm in a duplicate measurement of Allende powder which were about 35% lower than their previously (Makishima and Nakamura, 1997) reported value.

(3) Barrat et al. (2012) analyzed Pb abundances in six replicates of Smithsonian Allende powder (USNM 3529, split/position: 14/2, 14/22 and 15/3) using BHVO2 as standard. They used $^{169}$Tm as internal standard and monitored only $^{208}$Pb. Their determined Pb abundance is 1.27 ± 0.05 ppm (RSD: 4.1%, n = 6).

(4) Strack et al. (2012) analyzed a 30g chunk sample of Allende meteorite using isotope dilution method. They monitored only $^{207/208}$Pb following the procedure of Willbold et al. (2003). Their Pb abundance is 1.52 ± 0.26 ppm (17.3%, n = 39).

In external calibration techniques, terrestrial standards (e.g., Spex and BHVO2) were used whose Pb isotopic composition is different than those of cosmochemical samples (here Allende). For instance, $^{208}$Pb abundance in BHVO2 is 52.08% (Baker et al. 2004) whereas $^{208}$Pb abundance in Allende is 56.95% (Tatsumoto et al., 2007). So the slope of the calibration line using terrestrial standards will be lower than that of cosmochemical samples and may provide an erroneous data for Pb.

On the other hand, isotope dilution technique is free from the slope of calibration line. But we need to use an appropriate Pb isotopic composition to determine the Pb abundances in cosmochemical samples. Tatsumoto et al. (1973) determined the Pb isotopic composition as well as the Pb abundance (by MS-ID) in Allende sample. Their obtained value is 1097 ppb Pb in Smithsonian Allende powder. They used four significant figures in reporting the Pb abundance, which imply that their precision was much better than those of other literature data (mentioned in Table 2.18). So, in Fig. 2.6, Pb abundances in Allende meteorite of this study as well as the previous literature data are normalized to Tatsumoto et al. (1973) data. Except A4, all data of our experiment are in good agreement with Tatsumoto et al. (1973). Nevertheless, Allende powder is known to be heterogeneous for Pb (Barrat et al., 2012) and our data is within the range of Jarosewich et al. (1987).

In Bi determination, we used Pb/Bi ratio. For calibrating the Pb/Bi line, Spex solution was used. But Spex and Allende have different Pb isotopic composition. So their

corresponding calibration lines will have different slopes as shown schematically in Fig. 2.5. As the isotopic abundance of $^{209}$Bi is 100%, the slope of the calibration line is solely dependent on the isotopic abundance of $^{208}$Pb. To eliminate the problem regarding isotopic variation, our experimental counts per second (cps) were normalized by the corresponding isotopic abundances both for the Spex and Allende samples. The reproducibility for Bi determination is 7.8% and the Bi abundances in Allende meteorites are in good agreement with those of literature data (Chicago mean).

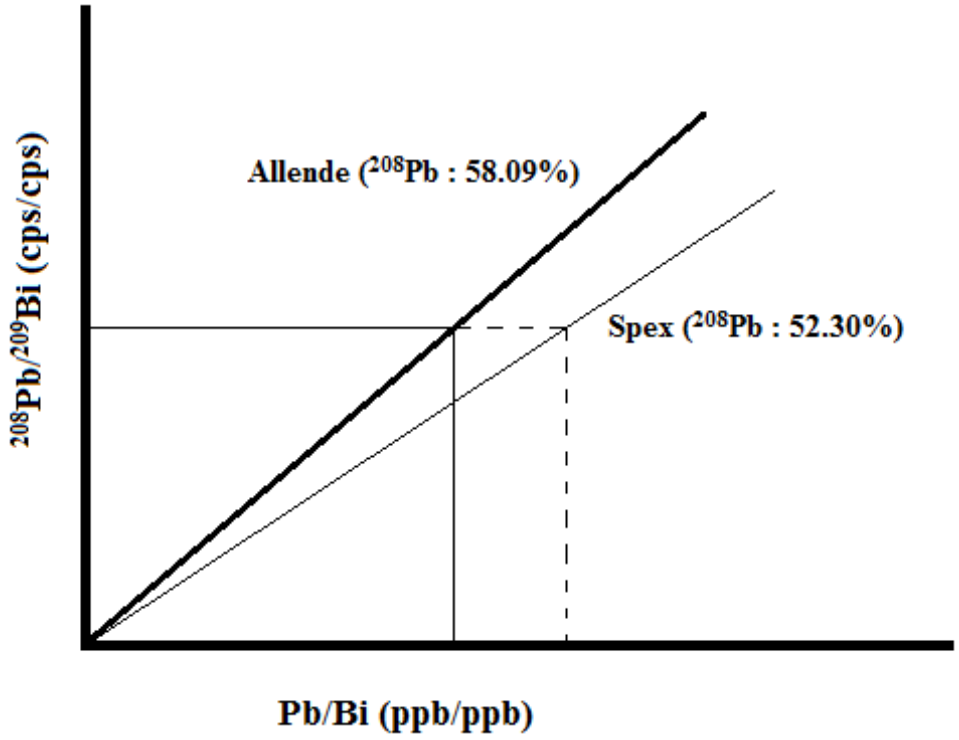


**Fig. 2.5** Schematic calibration lines for Spex and Allende showing the effect of isotopic variation on the slope of calibration line.

Other than the cosmochemical standard (here Allende), in this study six replicates of JB2 (basalt standard provided by Geological Survey of Japan) were also analyzed for Pb and Bi. Lead-isotopic composition from Baker et al. (2004) for JB2 was used for Pb determination by MS-ID. Lead and Bi abundances in JB2 are summarized in Table 2.19. Lead and Bi abundances in JB2 are in good agreement with those of literature data (Imai et al.,1995; Makishima et al., 1997; Jochum and Jenner, 1994 and Makishima and Nakamura, 2006).

*Zinc*

Spectral interference is a major concern in measuring accurate isotopic ratios in mass spectrometry. There are several sources of spectral interferences; isobaric ions, multi-charged cations of single atoms and molecular ions. The first two interferences can be easily eliminated by chemical separation of corresponding interfering elements. The contribution of molecular ions can also be decreased by separating co-existing elements, especially, in thermal ionization mass spectrometry. In ICP-MS, however, such a contribution doesn't change significantly even with the separation of matrix elements, because most molecular ions are contributed from ambient gases (Ar and air) and solvents, and these ions are unavoidably introduced into the ICP-MS instrument. Table 2.14 summarizes Zn isotopes and their possible spectral interferences. In the isotopic measurement of Zn, $^{64}$Zn and $^{70}$Zn have isobaric interferences of $^{64}$Ni and $^{70}$Ge, respectively, and, hence, the remaining three isotopes ($^{66}$Zn, $^{67}$Zn and $^{68}$Zn) were monitored for isotope dilution calculation. These three isotopes of Zn, however, may sustain interferences of double-charged Ba isotopes, $^{132}$Ba, $^{134}$Ba and $^{136}$Ba, respectively. In the matrix separation ICP-MS, these interferences can be eliminated by chemical separation. In ICP-MS without matrix-separation, their contributions were corrected by measuring both Ba and Zn standard solutions. As $^{136}$Ba has higher isotope abundances than those of $^{132}$Ba and $^{134}$Ba, $^{136}Ba^{+}$ was monitored together with $Zn^{+}$ in order to correct interferences of $Ba^{2+}$. The correction was carried out by applying mathematical equations to the analytical results of the Ba standard solution. In this calculation, mass fractionation of Zn and Ba were always considered. Zinc contents were determined by using $^{66}$Zn/$^{67}$Zn and $^{67}$Zn/$^{68}$Zn ratios in isotope dilution calculation.

**Table 2.14** Relative isotope abundances of Zn and possible mass interferences.

| Zn isotope | Possible mass interferences |
|---|---|
| 64 | $^{48}Ca^{16}O^{+}$, $^{48}Ti^{16}O^{+}$, $^{24}Mg^{40}Ar^{+}$, $^{50}Ti^{14}N^{+}$, $^{50}V^{14}N^{+}$, $^{50}Cr^{14}N^{+}$, $^{52}Cr^{12}C^{+}$, $^{64}Ni^{+}$ |
| 66 | $^{50}Ti^{16}O^{+}$, $^{50}V^{16}O^{+}$, $^{50}Cr^{16}O^{+}$, $^{26}Mg^{40}Ar^{+}$, $^{52}Cr^{14}N^{+}$, $^{54}Cr^{12}C^{+}$, $^{54}Fe^{12}C^{+}$, $^{132}Ba^{2+}$ |
| 67 | $^{51}V^{16}O^{+}$, $^{27}Al^{40}Ar^{+}$, $^{53}Cr^{14}N^{+}$, $^{55}Mn^{12}C^{+}$, $^{134}Ba^{2+}$ |
| 68 | $^{52}Cr^{16}O^{+}$, $^{54}Cr^{14}N^{+}$, $^{54}Fe^{14}N^{+}$, $^{56}Fe^{12}C^{+}$, $^{136}Ba^{2+}$, $^{136}Ce^{2+}$ |
| 70 | $^{54}Cr^{16}O^{+}$, $^{54}Fe^{16}O^{+}$, $^{56}Fe^{14}N^{+}$, $^{58}Fe^{12}C^{+}$, $^{58}Ni^{12}C^{+}$, $^{70}Ge^{+}$ |

Table 2.15 and 2.16 summarize analytical results of the two reference samples (JB2 and Allende) for Zn by ICP-MS with chemical separation of matrix elements. Literature values are shown for comparison. Individual Zn values were determined within 1% as relative standard deviation (1σ) for twenty times repeated measurements for one experimental run. Replicate analyses also gave highly reproducible values as well as the Zn values calculated by using $^{66}Zn/^{67}Zn$ and $^{68}Zn/^{67}Zn$ ratios are internally consistent. Our Zn values are in excellent agreement with literature values for the two reference samples (JB2 and Allende), implying that the data obtained are accurate as well as precise. This further proves that the chemical procedure used is effective in reducing possible interferences. It also became obvious that molecular ions from ambient gas and solvent didn't affect Zn values under the experimental condition of this study.

**Table 2.15** Zinc abundance in JB2.

| | Zn (ppm) | | | |
|---|---|---|---|---|
| | Without matrix separation | | Matrix separation | |
| | $^{66}Zn/^{67}Zn$ | $^{68}Zn/^{67}Zn$ | $^{66}Zn/^{67}Zn$ | $^{68}Zn/^{67}Zn$ |
| This work | | | | |
| JB2-1 | 107 ± 1 | 127 ± 2 | 105 ± 1 | 104 ± 1 |
| JB2-2 | 106 ± 1 | 130 ± 2 | 107 ± 1 | 106 ± 1 |
| JB2-3 | 108 ± 2 | 118 ± 3 | 105 ± 1 | 104 ± 1 |
| JB2-4 | 112 ± 1 | 137 ± 2 | | |
| JB2-5 | 120 ± 1 | 135 ± 2 | | |
| JB2-6 | 109 ± 1 | 137 ± 3 | | |
| Average : | **110** | **131** | **106** | **105** |
| SD : | 5 | 7 | 1 | 1 |
| RSD [%] : | 5 | 6 | 1 | 1 |
| Literature data | | | | |
| Imai et al. (1995) | | 108 | | |
| Makishima and Nakamura (2006) | | 107 ± 10 | | |

Zinc was also determined by ICP-MS without matrix separation for the two reference samples (JB2 and Allende). Two different analytical modes (STD mode and KED mode) were applied for Allende sample. Analytical results are summarized in Table 2.15 and 2.16. Literature data and mean values of matrix-separation ICP-MS data (Table 2.15 and 2.16) also are given for comparison.

**Table 2.16** Zinc abundance in Allende.

| | Zn (ppm): Without matrix separation | | | |
|---|---|---|---|---|
| | STD mood | | KED mood | |
| | $^{66}Zn/^{67}Zn$ | $^{68}Zn/^{67}Zn$ | $^{66}Zn/^{67}Zn$ | $^{68}Zn/^{67}Zn$ |
| This work | | | | |
| Allende | 121 ± 1 | 120 ± 1 | 127 ± 3 | 125 ± 2 |
| Allende | 118 ± 1 | 117 ± 1 | 123 ± 2 | 122 ± 2 |
| Allende* | 186 ± 2 | 185 ± 2 | 196 ± 5 | 193 ± 4 |
| Average : | **120** | **119** | **125** | **124** |
| Uncertainty : | 1 | 1 | 2 | 1 |
| Uncertainty [%] : | 0.8 | 0.8 | 1.6 | 0.8 |
| | | | | |
| Literature data | Table 2.13 | | | |

*Excluded from the mean

For Allende (Table 2.16) good agreement can be seen in Zn data between $^{66}Zn/^{67}Zn$-based values and $^{68}Zn/^{67}Zn$-based values in STD mode and their values are in excellent agreement with a literature value as well as mean values of matrix-separation ICP-MS (Table 2.13), which clearly implies that neither double-charged Ba ions nor molecular ions affect Zn values for Allende. As a trial, the $Ba^{2+}$ contribution was considered in calculating KED mode data. As seen in Table 2.16, Zn values by KED mode are a little higher than those from STD mode, but both data are mostly consistent with each other. Because a Ba/Zn content ratio in Allende (0.043) (Jarosewich et al., 1987) is low, the correction for $Ba^{2+}$ was found to be less than 1% in both KED and STD modes.

Between the two reference samples (JB2 and Allende) analyzed in this study, Ba/Zn ratios for JB-2 (2.1) (Imai et al., 1995) is much higher than that for Allende (0.043) (Jarosewich et al., 1987). Geological rock samples like JB-2, generally have higher Ba/Zn content ratios than chondritic meteorites like Allende. Therefore, the correction of $Ba^{2+}$ may become necessary for the determination of Zn for such geological samples. For JB-2, either $Ba^{2+}$- uncorrected Zn data are shown in Table 2.15. For JB-2, without the correction for $Ba^{2+}$, Zn values obtained by $^{68}Zn/^{67}Zn$ ratio are systematically larger (by 30%) than the literature value (and matrix-separation values) by both STD and KED mode measurements. Being different from the case for $^{68}Zn/^{67}Zn$ ratio, Zn values obtained by $^{66}Zn/^{67}Zn$ ratio for STD mode data are consistent with the literature values even without the correction for Ba. This is because the contribution of $^{132}Ba^{2+}$ to $^{66}Zn^{+}$ is about 80 times smaller than that of $^{136}Ba^{2+}$ to $^{68}Zn^{+}$.

*Cadmium, Indium and Thallium*

Cadmium, In and Tl abundances in four replicate measurements of Allende (Table 2.20) are consistent with those of literature data. Cadmium was determined by using $^{110}Cd/^{111}Cd$ and $^{112}Cd/^{111}Cd$ ratio and were found to be internally consistent.

Replicate measurements of Allende are also consistent with the literature data (Paul and Lipschutz, 1990 and the references therein). In Fig 2.7, Allende data from this study as well as Chicago means (Paul and Lipschutz, 1990 and the references therein) are normalized to Purdue means (Paul and Lipschutz, 1990 and the references therein) for Zn, Cd, Bi, Tl and In, and are found to be consistent with the literature abundances within the limit of uncertainty.

**Table 2.17** Lead and Bi abundances in Smithsonian Allende powder.

| | Weight | 208/207 Pb | | | 206/207 Pb | | | 204/207 Pb | | | 208Pb-209Bi | | |
|---|---|---|---|---|---|---|---|---|---|---|---|---|---|
| | [g] | ppm | SD | RSD | ppm | SD | RSD | ppm | SD | RSD | ppb | SD | RSD |
| 140527 | | | | | | | | | | | | | |
| Allende (22/6) | 0.09950 | 1.04 | 0.03 | 3.3 | 1.01 | 0.04 | 3.8 | 1.06 | 0.04 | 3.9 | 45.2 | 0.6 | 1.4 |
| Allende (22/6) | 0.10040 | 1.14 | 0.03 | 3.0 | 1.14 | 0.04 | 3.2 | 1.14 | 0.04 | 3.6 | 43.0 | 0.7 | 1.7 |
| 140701 | | | | | | | | | | | | | |
| Allende (22/6) | 0.10411 | 1.09 | 0.01 | 0.7 | 1.06 | 0.01 | 0.9 | 1.11 | 0.03 | 2.4 | 51.9 | 0.5 | 1.0 |
| Allende (22/6) | 0.09990 | 1.42* | 0.01 | 0.5 | 1.53* | 0.01 | 0.9 | 1.37* | 0.03 | 1.8 | 42.0* | 1.0 | 2.3 |
| 140413 | | | | | | | | | | | | | |
| Allende (22/6) | 0.01069 | 1.17 | 0.03 | 2.8 | 1.18 | 0.03 | 2.6 | 1.18 | 0.07 | 6.1 | 47.6 | 0.6 | 1.2 |
| Allende (22/6) | 0.01093 | 1.17 | 0.02 | 2.0 | 1.20 | 0.02 | 1.9 | 1.16 | 0.05 | 4.6 | 42.1 | 0.5 | 1.1 |
| Allende (22/6) | 0.01084 | 1.20 | 0.03 | 2.6 | 1.22 | 0.04 | 2.9 | 1.18 | 0.06 | 5.2 | 44.8 | 0.6 | 1.3 |
| Mean | | 1.14 | | | 1.14 | | | 1.14 | | | 45.8 | | |
| SD | | 0.06 | | | 0.08 | | | 0.05 | | | 3.6 | | |
| RSD [%] | | 5.2 | | | 7.3 | | | 4.1 | | | 7.8 | | |

*Excluded from the mean. Lead isotopic composition of Smithsonian Allende powder is used from Tatsumoto et al. (1973).

**Table 2.18** Literature data for Pb and Bi in Allende meteorite (all samples are Smithsonian powder unless otherwise indicated).

| | Pb [ppm] | Bi [ppb] | References |
|---|---|---|---|
| Purdue mean | | 48.6 ± 3.4 | Paul and Lipschutz (1990) and the references therein |
| Chicago mean | | 46.4 ± 2.8 | Paul and Lipschutz (1990) and the references therein |
| MS-ID | 1.097 | | Tatsumoto et al. (1973) |
| MS-ID | 1.52 ± 0.26 | | Stracke et al. (2012) [~30 g chunk sample] |
| ICP-SFMS | 1.27 ± 0.05 | | Barrat et al. (2012) |
| ICP-QMS | 1.09 | 42.0 | Makishima and Nakamura (2006) |
| FI-ICP-MS | 1.69 | | Makishima and Nakamura (1997) |
| Compiled | 1.39 ± 0.25 | | Recommended value from Jarosewich et al. (1987) |

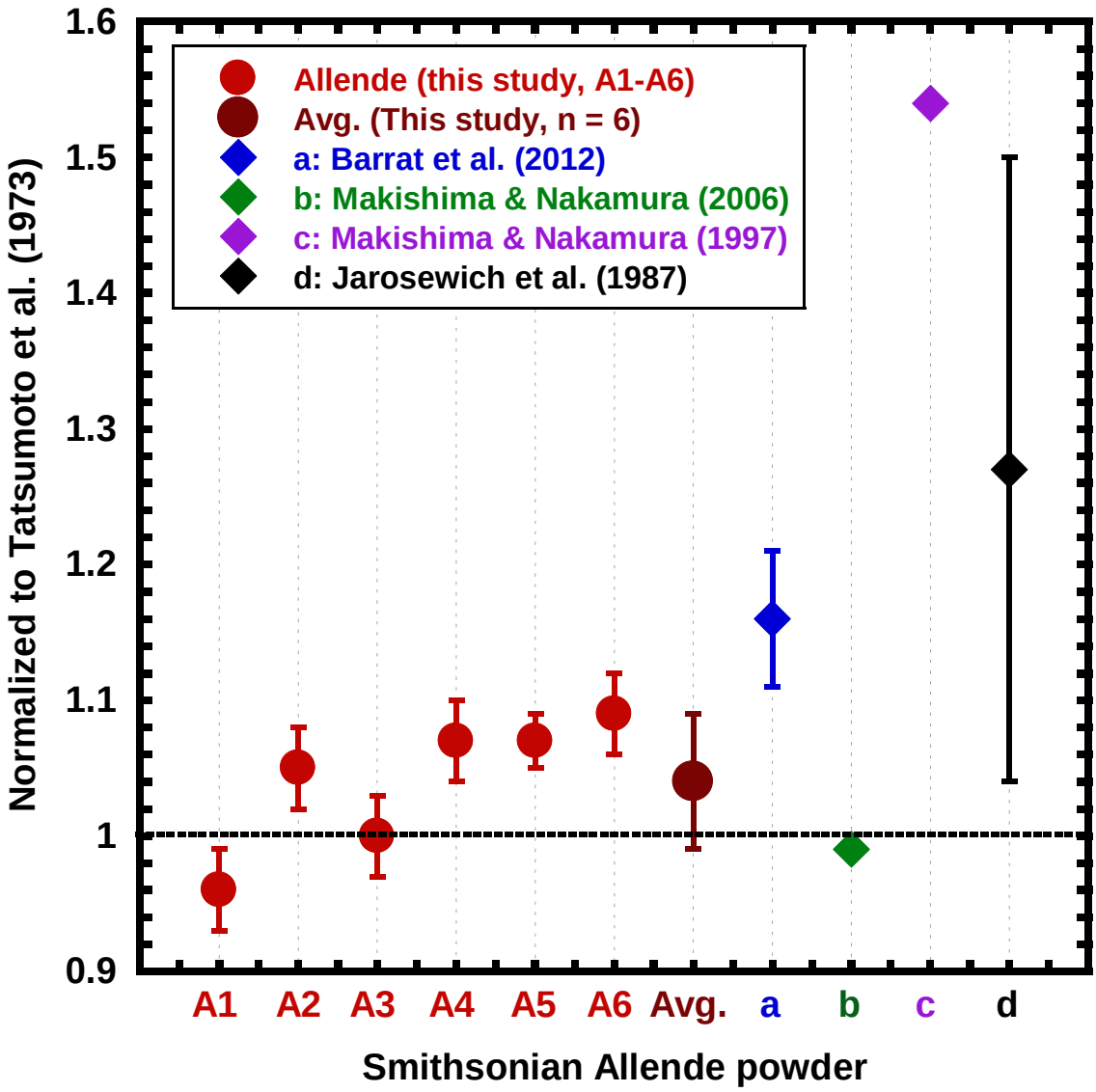


**Fig. 2.6** Lead abundance in Allende meteorite is normalized to the Pb abundance obtained by MS-ID data (Tatsumoto et al., 1973).

**Table 2.19** Lead and Bi abundance in JB2.

| JB2 | Pb (ppm) | | | Bi |
|---|---|---|---|---|
| | $^{208}Pb/^{207}Pb$ | $^{206}Pb/^{207}Pb$ | $^{204}Pb/^{207}Pb$ | (ppb) |
| This work | | | | |
| JB2-1 | 5.44 ± 0.16 | 5.10 ± 0.19 | 5.69 ± 0.18 | 28.6 ± 0.5 |
| JB2-2 | 4.96 ± 0.11 | 4.86 ± 0.12 | 5.16 ± 0.16 | 29.2 ± 0.5 |
| JB2-3 | 4.93 ± 0.10 | 4.72 ± 0.10 | 5.09 ± 0.22 | 28.8 ± 0.5 |
| JB2-4 | 5.83 ± 0.03 | 5.79 ± 0.03 | 5.83 ± 0.03 | 29.0 ± 0.6 |
| JB2-5 | 5.25 ± 0.02 | 5.21 ± 0.02 | 5.24 ± 0.02 | 29.0 ± 0.5 |
| JB2-6 | 5.17 ± 0.03 | 5.14 ± 0.04 | 5.13 ± 0.03 | 28.3 ± 0.6 |
| Average : | **5.26** | **5.14** | **5.36** | **28.8** |
| SD : | 0.34 | 0.37 | 0.32 | 0.3 |
| RSD [%] : | 6.4 | 7.2 | 6.0 | 1.1 |
| | | | | |
| Literature data[a] | | | | |
| Recommended | | 5.36 | | 33 |
| Imai et al. (1995) | | 5.16 | | 33 |
| Makishima et al. (1997) | | 5.28 | | |
| Jochum and Jenner (1994) | | 4.94 | | 30 |
| Makishima and Nakamura (2006) | | 4.88 | | 27.9 |

*****Lead isotopic composition is taken from Baker et al. (2004) for JB2.

**Table 2.20** Zinc, Pb, Cd, Bi, Tl and In abundances in Allende meteorite.

| Allende | Zn (ppm) | Pb (ppm) | Cd (ppb) | Bi (ppb) | Tl (ppb) | In (ppb) |
|---|---|---|---|---|---|---|
| This work | | | | | | |
| Allende-1 | 122 ± 1 | 1.05 ± 0.03 | 457 ± 14 | 45.1 ± 0.6 | 56.7 ± 1.0 | 30.2 ± 0.8 |
| Allende-2 | 126 ± 1 | 1.14 ± 0.03 | 470 ± 13 | 43.0 ± 0.7 | 57.1 ± 1.0 | 29.5 ± 0.8 |
| Allende-3 | 119 ± 1 | 1.09 ± 0.01 | 453 ± 4 | 51.9 ± 0.5 | 57.5 ± 0.3 | 30.4 ± 0.9 |
| Allende-4 | 119 ± 2 | 1.42 ± 0.01 | 471 ± 3 | 42.1 ± 1.0 | 57.7 ± 0.3 | 29.2 ± 0.4 |
| **Average** | **122** | **1.18** | **463** | **45.6** | **57.3** | **29.8** |
| SD | 3 | 0.17 | 9 | 4.4 | 0.4 | 0.6 |
| RSD | 2.7 | 14.3 | 2.0 | 9.7 | 0.8 | 1.9 |
| | | | | | | |
| Literature data | | | | | | |
| Purdue mean[a] | 116 ± 7 | | 505 ± 56 | 48.6 ± 3.4 | 61.0 ± 4.7 | 30.3 ± 3.4 |
| Chicago mean[a] | 116 ± 12 | | 466 ± 30 | 46.4 ± 2.8 | 61.2 ± 3.9 | 28.8 ± 6.7 |
| Compiled[b] | 110 ± 5 | 1.39 ± 0.25 | | | | 29 ± 1 |
| MS-ID[c] | | 1.097 | | | | |
| MS-ID[d] | | 1.52 ± 0.26 | | | | |
| ICP-SFMS[e] | | 1.27 ± 0.05 | | | | |
| ICP-QMS[f] | | 1.09 | | 42.0 | 56.5 | 28.1 |
| FI-ICP-MS[g] | | 1.69 | | | | |

[a]Paul and Lipschutz (1990) and the references therein; [b]Recommended data from Jarosewich et al. (1987); [c]Tatsumoto et al. (1973); [d]Stracke et al. (2012) ~ 30 g Allende chunk samples (n=39); [e]Barrat et al. (2012); [f]Makishima and Nakamura (2006); [g] Makishima and Nakamura (1997).

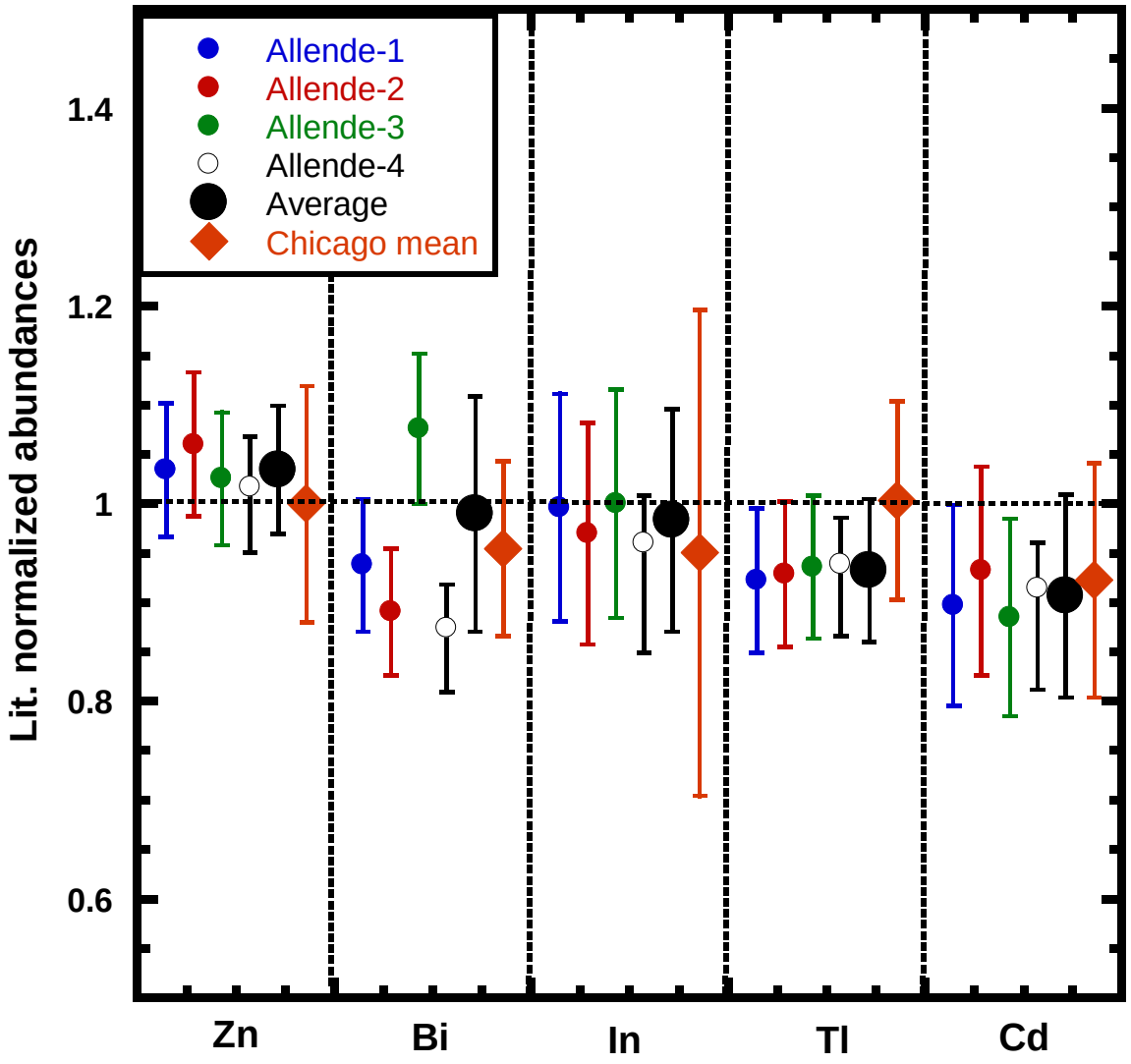


**Fig. 2.7** Purdue-mean (Paul and Lipschutz, 1990) normalized Zn, Cd, Bi, Tl and In abundances in Allende meteorite of this work. Black diamond represents Purdue-mean normalized Chicago-mean value.

## 2.5 Inductively coupled plasma atomic emission spectrometry for P determination

Phosphorus abundances in R chondrites were determined by ICP-AES using SPS 7800 (SSI-nanotechnology products, Chiba, Japan) following the procedure of Asoh and Ebihara (2013) with small modification. To do so, commercially available high purity phosphorus standard solution and beryllium solution (as internal monitor) were used. Analytical wavelengths of 213.648 nm and 234.861 nm were chosen for phosphorus and beryllium measurements, respectively, to have minimal spectral interference. Matrix matching method was used rather than ion-exchange separation. For ICP-AES experiment, we use the same stock solution of ICP-MS experiment (for REE, Th and U determination) with ~600 dilution factor.

### 2.5.1 Accuracy and precision

Accuracy and precision of ICP-AES experiment have been ensured by repeated analyses of Allende samples. The reproducibility of seven replicate measurements was just 1.8% (1σ) and the P abundances in this experiment are in good agreement with those of literature data (Table 2.21). Wolf and Palme (2001) used XRF coupled with standard addition method and reported a very precise (0.67%, 1σ) P data for Allende. In Fig 2.8, P abundances of this experiment were normalized to that of wolf and Palme (2001) and found to be consistent within the limit of uncertainty.

**Table 2.21** Phosphorus abundance (with 1σ uncertainty) in Allende sample obtained by ICP-AES and compared with literature data.

| Allende (A, Split/Position: 22/6) | P (ppm) |
|---|---|
| A1 | 1046 ± 26 |
| A2 | 1053 ± 25 |
| A3 | 1058 ± 19 |
| A4 | 1094 ± 21 |
| A5 | 1074 ± 23 |
| **Average (n=5)** | **1065** |
| SD | 19 |
| RSD (1σ, %) | 1.8 |
| | |
| Jarosewich et. al. (1987) | 1048 |
| Wolf & Palme (2001) | 1052 |
| Stracke et. al. (2012) | 1067 |

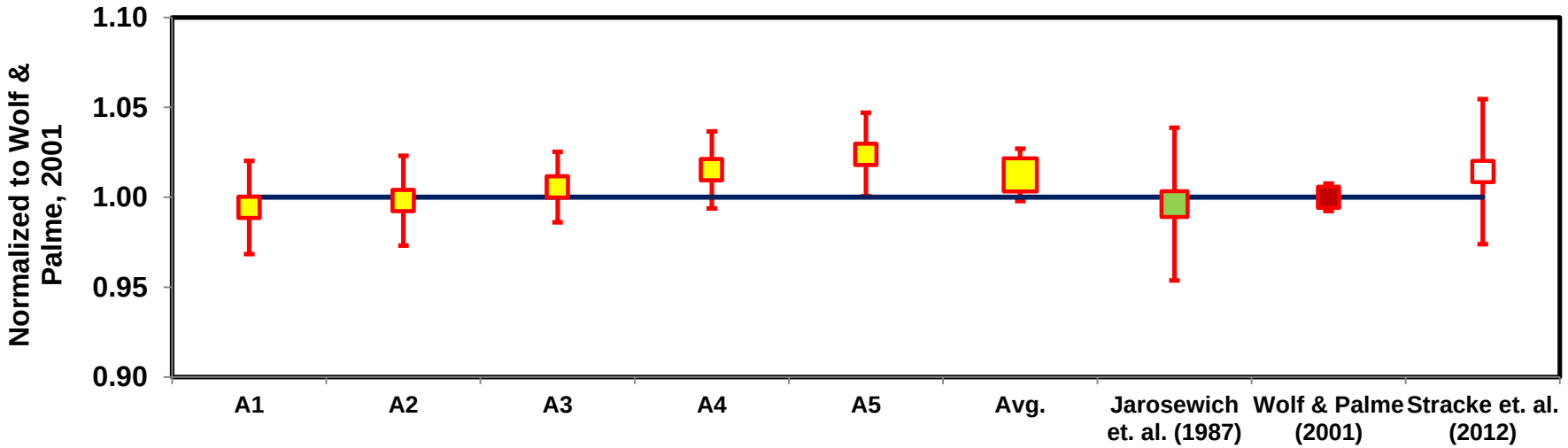


**Fig. 2.8** Literature (Wolf and Palme, 2001) normalized phosphorus abundances in Smithsonian Allende powder. Individual uncertainties are due to the standard deviation of replicate (n=3) measurements of same sample by Inductively Coupled Plasma Mass Spectrometry. Average of this study is also presented with the standard deviation (n=5).

# Chapter-3

## Results

### 3.1 Major, minor and trace elemental abundance: INAA data

Using instrumental neutron activation analysis, bulk chemical composition of twenty four elements (Na, Mg, Al, Ca, Sc, V, Cr, Mn, Fe, Co, Ni, Zn, As, Se, Br, Sb, La, Sm, Eu, Yb, Lu, Os Ir and Au) in R chondrites have been determined (Table 3.1). In Fig 3.1, CI, Cr-normalized abundance pattern is shown. Ivuna-like carbonaceous chondrites (CI) are supposed to have the representative chemical composition of the solar nebula (e.g., Anders and Ebihara, 1982; Anders and Grevesse, 1989; Lodders, 2003; Palme and Jones, 2003). So, by normalizing chemical abundances of R chondrites by CI abundance (Anders and Grevesse, 1989), we can have the idea about the elemental fractionations. CI-normalized abundances are generally further normalized by Mg abundance to remove the effect of dilution by water and organic matter in CI chondrites (Davis, 2005). But in this study, CI normalized abundances were further normalized by Cr abundance instead of Mg abundance since the analytical uncertainty (1σ, from counting statistics) for Cr is lower than that for Mg.

In Fig 3.1, individual R chondrites and R-mean (n=15, red line) are plotted along with the ordinary chondrites (H, L and LL) (Kallemeyn et al., 1989). Elements are plotted in terms of volatility to right (Lodders, 2003). Lithophile elemental abundance pattern in R chondrites are almost flat and are comparable with that of ordinary (Kallemeyn et al., 1989) chondrites (Fig 3.1). This flat lithophile abundance pattern is also consistent with Isa et al. (2014). A mean CI-normalized Na and Mn abundances are 1.32 ± 0.07 and 1.21 ± 0.04, respectively, which are comparable with those of ordinary chondrites (Kallemeyn et al., 1989) but higher than those of carbonaceous (Kallemeyn and Wasson, 1981; Kallemeyn et al., 1991) and enstatite (Kallemeyn and Wasson, 1986) chondrites. In carbonaceous and enstatite chondrites, CI-normalized Na and Mn abundances are less than unity. Siderophile elemental abundance pattern is intermediate between H and L chondrites. But the volatile elements (Zn and Se) abundances are higher than those of ordinary chondrites. A mean iron content in R chondrites is 24.6 ± 0.7 (%, 1σ, n=15, this study) whereas the mean iron contents are 27.1 ± 0.7 (%, 1σ, n=22), 21.6 ± 0.5 (%, 1σ, n=20) and 18.4 ± 0.4 (%, 1σ, n=16) in H, L and LL chondrites (Kallemeyn et al., 1989), respectively. That is, bulk iron contents in R chondrites are intermediate between H and L chondrites. Bulk Ir contents in R chondrites also show the same trend. CI-normalized Ni/Co ratios (~0.9) in R chondrites are comparable with those of ordinary chondrites (Kallemeyn et al., 1989).

**Table 3.1** Major and trace element abundances obtained by INAA for R chondrites of this work (uncertainties are due to counting statistics, 1σ).

| | | PRE 95411.21 (R3) | ALH 85151.41 (R3.6) | Y 793575.44 (R3.8) | Y 983270.56 (R4) | A 881988.68 (R4) |
|---|---|---|---|---|---|---|
| Na | ppm | 6460 ± 20 | 6280 ± 20 | 6710 ± 30 | 5620 ± 20 | 6730 ± 20 |
| Mg | % | 13.3 ± 1.1 | 13.9 ± 1.2 | 12.4 ± 1.1 | 13.0 ± 1.1 | 13.6 ± 1.2 |
| Al | % | 1.01 ± 0.01 | 1.02 ± 0.01 | 1.01 ± 0.01 | 0.99 ± 0.01 | 1.07 ± 0.01 |
| Ca | % | 1.22 ± 0.18 | 1.21 ± 0.19 | 1.10 ± 0.16 | 1.27 ± 0.18 | 1.27 ± 0.20 |
| Sc | ppm | 7.60 ± 0.03 | 7.57 ± 0.03 | 7.86 ± 0.04 | 7.55 ± 0.03 | 7.74 ± 0.04 |
| V | ppm | 66.0 ± 3.1 | 69.9 ± 3.2 | 70.9 ± 3.4 | 68.0 ± 3.1 | 70.6 ± 3.2 |
| Cr | ppm | 3610 ± 20 | 3590 ± 20 | 3650 ± 20 | 3570 ± 20 | 3560 ± 20 |
| Mn | ppm | 2470 ± 90 | 2420 ± 90 | 2270 ± 90 | 2330 ± 90 | 2570 ± 90 |
| Fe | % | 24.7 ± 0.1 | 24.6 ± 0.1 | 25.2 ± 0.1 | 24.3 ± 0.1 | 22.8 ± 0.1 |
| Co | ppm | 732 ± 8 | 694 ± 7 | 639 ± 6 | 645 ± 6 | 476 ± 5 |
| Ni | % | 1.66 ± 0.01 | 1.41 ± 0.01 | 1.15 ± 0.01 | 1.25 ± 0.01 | 0.741 ± 0.006 |
| Zn | ppm | 148 ± 12 | 153 ± 12 | 146 ± 12 | 161 ± 14 | 152 ± 15 |
| As | ppm | 2.06 ± 0.21 | 1.65 ± 0.15 | 2.18 ± 0.27 | 1.85 ± 0.21 | 1.95 ± 0.23 |
| Se | ppm | 12.3 ± 1.0 | 15.0 ± 0.8 | 15.3 ± 0.8 | 15.8 ± 1.1 | 10.7 ± 1.0 |
| Br | ppb | 950 ± 190 | 470 ± 100 | 430 ± 150 | 590 ± 160 | 710 ± 180 |
| Sb | ppb | 97.6 ± 16.8 | 68.2 ± 12.8 | 70.3 ± 24.6 | 73.1 ± 15.0 | 74.5 ± 15.1 |
| La | ppb | 287 ± 19 | 285 ± 17 | 293 ± 36 | 272 ± 29 | 309 ± 24 |
| Sm | ppb | 197 ± 5 | 197 ± 3 | 204 ± 5 | 200 ± 6 | 196 ± 5 |
| Eu | ppb | 82 ± 15 | 68 ± 16 | 76 ± 14 | 79 ± 14 | 67 ± 12 |
| Yb | ppb | 200 ± 31 | 197 ± 40 | 215 ± 35 | 185 ± 37 | 203 ± 44 |
| Lu | ppb | 29 ± 5 | 30 ± 4 | 33 ± 7 | 34 ± 7 | 34 ± 6 |
| Os | ppb | 740 ± 90 | 670 ± 130 | 690 ± 90 | 450 ± 60 | 470 ± 70 |
| Ir | ppb | 598 ± 6 | 602 ± 7 | 637 ± 6 | 613 ± 6 | 507 ± 4 |
| Au | ppb | 150 ± 1 | 73.0 ± 0.9 | 62.5 ± 1.0 | 63.2 ± 0.8 | 134 ± 1 |

*(Continued)*

**Table 3.1**

| | | MIL 07440.8 (R4) | LAP 03639.33 (R4) | Y 983720.81 (R4) | Y 983097.81 (R5) | LAP 04840.12 (R6) |
|---|---|---|---|---|---|---|
| Na | ppm | 6840 ± 30 | 7050 ± 30 | 6210 ± 20 | 7120 ± 20 | 6830 ± 20 |
| Mg | % | 13.8 ± 1.2 | 12.5 ± 1.1 | 13.2 ± 1.1 | 14.1 ± 1.2 | 14.0 ± 1.2 |
| Al | % | 1.02 ± 0.01 | 1.03 ± 0.01 | 1.05 ± 0.01 | 1.04 ± 0.01 | 1.04 ± 0.01 |
| Ca | % | 1.12 ± 0.19 | 1.28 ± 0.18 | 1.07 ± 0.18 | 1.16 ± 0.18 | 1.13 ± 0.18 |
| Sc | ppm | 7.79 ± 0.04 | 8.04 ± 0.04 | 8.04 ± 0.03 | 7.91 ± 0.04 | 7.74 ± 0.04 |
| V | ppm | 65.8 ± 3.0 | 64.9 ± 2.8 | 67.3 ± 3.0 | 67.0 ± 3.0 | 63.6 ± 3.1 |
| Cr | ppm | 3660 ± 20 | 3580 ± 20 | 3660 ± 20 | 3650 ± 20 | 3660 ± 20 |
| Mn | ppm | 2480 ± 90 | 2340 ± 90 | 2410 ± 90 | 2480 ± 90 | 2420 ± 90 |
| Fe | % | 25.2 ± 0.1 | 24.6 ± 0.1 | 25.1 ± 0.1 | 23.5 ± 0.1 | 24.8 ± 0.1 |
| Co | ppm | 674 ± 7 | 726 ± 7 | 494 ± 5 | 713 ± 7 | 673 ± 7 |
| Ni | % | 1.17 ± 0.01 | 1.46 ± 0.01 | 0.969 ± 0.005 | 1.34 ± 0.01 | 1.34 ± 0.01 |
| Zn | ppm | 149 ± 11 | 155 ± 11 | 147 ± 12 | 172 ± 14 | 163 ± 14 |
| As | ppm | 2.32 ± 0.30 | 1.96 ± 0.30 | 1.75 ± 0.20 | 2.02 ± 0.25 | 1.94 ± 0.19 |
| Se | ppm | 15.4 ± 0.8 | 12.8 ± 0.9 | 12.1 ± 0.8 | 13.3 ± 1.1 | 14.0 ± 0.9 |
| Br | ppb | 590 ± 180 | 720 ± 230 | 590 ± 150 | 810 ± 210 | 380 ± 90 |
| Sb | ppb | 95.9 ± 16.1 | 100 ± 20 | 91.7 ± 16.1 | 49.5 ± 13.6 | 53.5 ± 16.3 |
| La | ppb | 286 ± 24 | 262 ± 28 | 270 ± 26 | 328 ± 26 | 284 ± 20 |
| Sm | ppb | 190 ± 7 | 193 ± 6 | 195 ± 4 | 205 ± 6 | 189 ± 5 |
| Eu | ppb | 61 ± 17 | 87 ± 17 | 87 ± 14 | 86 ± 16 | 88 ± 17 |
| Yb | ppb | 239 ± 38 | 217 ± 37 | 190 ± 25 | 205 ± 33 | 247 ± 36 |
| Lu | ppb | 34 ± 7 | 29 ± 6 | 37 ± 6 | 36 ± 5 | 35 ± 8 |
| Os | ppb | 660 ± 90 | 650 ± 130 | 700 ± 90 | 509 ± 84 | 565 ± 76 |
| Ir | ppb | 604 ± 3 | 552 ± 3 | 554 ± 3 | 536 ± 6 | 566 ± 6 |
| Au | ppb | 199 ± 1 | 66.9 ± 1.6 | 82.3 ± 1.1 | 178 ± 1 | 176 ± 1 |

*(Continued)*

**Table 3.1**

| | | MIL 11207.8 (R6) | Y 980702.61 (R6) | Y 980703.71 (R6) | LAP 02238.13 (R) | PCA 91002.64 (R3.8-6) |
|---|---|---|---|---|---|---|
| Na | ppm | 6570 ± 20 | 6490 ± 20 | 6730 ± 20 | 6540 ± 20 | 6520 ± 20 |
| Mg | % | 14.3 ± 1.2 | 14.4 ± 1.2 | 15.1 ± 1.3 | 13.8 ± 1.2 | 12.9 ± 1.1 |
| Al | % | 1.06 ± 0.01 | 1.06 ± 0.01 | 1.32 ± 0.02 | 1.02 ± 0.01 | 1.01 ± 0.01 |
| Ca | % | 1.27 ± 0.18 | 1.33 ± 0.19 | 1.09 ± 0.16 | 0.94 ± 0.15 | 1.20 ± 0.17 |
| Sc | ppm | 8.23 ± 0.03 | 7.86 ± 0.04 | 8.17 ± 0.04 | 7.79 ± 0.03 | 7.75 ± 0.04 |
| V | ppm | 71.4 ± 3.1 | 64.5 ± 3.0 | 70.9 ± 3.2 | 67.8 ± 3.0 | 67.7 ± 3.1 |
| Cr | ppm | 3630 ± 20 | 3640 ± 20 | 3700 ± 20 | 3640 ± 20 | 3580 ± 20 |
| Mn | ppm | 2440 ± 90 | 2460 ± 90 | 2370 ± 90 | 2310 ± 90 | 2280 ± 90 |
| Fe | % | 25.5 ± 0.1 | 24.2 ± 0.1 | 24.7 ± 0.1 | 24.6 ± 0.1 | 25.1 ± 0.1 |
| Co | ppm | 655 ± 7 | 649 ± 6 | 678 ± 7 | 707 ± 7 | 719 ± 7 |
| Ni | % | 1.19 ± 0.01 | 1.20 ± 0.01 | 1.26 ± 0.01 | 1.48 ± 0.01 | 1.45 ± 0.01 |
| Zn | ppm | 158 ± 13 | 140 ± 11 | 133 ± 12 | 169 ± 14 | 146 ± 13 |
| As | ppm | 2.38 ± 0.21 | 1.87 ± 0.22 | 2.24 ± 0.28 | 1.46 ± 0.19 | 2.02 ± 0.19 |
| Se | ppm | 10.9 ± 0.7 | 12.2 ± 1.1 | 12.2 ± 0.9 | 14.1 ± 0.9 | 14.3 ± 1.0 |
| Br | ppb | 270 ± 70 | 1270 ± 310 | 1350 ± 340 | 780 ± 180 | 990 ± 190 |
| Sb | ppb | 94.8 ± 15.3 | 79.7 ± 14.6 | 76.9 ± 16.9 | 95.7 ± 17.5 | 71.6 ± 14.7 |
| La | ppb | 330 ± 30 | 293 ± 20 | 321 ± 21 | 296 ± 21 | 309 ± 19 |
| Sm | ppb | 211 ± 5 | 201 ± 5 | 206 ± 7 | 195 ± 5 | 201 ± 5 |
| Eu | ppb | 87 ± 12 | 87 ± 16 | 73 ± 14 | 86 ± 14 | 73 ± 12 |
| Yb | ppb | 198 ± 31 | 212 ± 29 | 217 ± 33 | 180 ± 44 | 209 ± 35 |
| Lu | ppb | 32 ± 5 | 29 ± 6 | 28 ± 6 | 30 ± 6 | 31 ± 7 |
| Os | ppb | 670 ± 90 | 680 ± 90 | 620 ± 70 | 1110 ± 110 | 640 ± 100 |
| Ir | ppb | 616 ± 6 | 537 ± 5 | 549 ± 6 | 633 ± 7 | 598 ± 7 |
| Au | ppb | 218 ± 1 | 169 ± 1 | 171 ± 1 | 307 ± 2 | 174 ± 1 |

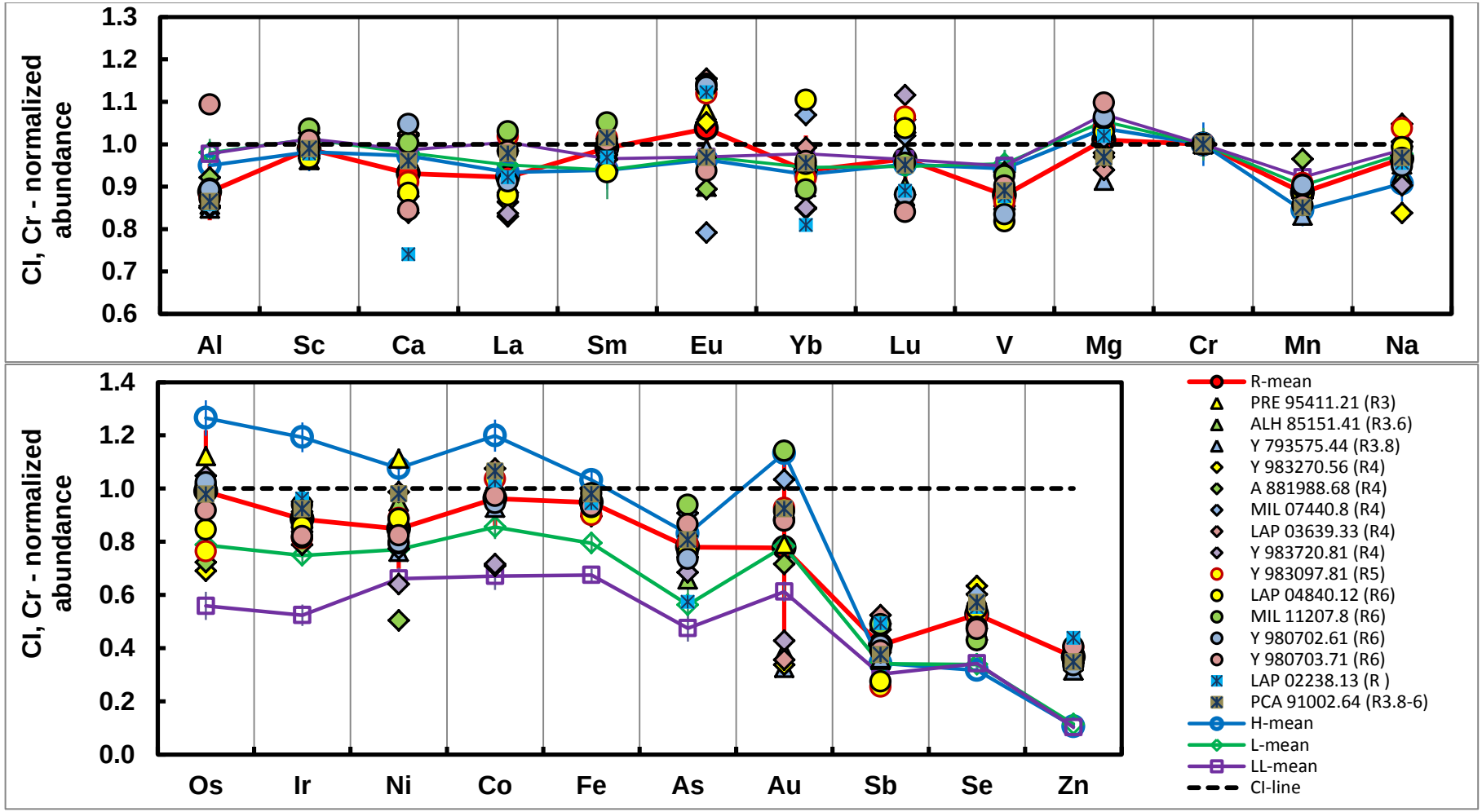


**Fig. 3.1** CI, Cr-normalized elemental abundances for the R chondrites and compared with H, L and LL chondrites mean value (Kallemeyn et al., 1989). Heavy red lines represents the mean value for R chondrites of this study with 1σ uncertainty (n=15). Lithophile elements are plotted at the top and siderophile and chalcophile elements at the bottom. Elements are arranged from left to right in order of decreasing nebular condensation temperature.

### 3.2 REEs, Th and U abundances: ICP-MS data

Detailed abundances of REEs, Th and U in R chondrites are listed in Table 3.2. Uncertainties (1σ) are due to repeated scanning of ICP-MS instrument (n=30). For all elements uncertainties (in %) are less than 4% except that for U (RSD < 5%). R- Chondrite mean value is calculated from the average of 15 R chondrites of this study and RSD is less than 5%, except that for U (RSD = 5.3%). CI-normalized REE, Th & U abundance patterns are shown in Fig. 3.2. In the CI-normalized abundance patterns heavy rare earth elements (HREE) are faintly enriched compared with the light rare earth elements (LREE) and show a subtle positive Ce anomaly.

**Table 3.2** REE, Th, and U abundances (in ppb with 1σ uncertainty) obtained by ICP-MS for R chondrites of this work.

| | PRE 95411.21 (R3) | ALH 85151.41 (R3.6) | Y 793575.44 (R3.8) | Y 983270.56 (R4) | A 881988.68 (R4) | MIL 07440.8 (R4) | LAP 03639.33 (R4) | Y 983720.81 (R4) |
|---|---|---|---|---|---|---|---|---|
| La | 302 ± 5 | 301 ± 4 | 292 ± 5 | 289 ± 4 | 310 ± 6 | 300 ± 5 | 288 ± 7 | 284 ± 7 |
| Ce | 824 ± 14 | 817 ± 10 | 803 ± 11 | 811 ± 11 | 854 ± 14 | 817 ± 13 | 828 ± 17 | 821 ± 17 |
| Pr | 115 ± 2 | 114 ± 2 | 115 ± 2 | 115 ± 2 | 116 ± 2 | 113 ± 2 | 114 ± 2 | 117 ± 2 |
| Nd | 593 ± 9 | 597 ± 10 | 604 ± 9 | 602 ± 10 | 602 ± 12 | 587 ± 12 | 587 ± 11 | 593 ± 11 |
| Sm | 196 ± 5 | 192 ± 5 | 199 ± 6 | 199 ± 5 | 199 ± 6 | 188 ± 5 | 191 ± 5 | 192 ± 5 |
| Eu | 75.3 ± 1.8 | 76.0 ± 1.4 | 77.7 ± 1.5 | 74.1 ± 1.6 | 78.0 ± 1.7 | 75.8 ± 1.4 | 73.2 ± 1.7 | 77.2 ± 2.5 |
| Gd | 260 ± 7 | 263 ± 6 | 264 ± 5 | 257 ± 7 | 267 ± 6 | 256 ± 6 | 261 ± 6 | 256 ± 8 |
| Tb | 47.7 ± 1.0 | 47.5 ± 0.8 | 48.1 ± 1.0 | 46.8 ± 1.0 | 48.7 ± 0.9 | 47.2 ± 1.1 | 48.7 ± 1.2 | 47.3 ± 1.5 |
| Dy | 320 ± 6 | 321 ± 5 | 322 ± 5 | 312 ± 5 | 326 ± 4 | 315 ± 6 | 330 ± 6 | 317 ± 5 |
| Ho | 73.3 ± 1.0 | 73.3 ± 1.1 | 73.2 ± 1.2 | 70.8 ± 1.5 | 74.4 ± 1.3 | 72.0 ± 1.5 | 75.7 ± 1.1 | 72.7 ± 1.3 |
| Er | 213 ± 4 | 212 ± 4 | 210 ± 4 | 204 ± 4 | 216 ± 3 | 209 ± 5 | 221 ± 5 | 208 ± 3 |
| Tm | 33.0 ± 0.8 | 33.0 ± 0.8 | 32.2 ± 0.6 | 31.6 ± 0.6 | 33.7 ± 0.7 | 32.1 ± 0.7 | 34.3 ± 0.8 | 32.3 ± 0.9 |
| Yb | 214 ± 3 | 216 ± 4 | 219 ± 3 | 207 ± 4 | 221 ± 4 | 212 ± 4 | 228 ± 6 | 220 ± 4 |
| Lu | 32.3 ± 0.6 | 32.6 ± 0.7 | 31.8 ± 0.8 | 30.7 ± 0.7 | 33.3 ± 0.6 | 32.6 ± 0.6 | 34.8 ± 1.0 | 32.0 ± 0.8 |
| Th | 38.8 ± 0.9 | 40.3 ± 1.0 | 41.1 ± 1.0 | 37.6 ± 1.1 | 41.2 ± 1.0 | 41.1 ± 1.4 | 42.3 ± 1.1 | 42.5 ± 1.2 |
| U | 10.4 ± 0.4 | 11.1 ± 0.3 | 10.7 ± 0.3 | 9.87 ± 0.34 | 11.4 ± 0.6 | 10.2 ± 0.3 | 11.2 ± 0.4 | 11.6 ± 0.4 |

*(Continued)*

**Table 3.2**

| | Y 983097.81 (R5) | LAP 04840.12 (R6) | MIL 11207.8 (R6) | Y 980702.61 (R6) | Y 980703.71 (R6) | LAP 02238.13 (R) | PCA 91002.64 (R3.8-6) | R chondrites (Mean) | | |
|---|---|---|---|---|---|---|---|---|---|---|
| | | | | | | | | ppb | SD | RSD |
| La | 324 ± 4 | 284 ± 3 | 321 ± 4 | 314 ± 4 | 318 ± 4 | 306 ± 4 | 323 ± 4 | 304 | 14 | 4.6 |
| Ce | 887 ± 11 | 768 ± 8 | 873 ± 9 | 835 ± 9 | 837 ± 12 | 799 ± 11 | 846 ± 11 | 828 | 30 | 3.6 |
| Pr | 121 ± 2 | 108 ± 2 | 121 ± 2 | 117 ± 2 | 118 ± 2 | 115 ± 2 | 120 ± 3 | 116 | 3 | 2.9 |
| Nd | 616 ± 9 | 548 ± 8 | 613 ± 9 | 596 ± 10 | 601 ± 9 | 580 ± 10 | 604 ± 10 | 595 | 16 | 2.7 |
| Sm | 206 ± 5 | 185 ± 4 | 209 ± 6 | 204 ± 6 | 206 ± 5 | 198 ± 8 | 208 ± 9 | 198 | 7 | 3.8 |
| Eu | 77.8 ± 1.9 | 71.7 ± 1.6 | 77.3 ± 1.5 | 76.7 ± 1.7 | 78.1 ± 2.0 | 74.1 ± 1.7 | 77.9 ± 1.7 | 76.0 | 2.0 | 2.6 |
| Gd | 269 ± 7 | 246 ± 7 | 271 ± 6 | 264 ± 6 | 264 ± 7 | 257 ± 6 | 265 ± 7 | 261 | 6 | 2.4 |
| Tb | 49.2 ± 1.0 | 45.6 ± 0.8 | 49.9 ± 1.1 | 48.8 ± 1.1 | 49.0 ± 0.7 | 47.2 ± 1.0 | 49.2 ± 1.4 | 48.1 | 1.1 | 2.4 |
| Dy | 328 ± 6 | 306 ± 6 | 333 ± 6 | 326 ± 6 | 328 ± 5 | 318 ± 5 | 330 ± 7 | 322 | 8 | 2.4 |
| Ho | 75.6 ± 1.1 | 70.6 ± 1.4 | 76.3 ± 1.6 | 75.6 ± 1.2 | 75.7 ± 1.4 | 73.6 ± 1.4 | 75.2 ± 1.6 | 73.9 | 1.8 | 2.5 |
| Er | 219 ± 4 | 206 ± 4 | 223 ± 4 | 219 ± 4 | 221 ± 5 | 214 ± 5 | 222 ± 4 | 214 | 6 | 2.9 |
| Tm | 33.5 ± 0.6 | 31.5 ± 0.6 | 33.8 ± 0.8 | 33.3 ± 0.7 | 34.0 ± 0.8 | 32.6 ± 0.8 | 33.8 ± 1.0 | 33.0 | 0.9 | 2.7 |
| Yb | 223 ± 4 | 213 ± 4 | 227 ± 5 | 226 ± 5 | 227 ± 5 | 218 ± 4 | 227 ± 5 | 220 | 7 | 3.0 |
| Lu | 34.2 ± 0.6 | 32.9 ± 0.8 | 34.7 ± 0.9 | 34.6 ± 1.0 | 34.9 ± 1.0 | 33.5 ± 0.7 | 34.2 ± 0.9 | 33.3 | 1.3 | 3.9 |
| Th | 40.7 ± 1.9 | 37.9 ± 0.9 | 41.1 ± 1.1 | 41.4 ± 1.0 | 41.8 ± 1.0 | 38.7 ± 1.9 | 40.1 ± 3.1 | 40.4 | 1.5 | 3.8 |
| U | 11.0 ± 0.9 | 9.58 ± 0.37 | 10.6 ± 0.4 | 10.6 ± 0.4 | 10.8 ± 0.4 | 9.90 ± 0.76 | 10.1 ± 1.2 | 10.6 | 0.6 | 5.8 |

RSD: 1σ and n=15

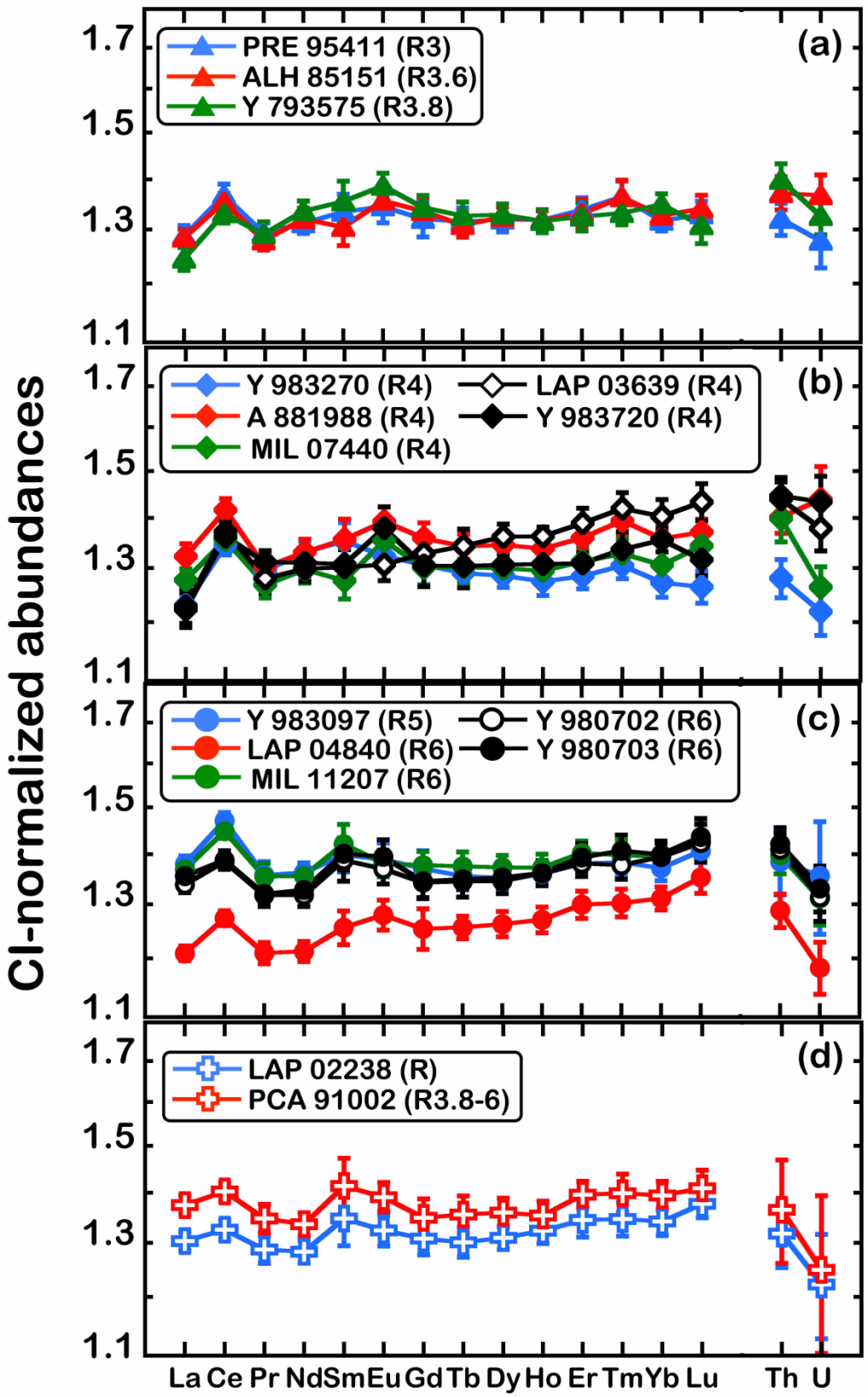


**Fig. 3.2:** CI- (Anders & Grevesse, 1989) normalized REEs, Th and U abundance patterns in R chondrites with 1σ uncertainty (triangles represent R3 – R3.4, diamonds represent R4, circles represent R5 – R6 and blank cross represent brecciated R chondrites).

### 3.3 Phosphorus abundance in R chondrites: ICP-AES data

Table 3.4 shows the phosphorus abundances in R chondrites of this study as well as the literature values from Palme et al. (1996). In this study, mean phosphorus abundance is 1230 ± 70 ppm, which is consistent with that for the fall R chondrite- Rumuruti. In Fig 3.3, CI-normalized phosphorus abundances in R chondrites of this study along with the literature values and phosphorus abundances in other chondritic groups (Wasson and Kallemeyn, 1988) are plotted. In most of the cases, phosphorus abundances are comparable with that of CI chondrites. Phosphorus abundances in other chondritic groups are comparatively lower than the R chondrites.

**Table 3.4** Phosphorus abundance (with 1σ uncertainty) in R chondrites obtained by ICP-AES and compared with literature data.

| R chondrites | P (ppm) |
|---|---|
| This work | |
| PRE 95411.21 (R3) | 1221 ± 17 |
| ALH 85151.41 (R3.6) | 1273 ± 39 |
| Y 793575.44 (R3.8) | 1267 ± 20 |
| Y 983270.56 (R4) | 1403 ± 50 |
| A 881988.68 (R4) | 1152 ± 24 |
| MIL 07440.8 (R4) | 1261 ± 47 |
| LAP 03639.33 (R4) | 1252 ± 22 |
| Y 983720.81(R4) | 1309 ± 4 |
| Y 983097.81(R5) | 1101 ± 29 |
| LAP 04840.12 (R6) | 1316 ± 8 |
| MIL 11207.8 (R6) | 1260 ± 17 |
| Y 980702.61(R6) | 1208 ± 36 |
| Y 980703.71(R6) | 1234 ± 48 |
| LAP 02238.13 (R) | 1290 ± 36 |
| PCA 91002.64 (R3.8-6) | 1224 ± 49 |
| Average : | **1254** |
| SD : | 70 |
| RSD [%] : | 5.6 |
| | |
| Literature data[a] | |
| Acfer 217 (R3.8-5) | 1217 |
| Rumuruti (R3.8-6) | 1260 |
| Dar al Gani 013 (R3.5-6) | 1320 |

[a]Palme et al. (1996)

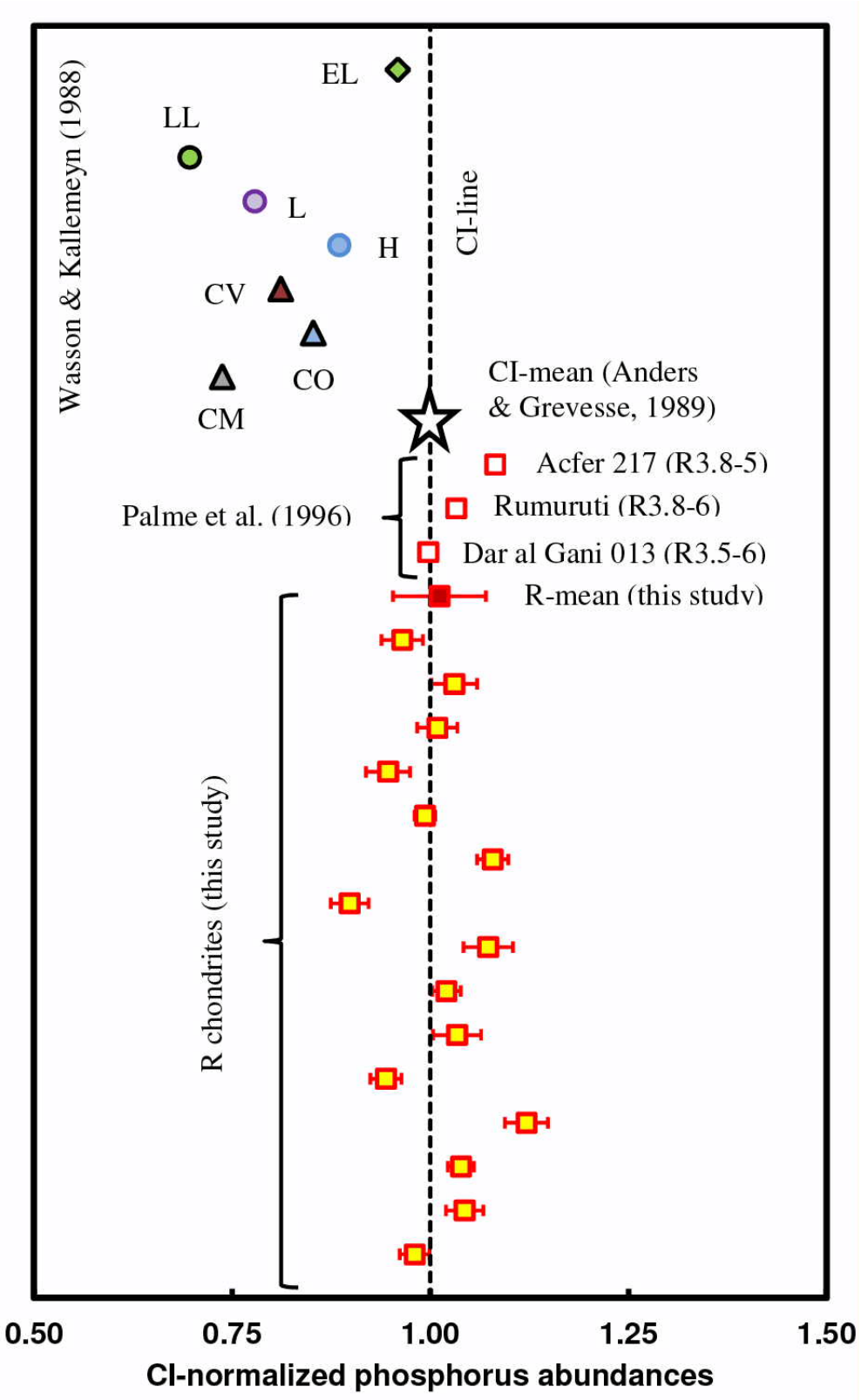


**Fig. 3.3** CI-(Anders & Grevesse, 1989) normalized phosphorus abundances in R chondrites along with the literature values for R chondrites (Palme et al., 1996) and the other chondritic group (Wasson and Kallemeyn, 1988).

### 3.4 Volatile elements abundances in R chondrites: MS-ID

Lead and Bi abundances in R chondrites are shown in Table 3.5. There is a significant difference in Pb isotopic composition between the terrestrial and cosmochemical samples. First we assume that Pb isotopic composition in R chondrites is similar with that of Allende meteorite (Bouvier et al., 2007). Then the Pb-isotopic composition was determined in this study and was found to be similar (within the analytical uncertainty) with that of Allende Pb-isotopic composition determined by Bouvier et al. (2007). In this study, $^{204}$Pb, $^{206}$Pb, $^{207}$Pb and $^{208}$Pb isotopes were monitored and $^{207}$Pb spike was used. So, it was possible to determine Pb abundance from $^{204}$Pb/$^{207}$Pb, $^{206}$Pb/$^{207}$Pb and $^{208}$Pb/$^{207}$Pb ratios. In isotope dilution technique, if inappropriate isotopic abundances is used for data reduction, then each ratios (here $^{204}$Pb/$^{207}$Pb, $^{206}$Pb/$^{207}$Pb and $^{208}$Pb/$^{207}$Pb) will provide inconsistent data. In our calculation, we get internally consistent Pb abundance data from different isotopic ratios which imply that our assumption about the Pb isotopic composition of R chondrites was applicable without significant compromising of data accuracy. In contrast to all other R chondrites of this study, MIL 11207.8 (weathering category: Ce) gives different Pb abundances from different isotopic ratios (here $^{204}$Pb/$^{207}$Pb, $^{206}$Pb/$^{207}$Pb and $^{208}$Pb/$^{207}$Pb). A probable effect of terrestrial weathering on such variation will be discussed in discussion part. Bismuth abundances in R chondrites were determined from Pb/Bi. Relative standard deviations for Bi abundances are less than 3%.

Zinc abundances in R chondrites were determined from $^{66}$Zn/$^{67}$Zn and $^{68}$Zn/$^{67}$Zn ratio. They are internally consistent and also consistent with the INAA data (except for some cases, MS-ID data is little bit higher than those of INAA data. But the % of uncertainty in MS-ID data is about one-third of the % of uncertainty in INAA data. Similarly, for Cd determination, $^{110}$Cd/$^{111}$Cd and $^{112}$Cd/$^{111}$Cd ratios were used and were found to be internally consistent, except for LAP 02238.13. Zinc, Cd, In and Tl abundances in R chondrites are shown in Table 3.6 to 3.8, sequentially. All the data shown in these tables are blank corrected. In Table 3.9, procedure blank data are shown. Except some contamination (shown in italics in Table 3.9), procedure blank is mostly comparable with those of instrumental uncertainty. In the case of Tl, for some samples (Y 793575.44, A 881988.68, MIL 07440.8 and LAP 03639.33), relative standard deviation is higher than those of the other R chondrites. These R chondrites contain a very low amount of Tl.

**Table 3.5** Lead and Bi abundances in R chondrites.

| | R chondrites | 208/207 Pb | | | 206/207 Pb | | | 204/207 Pb | | | 208Pb-209Bi | | |
|---|---|---|---|---|---|---|---|---|---|---|---|---|---|
| | | ppm | ± | [%] | ppm | ± | [%] | ppm | ± | [%] | ppb | ± | [%] |
| 1 | PRE 95411.21 (R3) | 1.33 | 0.03 | 2.6 | 1.30 | 0.04 | 2.8 | 1.34 | 0.04 | 3.1 | 57.4 | 0.6 | 1.0 |
| 2 | ALH 85151.41 (R3.6) | 1.26 | 0.03 | 2.7 | 1.25 | 0.04 | 2.9 | 1.27 | 0.04 | 3.1 | 53.6 | 0.9 | 1.7 |
| 3 | Y 793575.44 (R3.8) | 0.373 | 0.033 | 8.9 | 0.385 | 0.035 | 9.2 | 0.371 | 0.035 | 9.5 | 13.6 | 0.4 | 2.9 |
| 4 | Y 983270.56 (R4) | 0.942 | 0.034 | 3.6 | 0.904 | 0.04 | 3.9 | 0.965 | 0.04 | 4.4 | 42.4 | 0.5 | 1.2 |
| 5 | A 881988.68 (R4) | 1.04 | 0.03 | 3.2 | 1.01 | 0.04 | 3.7 | 1.06 | 0.04 | 3.8 | 34.4 | 0.5 | 1.5 |
| 6 | MIL 07440.8 (R4) | 1.05 | 0.03 | 3.2 | 1.01 | 0.04 | 3.6 | 1.07 | 0.04 | 3.9 | 46.3 | 0.7 | 1.6 |
| 7 | LAP 03639.33 (R4) | 0.948 | 0.034 | 3.5 | 0.851 | 0.035 | 4.1 | 1.003 | 0.043 | 4.3 | 64.8 | 0.9 | 1.4 |
| 8 | Y 983720.81 (R4) | 0.950 | 0.034 | 3.5 | 0.872 | 0.04 | 4.2 | 0.99 | 0.04 | 4.2 | 39.0 | 0.6 | 1.6 |
| 9 | Y 983097.81 (R4) | 0.963 | 0.007 | 0.7 | 0.946 | 0.01 | 1.3 | 0.98 | 0.02 | 2.2 | 16.8 | 0.5 | 2.9 |
| 10 | LAP 04840.12 (R6) | 0.807 | 0.008 | 0.9 | 0.807 | 0.011 | 1.4 | 0.802 | 0.025 | 3.1 | 26.9 | 0.4 | 1.6 |
| 11 | MIL 11207.8 (R6) | 2.28 | 0.02 | 0.7 | 2.88 | 0.03 | 0.9 | 2.03 | 0.03 | 1.7 | 49.3 | 0.7 | 1.5 |
| 12 | Y 980702.61 (R6) | 0.864 | 0.008 | 1.0 | 0.863 | 0.009 | 1.0 | 0.870 | 0.022 | 2.6 | 25.8 | 0.5 | 2.1 |
| 13 | Y 980703.71 (R6) | 0.846 | 0.009 | 1.0 | 0.843 | 0.008 | 0.9 | 0.863 | 0.022 | 2.6 | 26.7 | 0.7 | 2.5 |
| 14 | LAP 02238.13 (R) | 1.19 | 0.01 | 0.9 | 1.20 | 0.01 | 1.2 | 1.18 | 0.03 | 2.2 | 56.0 | 1.0 | 1.7 |
| 15 | PCA 91002.64 (R3.8-6) | 1.59 | 0.01 | 0.8 | 1.58 | 0.02 | 1.1 | 1.60 | 0.03 | 2.0 | 71.7 | 0.9 | 1.3 |

Uncertainties (1σ) are due to standard deviation of 20 scans of single sample by ICP-MS (iCAP – Thermo Scientific) and for blank correction.

**Table 3.6** Zinc abundances in R chondrites.

| | | 66/67 Zn | | | 68/67 Zn | | | INAA | | |
|---|---|---|---|---|---|---|---|---|---|---|
| | | ppm | ± | [%] | ppm | ± | [%] | ppm | ± | [%] |
| 1 | PRE 95411.21 (R3) | 164 | 1 | 0.8 | 163 | 2 | 1.1 | 148 | 12 | 8.1 |
| 2 | ALH 85151.41 (R3.6) | 172 | 1 | 0.9 | 172 | 1 | 0.7 | 148 | 12 | 8.1 |
| 3 | Y 793575.44 (R3.8) | 164 | 1 | 0.8 | 164 | 2 | 1.0 | 135 | 12 | 8.9 |
| 4 | Y 983270.56 (R4) | 156 | 2 | 1.0 | 157 | 1 | 0.9 | 161 | 14 | 8.7 |
| 5 | A 881988.68 (R4) | 161 | 1 | 0.8 | 161 | 2 | 1.0 | 152 | 15 | 9.9 |
| 6 | MIL 07440.8 (R4) | 166 | 2 | 1.1 | 166 | 2 | 1.1 | 148 | 11 | 7.4 |
| 7 | LAP 03639.33 (R4) | 150 | 1 | 1.0 | 151 | 1 | 1.0 | 155 | 11 | 7.1 |
| 8 | Y 983720.81 (R4) | 156 | 1 | 0.8 | 156 | 1 | 0.7 | 147 | 12 | 8.2 |
| 9 | Y 983097.81 (R4) | 174 | 2 | 1.1 | 190 | 2 | 1.2 | 172 | 14 | 8.1 |
| 10 | LAP 04840.12 (R6) | 168 | 2 | 1.0 | 169 | 2 | 1.2 | 163 | 14 | 8.6 |
| 11 | MIL 11207.8 (R6) | 167 | 1 | 0.9 | 167 | 2 | 0.9 | 158 | 13 | 8.2 |
| 12 | Y 980702.61 (R6) | 133 | 1 | 0.9 | 133 | 2 | 1.2 | 143 | 11 | 7.7 |
| 13 | Y 980703.71 (R6) | 135 | 1 | 0.8 | 136 | 2 | 1.2 | 133 | 12 | 8.0 |
| 14 | LAP 02238.13 (R) | 161 | 1 | 0.8 | 162 | 1 | 0.9 | 169 | 14 | 8.0 |
| 15 | PCA 91002.64 (R3.8-6) | 156 | 2 | 1.1 | 156 | 2 | 1.0 | 146 | 13 | 8.9 |

**Table 3.7** Cadmium abundances in R chondrites.

| | | 110/111 Cd | | | 112/111 Cd | | |
|---|---|---|---|---|---|---|---|
| | | ppb | ± | [%] | ppb | ± | [%] |
| 1 | PRE 95411.21 (R3) | 527 | 16 | 3.0 | 518 | 16 | 3.0 |
| 2 | ALH 85151.41 (R3.6) | 238 | 10 | 4.1 | 238 | 8 | 3.5 |
| 3 | Y 793575.44 (R3.8) | 77.8 | 7.3 | 9.4 | 80.5 | 4.6 | 5.7 |
| 4 | Y 983270.56 (R4) | 258 | 9 | 3.5 | 255 | 8 | 3.0 |
| 5 | A 881988.68 (R4) | 243 | 10 | 4.2 | 239 | 9 | 3.9 |
| 6 | MIL 07440.8 (R4) | 232 | 10 | 4.1 | 237 | 9 | 3.6 |
| 7 | LAP 03639.33 (R4) | 230 | 9 | 3.7 | 228 | 10 | 4.2 |
| 8 | Y 983720.81 (R4) | 228 | 19 | 8.1 | 206 | 12 | 5.9 |
| 9 | Y 983097.81 (R4) | 20.0 | 1.5 | 7.4 | 16.5 | 2.2 | 13.4 |
| 10 | LAP 04840.12 (R6) | 179 | 2 | 1.1 | 172 | 5 | 3.2 |
| 11 | MIL 11207.8 (R6) | 215 | 3 | 1.2 | 207 | 9 | 4.1 |
| 12 | Y 980702.61 (R6) | 170 | 2 | 1.2 | 160 | 8 | 5.3 |
| 13 | Y 980703.71 (R6) | 179 | 2 | 1.2 | 172 | 7 | 3.9 |
| 14 | LAP 02238.13 (R) | 291 | 3 | 1.1 | 247 | 13 | 5.2 |
| 15 | PCA 91002.64 (R3.8-6) | 556 | 5 | 1.0 | 550 | 8 | 1.5 |

Uncertainties (1σ) are due to standard deviation of 20 scans of single sample by ICP-MS (iCAP – Thermo Scientific) and for blank correction.

**Table 3.8** Indium and Tl abundances in R chondrites.

| | | 113/115 In | | | 203/205 Tl | | |
|---|---|---|---|---|---|---|---|
| | | ppb | ± | [%] | ppb | ± | [%] |
| 1 | PRE 95411.21 (R3) | 44.5 | 1.2 | 2.6 | 112.3 | 1.3 | 1.1 |
| 2 | ALH 85151.41 (R3.6) | 36.9 | 0.5 | 1.4 | 51.4 | 1.0 | 2.0 |
| 3 | Y 793575.44 (R3.8) | 15.8 | 0.4 | 2.7 | 2.41 | 0.9 | 39.2 |
| 4 | Y 983270.56 (R4) | 31.5 | 4.1 | 13.0 | 42.0 | 1.0 | 2.4 |
| 5 | A 881988.68 (R4) | 32.9 | 0.9 | 2.9 | 2.90 | 0.94 | 32.6 |
| 6 | MIL 07440.8 (R4) | 29.1 | 3.6 | 12.4 | 7.49 | 0.95 | 12.6 |
| 7 | LAP 03639.33 (R4) | 25.3 | 1.1 | 4.4 | 6.63 | 0.95 | 14.3 |
| 8 | Y 983720.81 (R4) | 29.9 | 0.9 | 2.9 | 35.6 | 1.0 | 2.7 |
| 9 | Y 983097.81 (R4) | 12.1 | 0.3 | 2.3 | 2.88 | 0.08 | 2.9 |
| 10 | LAP 04840.12 (R6) | 38.9 | 0.6 | 1.7 | 37.4 | 0.3 | 0.7 |
| 11 | MIL 11207.8 (R6) | 39.5 | 0.7 | 1.7 | 17.2 | 0.1 | 0.8 |
| 12 | Y 980702.61 (R6) | 28.3 | 0.5 | 1.6 | 6.17 | 0.07 | 1.1 |
| 13 | Y 980703.71 (R6) | 28.1 | 0.4 | 1.6 | 6.58 | 0.07 | 1.1 |
| 14 | LAP 02238.13 (R) | 31.8 | 0.5 | 1.5 | 51.3 | 0.3 | 0.5 |
| 15 | PCA 91002.64 (R3.8-6) | 42.3 | 0.8 | 1.9 | 84.1 | 0.5 | 0.6 |

Uncertainties (1σ) are due to standard deviation of 20 scans of single sample by ICP-MS (iCAP – Thermo Scientific) and for blank correction.

Volatile elemental abundances in R chondrites are summarized in Table 3.10. In Table 3.10, $^{208/207}$Pb, $^{68/67}$Zn and $^{112/111}$Cd date are chosen for their relatively lower uncertainty. CI-normalized Zn, Pb, Bi, In, Tl and Cd abundances are plotted in Fig. 3.4. Except Zn, all the elements show systematic variation with the petrologic types with few exceptions. In Fig. 3.4, triangles represent R3 – R3.8, squares represent R4, diamond represents R5, circles represent R6 chondrites.

**Table 3.9** Procedure blank (1σ).

| | Zn | | | Pb | | | Bi | | | In | | | Tl | | | Cd | | |
|---|---|---|---|---|---|---|---|---|---|---|---|---|---|---|---|---|---|---|
| | ppm | ± | [%] | ppm | ± | [%] | ppb | ± | [%] | ppb | ± | [%] | ppb | ± | [%] | ppb | ± | [%] |
| 140527 | | | | | | | | | | | | | | | | | | |
| Blank-1 | *56* | *45* | *80.4* | *0.0125* | *0.0005* | 4.0 | 0.81 | 0.08 | 9.3 | 0.24 | 0.05 | 19.3 | *1.26* | *0.03* | *2.6* | *9.17* | *2.03* | *22.2* |
| Blank-2 | *94* | *32* | *34.0* | 0.0071 | 0.0004 | 5.6 | *1.07* | *0.10* | *9.7* | 0.35 | 0.06 | 18.4 | *1.37* | *0.04* | *2.7* | 3.52 | 0.52 | 14.8 |
| Blank-3 | *54* | *10* | *18.5* | 0.0079 | 0.0004 | 5.1 | 0.64 | 0.05 | 8.4 | 0.28 | 0.09 | 31.5 | *2.93* | *0.12* | *3.9* | 2.59 | 0.42 | 16.1 |
| 140701 | | | | | | | | | | | | | | | | | | |
| Blank-4 | 0.72 | 0.08 | 11.2 | 0.0095 | 0.0004 | 4.7 | *1.02* | *0.08* | *8.1* | 1.33 | 0.06 | 4.2 | 0.25 | 0.01 | 4.6 | 4.79 | 0.28 | 5.9 |
| Blank-5 | *14.6* | *0.8* | *5.5* | 0.0036 | 0.0004 | 11.3 | 0.42 | 0.08 | 19.2 | 1.22 | 0.04 | 3.2 | 0.28 | 0.01 | 4.4 | 1.89 | 0.12 | 6.2 |
| Blank-6 | 0.62 | 0.06 | 9.6 | *0.0266* | *0.0012* | 4.4 | 0.78 | 0.07 | 8.7 | 1.51 | 0.07 | 4.7 | 0.34 | 0.01 | 3.9 | 1.80 | 0.11 | 5.9 |
| Blank-7 | 0.80 | 0.07 | 8.5 | 0.0027 | 0.0004 | 13.4 | 0.49 | 0.11 | 23.2 | *7.90* | *0.23* | *2.9* | 0.34 | 0.02 | 5.3 | 2.59 | 0.10 | 3.9 |
| 140413 | | | | | | | | | | | | | | | | | | |
| Blank-8 | | | | *0.0815* | *0.00297* | 3.6 | 1.58 | 0.11 | 6.7 | | | | | | | | | |
| **Average :** | **0.71** | | | **0.006** | | | **0.63** | | | **0.82** | | | **0.30** | | | **2.9** | | |
| SD : | 0.09 | | | 0.003 | | | 0.17 | | | 0.59 | | | 0.04 | | | 1.1 | | |
| RSD [%] : | 12.6 | | | 46.7 | | | 28 | | | 72 | | | 14 | | | 39 | | |

Italics are suspected to be contaminated.

**Table 3.10** Zinc, Pb, Bi, In, Tl and Cd abundances for R chondrites of this study. Zn, Pb, In, Tl and Cd were determined by isotope dilution technique whereas Bi was determined from Pb/Bi ratio.

| R chondrites | Type | Weathering* | Zn (ppm) | Pb (ppm) | In (ppb) | Bi (ppb) | Cd (ppb) | Tl (ppb) |
|---|---|---|---|---|---|---|---|---|
| This work | | | | | | | | |
| PRE 95411.21 | R3 | A/B | 164 ± 1 | 1.33 ± 0.03 | 44.5 ± 1.2 | 57.4 ± 0.6 | 527 ± 16 | 112.3 ± 1.3 |
| ALH 85151.41 | R3.6 | B(wi2) | 172 ± 1 | 1.26 ± 0.03 | 36.9 ± 0.5 | 53.6 ± 0.9 | 238 ± 10 | 51.4 ± 1.0 |
| Y 793575.44 | R3.8 | (wi4) | 164 ± 1 | 0.373 ± 0.033 | 15.8 ± 0.4 | 13.6 ± 0.4 | 77.8 ± 7.3 | 2.41 ± 0.94 |
| Y 983270.56 | R4 | A | 156 ± 2 | 0.942 ± 0.034 | 31.5 ± 4.1 | 42.4 ± 0.5 | 258 ± 9 | 42.0 ± 1.0 |
| A 881988.68 | R4 | (wi3) | 161 ± 1 | 1.04 ± 0.03 | 32.9 ± 0.9 | 34.4 ± 0.5 | 243 ± 10 | 2.90 ± 0.94 |
| MIL 07440.8 | R4 | Be | 166 ± 2 | 1.05 ± 0.03 | 29.1 ± 3.6 | 46.3 ± 0.7 | 232 ± 10 | 7.49 ± 0.95 |
| LAP 03639.33 | R4 | A/B | 150 ± 1 | 0.948 ± 0.034 | 25.3 ± 1.1 | 64.8 ± 0.9 | 230 ± 9 | 6.63 ± 0.95 |
| Y 983720.81 | R4 | A | 156 ± 1 | 0.950 ± 0.034 | 29.9 ± 0.9 | 39.0 ± 0.6 | 228 ± 19 | 35.6 ± 1.0 |
| Y 983097.81 | R5 | A | 174 ± 2 | 0.963 ± 0.007 | 12.1 ± 0.3 | 16.8 ± 0.5 | 20.0 ± 1.5 | 2.88 ± 0.08 |
| LAP 04840.12 | R6 | A/B | 168 ± 2 | 0.807 ± 0.008 | 38.9 ± 0.6 | 26.9 ± 0.4 | 179 ± 2 | 37.4 ± 0.3 |
| MIL 11207.8 | R6 | Ce | 167 ± 1 | 2.28 ± 0.02 | 39.5 ± 0.7 | 49.3 ± 0.7 | 215 ± 3 | 17.2 ± 0.1 |
| Y 980702.61 | R6 | ? | 133 ± 1 | 0.864 ± 0.008 | 28.3 ± 0.5 | 25.8 ± 0.5 | 170 ± 2 | 6.17 ± 0.07 |
| Y 980703.71 | R6 | ? | 135 ± 1 | 0.846 ± 0.009 | 28.1 ± 0.4 | 26.7 ± 0.7 | 179 ± 2 | 6.58 ± 0.07 |
| LAP 02238.13 | R | B(wi4) | 161 ± 1 | 1.19 ± 0.01 | 31.8 ± 0.5 | 56.0 ± 1.0 | 291 ± 3 | 51.3 ± 0.3 |
| PCA 91002.64 | R3.8-6 | A/B(wi1) | 156 ± 2 | 1.59 ± 0.01 | 42.3 ± 0.8 | 71.7 ± 0.9 | 556 ± 5 | 84.1 ± 0.5 |

Uncertainties (1σ) are due to standard deviation of 20 scans of single sample by ICP-MS (iCAP – Thermo Scientific) and for blank correction.

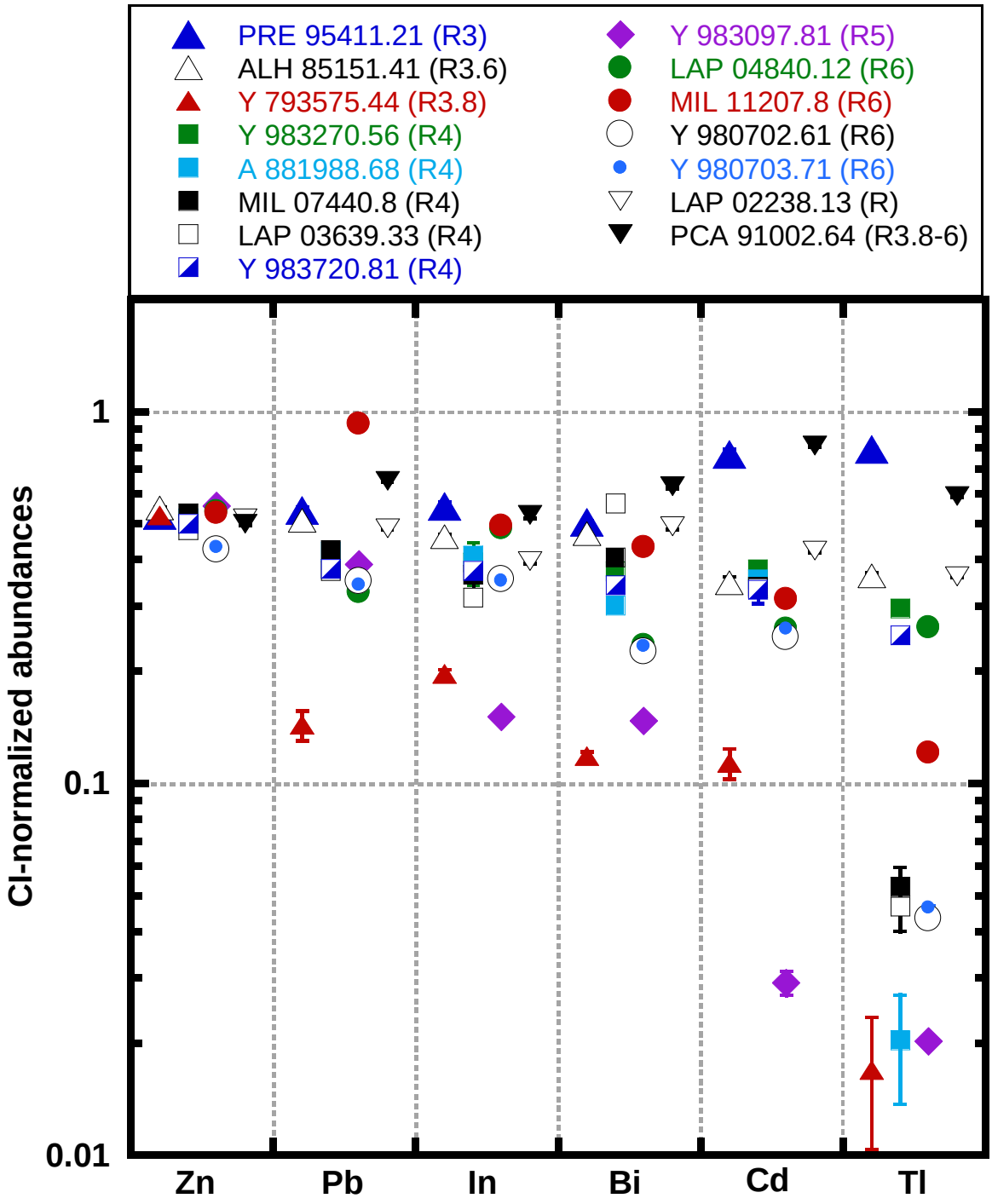


**Fig. 3.4:** CI-normalized abundances of Zn, Pb, Bi, In, Tl and Cd in a petrologic suite of R chondrites. Triangles represent R3 – R3.8, squares represent R4, diamonds represent R5, circles represent R6.

# Chapter-4

## Discussion

### 4.1 Comparison with Literature data and possible terrestrial weathering

Out of the 15 R chondrites of this study, PRE 95411, LAP 03639 and LAP 04840 (Isa et al., 2014), ALH 85151 (Rubin & Kallemeyn, 1989) and PCA 91002, Y 793575 (Kallemeyn et al., 1996) were previously analyzed by instrumental neutron activation analysis. In Fig. 4.1, elemental abundances of this study are normalized to the respective literature data. From Isa et al., 2014, no data for Mg, Al and V are available. In the literature-normalized plot, most of the data are in good agreement with those of literature data except that for Au and Br. In Table 4.1, scattered values of Au are shown from this study and the literature data as well. Even the different replicates of a same meteorite show very scattered abundance (Rubin et al., 1989; Kallemeyn et al., 1996, Xiao and Lipschutz, 1992) for Au. Rubin and Kallemeyn, 1994 suggested that the heterogeneities in Au abundances were caused by terrestrial weathering, i.e., that Au was redistributed in the meteorites by ground water transportation and electrochemical precipitation. Bromine values in R chondrites are appreciably scattered in this study as well as in literature data. These scattered values are also suspected to be a result of terrestrial weathering. Other than Au and Br, in Y 793575 and A 881988, Ni and Co abundances show some variation compared with that of literature data. In calculating the mean Ni and Co abundances in R chondrites, Isa et al. (2014) rejected the values from Y 793575 and A 881988, suspecting a probable weathering.

**Table 4.1** Scattered gold abundances in R chondrites

| R chondrites | This study [ppb] | Literature data [ppb] |
|---|---|---|
| PCA 91002.64 | 174 | |
| PCA 91002.20[a] | | 34.0 |
| PCA 91002.20[a] | | 194 |
| PCA 91002.23[a] | | 242 |
| PCA 91002.23[a] | | 62.0 |
| | | |
| Y-793575.44 | 62.5 | |
| Y-793575.100[a] | | 107 |
| Y-793575.100[a] | | 125 |
| | | |
| ALH 85151.41 | 73.0 | |
| ALH 85151.5[b] | | 73 |
| ALH 85151.5[b] | | 71 |
| ALH 85151.15[c] | | 136 |

[a]Kallemeyn et al., 1996; [b]Rubin et al., 1989
[c]Xiao and Lipschutz, 1992

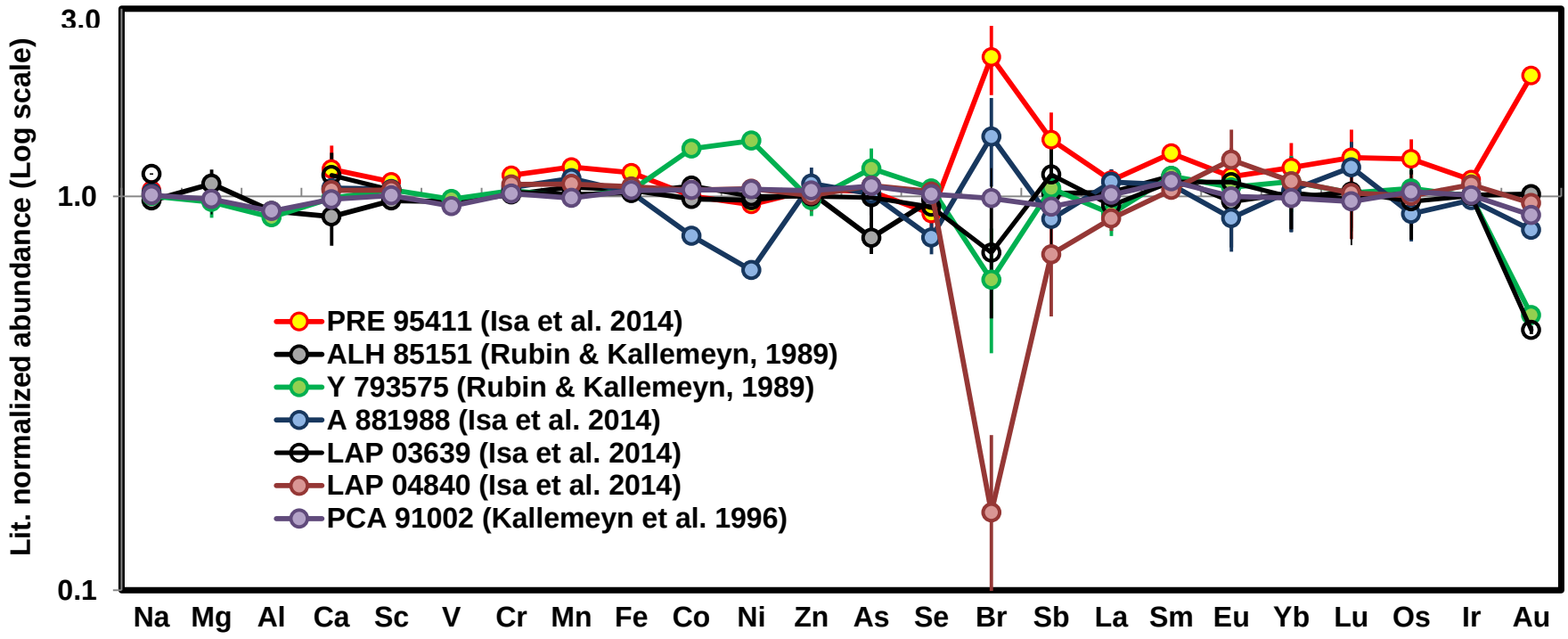


**Fig. 4.1** Bulk chemical composition of this study is normalized by the literature data for comparison. PRE 95411, LAP 03639, LAP 04840 (Isa et al., 2010), ALH 58150 (Rubin & Kallemeyn, 1989), Y-793575, PCA 91002 (Kallemeyn et al., 1996) are the common R chondrites in this work.

Rumuruti is the only fall R chondrite so far (Schulze et al., 1994) and is terrestrially unweathered. In Fig 4.2 Rumuruti normalized elemental abundances in R chondrites of this study along with the literature data (Rubin and Kallemeyn, 1989; Rubin and Kallemeyn, 1994; Kallemeyn et al., 1996; Isa et al., 2014 and Palme et al., 1996) are plotted. Yellow circles with red outlining represent the R chondrites of this study whereas the blank circles represent the literature data. For normalization, Rumuruti abundances were taken from Kallemenyn et al. (1996). For most of the elements, elemental abundances of this study lie within the 20% limit of the Rumuruti chondrite. The spreading of the abundances in Fig 4.2 also represents the analytical uncertainty. But the analytical uncertainties (1σ, counting statistics) for Au, Co and Ni are <3.0%, <1.0% and <2.0%, respectively. So the large variation of Au abundances in this study as well as in previous work is probably due to terrestrial weathering. For Co and Ni, only in few cases depleted abundances are observed which are not due to analytical uncertainties.

The analytical uncertainties for Br is ~30%, but the variations of Br abundances in Rumuruti normalized plot (Fig 4.2) are more than 30%. So, Br in R chondrites is suspected to be terrestrially altered. For Arsenic and Sb, the analytical uncertainties range from 20 to 25% which are comparable with their variations in Fig 4.2. Sodium, Mn, Zn and Se abundances of this study are consistent with those of literature data (Fig 4.1 and 4.2).

In this study, Pb abundances were determined by isotope dilution technique assuming the same Pb isotopic composition in R chondrites as in Allende. Four isotopes ($^{204}$Pb, $^{206}$Pb, $^{207}$Pb and $^{208}$Pb) were monitored in ICP-MS experiment and the spike was enriched with $^{207}$Pb. So, Pb abundances were measured from $^{204}$Pb/$^{207}$Pb, $^{206}$Pb/$^{207}$Pb and $^{208}$Pb/$^{207}$Pb isotopic ratio. For all R chondrites, Pb abundances obtained from $^{204}$Pb/$^{207}$Pb, $^{206}$Pb/$^{207}$Pb and $^{208}$Pb/$^{207}$Pb isotopic ratio are internally consistent, except for MIL 11207.8. In Fig 4.3, Pb abundances (in ppm) are plotted obtained from different isotopic ratios where MIL 11207.8 is far away from the regression line. A reasonable assumption is that Pb isotopic composition in MIL 11207.8 was somehow changed due to terrestrial weathering. Its weathering category is Ce (Severe rustiness with the presence of evaporates) which is also concomitant with the terrestrial alteration.

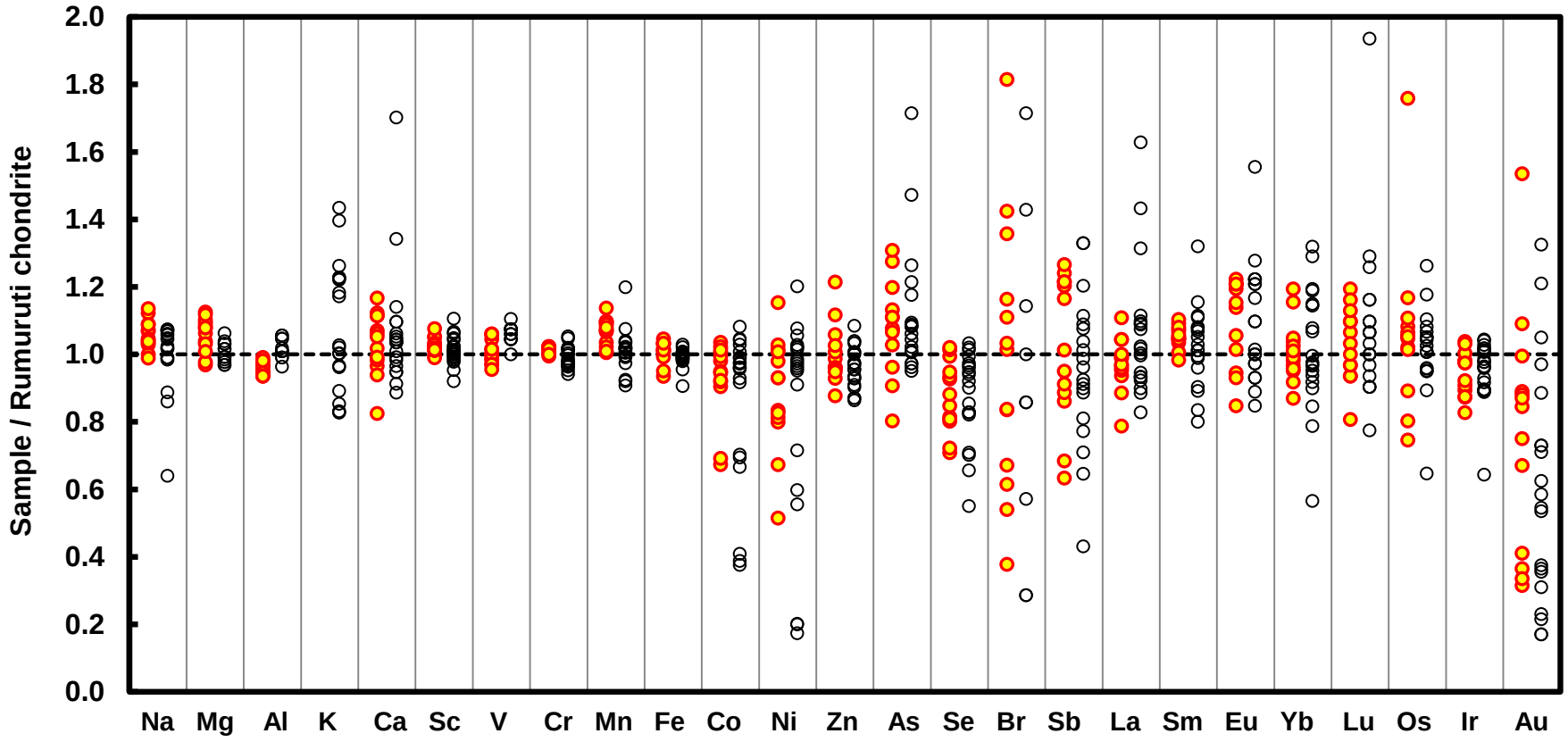


**Fig. 4.2** Rumuruti normalized elemental abundances for R chondrites. Yellow circles with red outline represent the R chondrites analyzed in this study and the blank circles represent the previous works (Rubin and Kallemeyn, 1989; Rubin and Kallemeyn, 1994; Kallemeyn et al., 1996; Isa et al., 2014 and Palme et al., 1996).

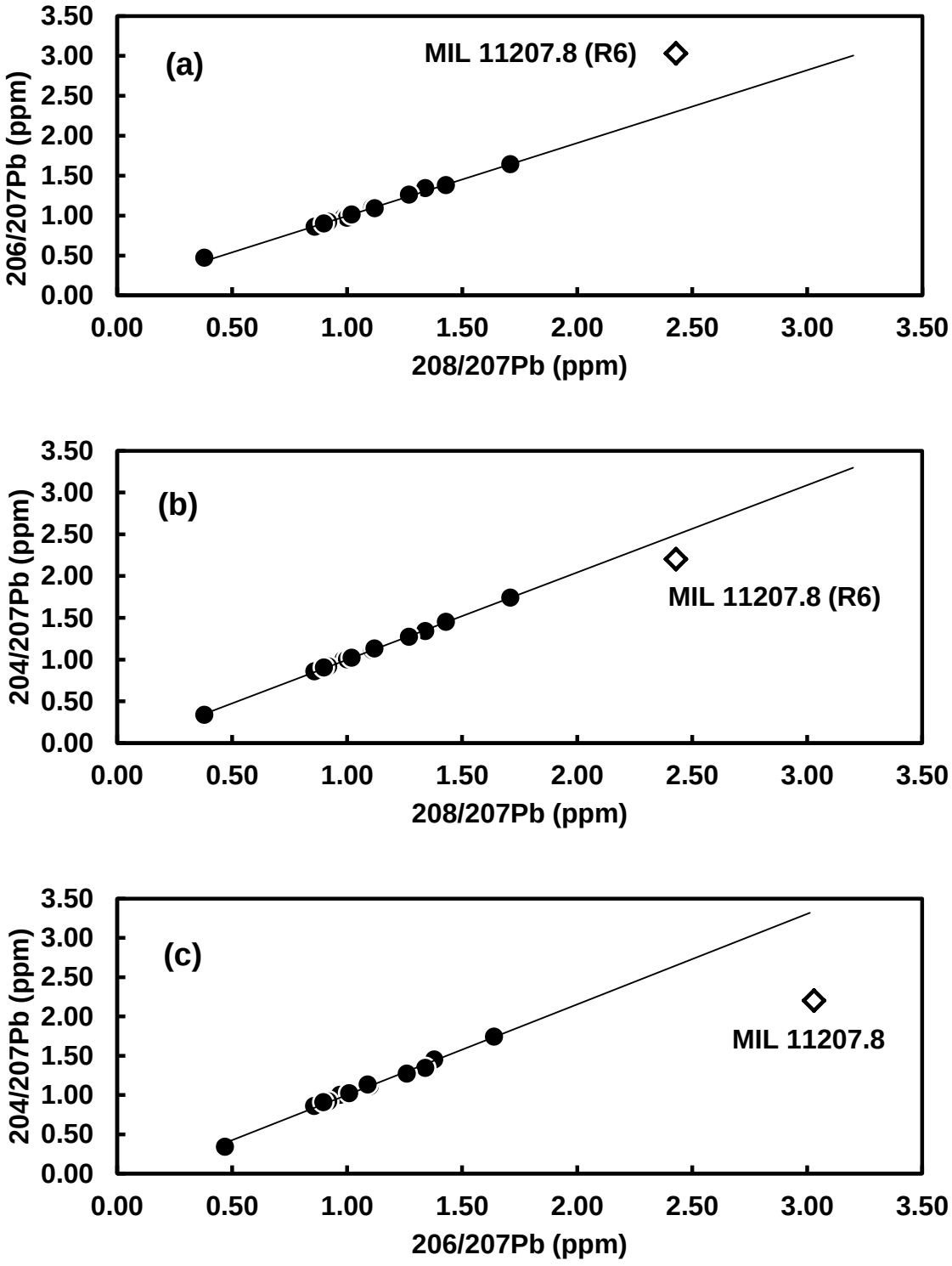


**Fig. 4.3** Lead abundances in R chondrites have determined by isotope dilution method assuming the same isotopic compositon in R chondrites as in Allende. Using $^{207}$Pb spike, we measured Pb abundance from $^{204}$Pb/$^{207}$Pb, $^{206}$Pb/$^{207}$Pb and $^{208}$Pb/$^{207}$Pb ratios. For all R chondrites Pb abundances are internally consistent, except for MIL 11207.8 which implies that MIL 11207.8 possesses a different Pb isotopic composition compared with those of other R chondrites. A simple explanation is Pb isotopic composition of MIL 11207.8 is altered by terrestrial weathering.

### 4.2 Taxonomic study: A bulk chemical composition approach

Kallemeyn et al. (1996) showed that Zn/Mn vs. Al/Mn plot can distinguishe the established chondritic groups as Al, Mn and Zn are widely separated in terms of nebular condensation temperatures. In Fig. 4.4 R chondrites of this study are well fit with the R chondrite classification depending on the bulk chemical compositions.

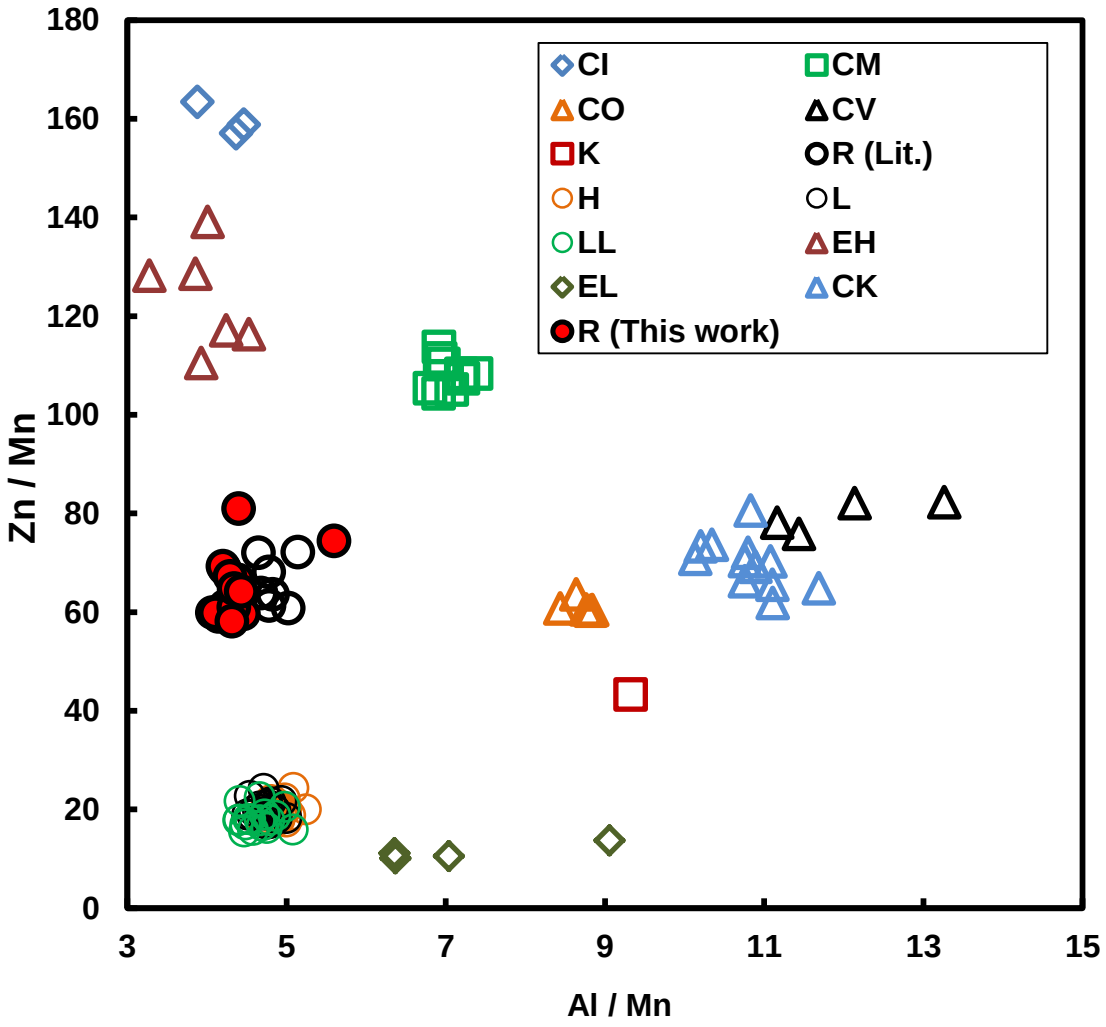


**Fig. 4.4** Various chondritic groups from distinct compositional clusters on a plot of Zn/Mn vs. Al/Mn along with the R chondrites of this study and of previous works (Rubin and Kallemeyn, 1989, 1994; Bischoff et al., 1994, Schulze et al., 1994; Kallemeyn et al., 1996; Palme et al., 1996; Isa et al., 2014). These three elements are widely separated in terms of nebular condensation temperatures (Al > Mn > Zn). R chondrites of this study tightly clustered with literature works and widely separated from that of other established chondritic groups (Kallemeyn and Wasson, 1981, 1986; Kallemeyn et al., 1989, 1991).

## 4.3 Nebular processes

### 4.3.1 Oxidation

Figure 4.5 shows the correlation of Zn and Se contents in various types of chondrites. Selenium is a chalcophile and mostly partitioned into the sulfide while Zn is found in almost all sorts of mineralogical phases in meteorites (Allen and Mason, 1973). Both of them share the same nebular condensation temperature (McSween and Huss, 2010), but they are fractionated. Enstatite chondrites are the most reduced chondritic meteorites whose Se abundances are comparable with those in the most oxidized noncarbonaceous R chondrite. But Zn abundances in R chondrite are remarkably higher than those in EL chondrite and comparable with CM chondrite abundances. Higher stability of ZnO in oxidized condition can be a plausible explanation for this Zn enrichment.

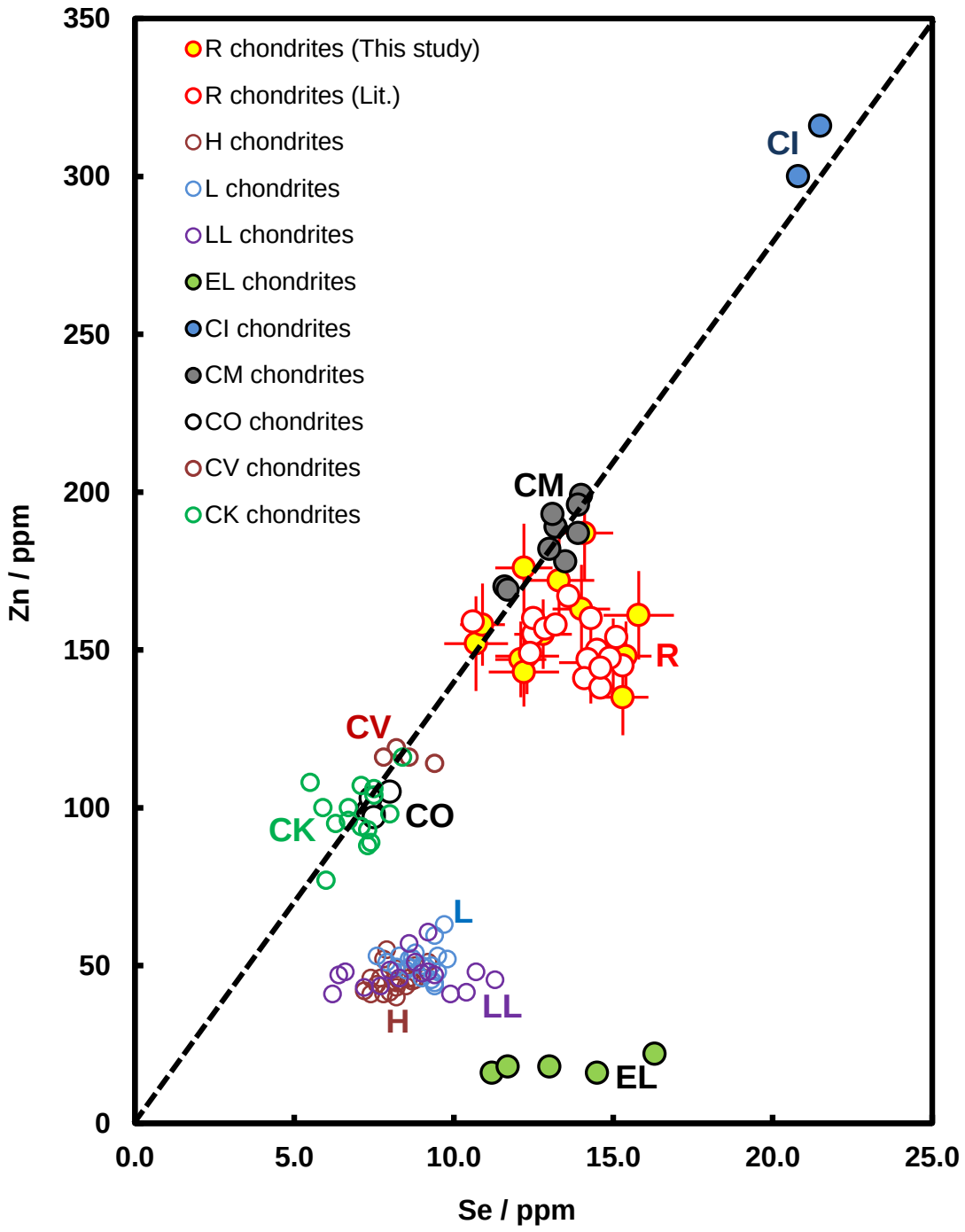


**Fig. 4.5** Zinc vs. Selenium plot for various chondritic groups along with the R chondrites of this study and of previous works (Rubin and Kallemeyn, 1989, 1994; Bischoff et al., 1994, Schulze et al., 1994; Kallemeyn et al., 1996; Palme et al., 1996; Isa et al., 2014). R chondrites are closely lying to the carbonaceous chondrite line and are distinctly separated from ordinary chondrites (Kallemeyn and Wasson, 1981, 1986; Kallemeyn et al., 1989, 1991).

### 4.3.2 HREE-LREE fractionation

It can be noticed that heavy rare earth elements (HREEs) are faintly enriched compared with light rare earth elements (LREEs) (Fig. 3.2). CI-normalized Nd/Yb and Pr/Tm ratios are plotted in Fig. 4.3. These ratios for R chondrites are systematically lower than CI values. Apparently, HREEs (represented by Tm and Yb) are enriched compared with LREEs (represented by Pr and Nd). In our ICP-MS experiment, we have corrected the interferences from LREE (oxides & hydroxides) and Ba on HREE determination, although in most of the cases such interference is less than 1%.

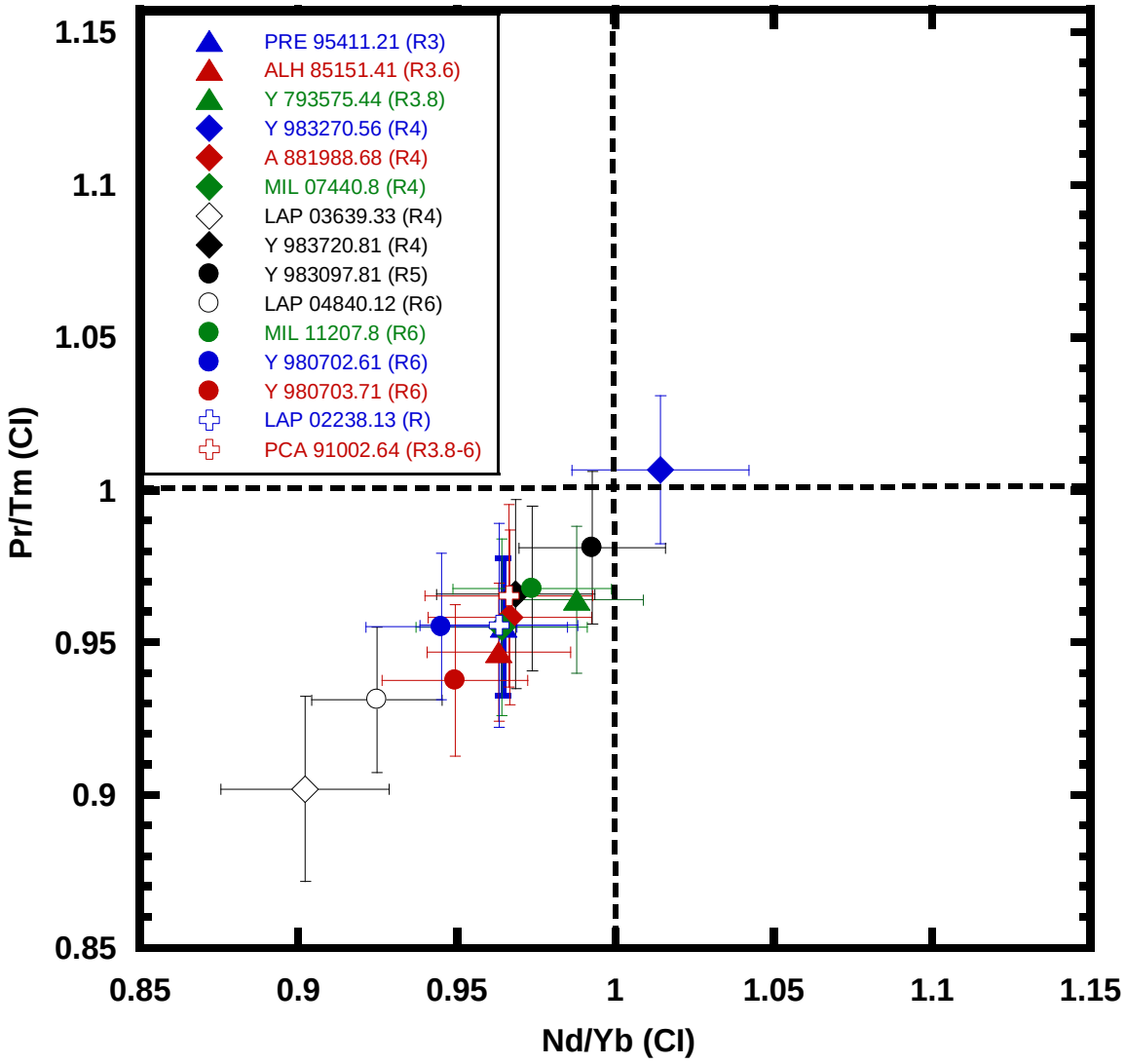


**Fig. 4.6** CI normalized (Anders and Grevesse, 1989) Pr/Tm-Nd/Yb plot to represent the HREE enrichment (represented by Tm and Yb) compared with that of LREE (represented by Pr and Nd). Here triangle presents the petrologic type 3, diamonds for type 4, circles for type 5 and 6, and blank plus for brecciated R chondrites.

Two possible explanations can be given for such HREE-LREE fractionation: (1) As La and other common REEs reside primarily in Ca-phosphate and to lesser extent in Ca-pyroxene in metamorphosed ordinary chondrites (Ebihara and Honda, 1983, 1984), it can be considered that the faint HREE-LREE fractionation observed here may be due to the heterogeneous distribution of these minerals in R chondrites. If this is so, the relative standard deviations (RSDs) for specific REEs in highly metamorphosed R chondrites (R5 – R6) should be lower compared with those of RSDs in R chondrites (R3 – R4) of low metamorphic grade. But in this study, no such significant variations have been observed. (2) Nebular process can be responsible for such small HREE-LREE fractionation in R chondrites. To explain the nebular process in R chondrites, an analogically well explained fractionated pattern of REEs, Th and U abundances in Allende meteorite can be considered. In Allende, HREEs are depleted compared with LREEs (Fig. 2.3). According to Boynton (1975) and Davis and Grossman (1979), high temperature early condensates (e.g., perovskite, hibonite, corundum etc.) enriched in refractory HREEs could have been removed from the nebular gas, making the remaining gas enriched in less refractory LREEs. It is likely that the Allende parent body formed from such later condensates of the remaining gas. In R chondrites, the inclination of CI-normalized REE pattern is opposite to the Allende pattern (except positive Tm anomaly) (Fig. 3.2). A simple interpretation is that R chondrites formed in the nebula where early condensates were relatively abundant.

### 4.3.3 Thorium-Uranium fractionation

REE fractionation pattern in R chondrites is opposite to that of Allende, however, Th-U fractionation patterns are the same both in R chondrites and in Allende. In the seven replicate measurements of Allende powder of this study, Th/U ratio is 4.10 ± 0.20 and is consistent with the literature (Tatsumoto et al., 1973, Shinotsuka et al., 1995; Makishima & Nakamura, 2006; Dauphas & Pourmand, 2011 and Barrat et al., 2012) value (3.90 ± 0.20). In R chondrites of this study, Th/U ratio is 3.81 ± 0.13.

Thorium and Er have the same nebular condensation temperature while U is less refractory compared with Th and Er (McSween and Huss, 2010). In Fig. 4, CI-normalized Th/Er and U/Er ratios are plotted. Obviously U/Er values are smaller but Th/Er values are larger than their corresponding CI ratios for most R chondrites. This suggests that in R chondrites Th and U are fractionated from CI chondrite values.

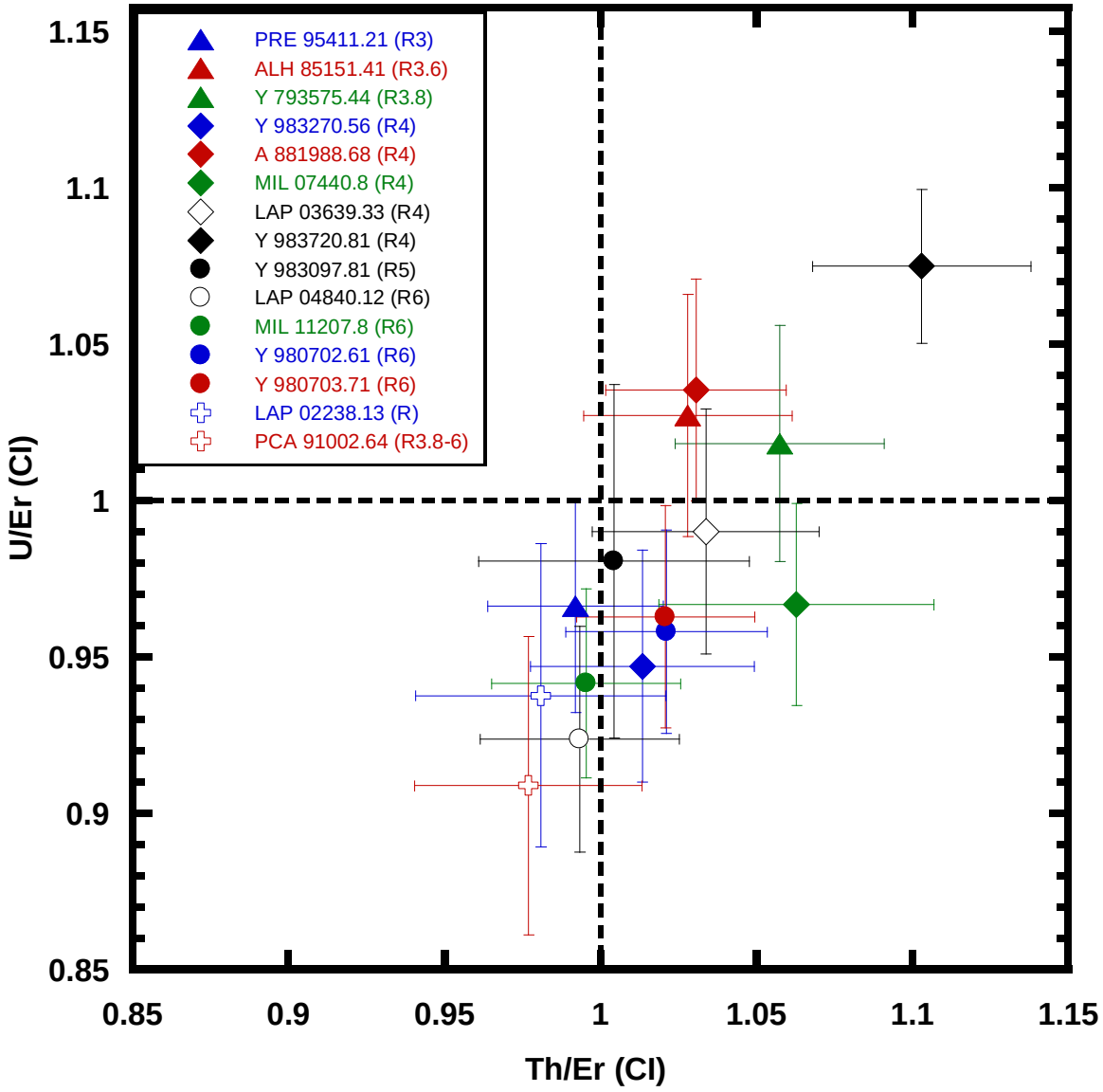


**Fig. 4.7** CI normalized (Anders and Grevesse, 1989) U/Er-Th/Er plot to represent the thorium-uranium fractionation in R chondrites. Here triangle presents the petrologic type 3, diamonds for type 4, circles for type 5 and 6, and blank plus for brecciated R chondrites.

### 4.4 Systematic variation of volatile elements in R chondrites

Among the 15 R chondrites of this study, MIL 11207.8 is heavily altered by terrestrial weathering. Y 793575.44 and LAP 02238.13 also represent some terrestrial alteration (Table 2.1). Gold abundances in Y 793575 is very low whereas in MIL 11207 is high. The same trend is observed in Fig. 4.8 for Pb, Bi, In, Tl and Cd abundances. So it would be a reasonable assumption that these two meteorites (MIL 11207 and Y 793575) are terrestrially altered than the other R chondrites in this study. Earlier works by Purdue and Chicago groups showed that the volatile elements are not much altered in lightly weathered finds (Laul et al., 1970; Keays et al., 1971; Case et al., 1973; Laul et al., 1973; Binz et al., 1976; Takahashi et al., 1798 etc.). So the rests of the R chondrites are not heavily altered and the volatile elements represent their pristine abundances. If highly weathered MIL 11207 and Y 793575 are disregarded, then we can observe a systematic variation of Pb, Bi, In, Tl and Cd in Fig. 4.8. In Fig. 4.8 brecciated and type 3 R chondrites are both showed by triangles as their volatile elements abundances are comparable with those of petrologic type 3. It would be reasonable to assume that LAP 02238.13 and PCA 91002.64 belong to type 3 clast.

In Fig 4.9 average CI-normalized abundances of petrologic type 3, 4 and 5/6 are plotted. MIL 11207.8 and Y 793575.44 are excluded from the average and LAP 02238.13 and PCA 91002.64 are included in type 3 average. Refractory siderophile elements (Ir, Co, Ni) and moderately volatile elements (Au, Se, Zn) do not show any fractionation within the petrologic types 3 to 6. But highly volatile elements (Pb, Bi, In, Tl, Cd) show fractionation within the petrologic types. Sometimes it is difficult to separate the petrologic types 3 from 4 or petrologic types 4 from 5/6, but petrologic types 3 and 6 can easily be distinguished from their volatile elements abundances. So, in the petrologic suite of R chondrites of this study, volatile elements are more depleted in higher petrologic types compared with those of lower petrologic types.

Other than volatile elements, in Fig. 4.8 and 4.9, refractory siderophile elements (Ir, Co and Ni) and moderately volatile element Au are plotted. Being siderophile elements, Ir, Co, Ni and Au are generally partitioned into the metal phase of chondrites. But R chondrites have almost no metal phase. So, the siderophile elements are believed to be partitioned into sulphides. Except Au, other siderophile elements are terrestrially unaltered (with very minor exception for Co and Ni). Among the volatile elements Zn, Bi and Cd are considered as lithophile; Se, In and Tl are chalcophile and only Pb is considered to be a

siderophile (Lodders et al. 2009). Selenium and Zn are unfractionated within the petrologic suite of R chondrites whereas Pb, Bi, In, Tl and Cd show systematic variation. The general trend for Pb and Bi are similar to that of In, Tl and Cd. So we can reasonably assume that the systematic variation of volatile elements with the petrologic types is not due to the terrestrial weathering. Two possible explanations can be given for such systematic variation- accretional condensation and (/or) parent body heating.

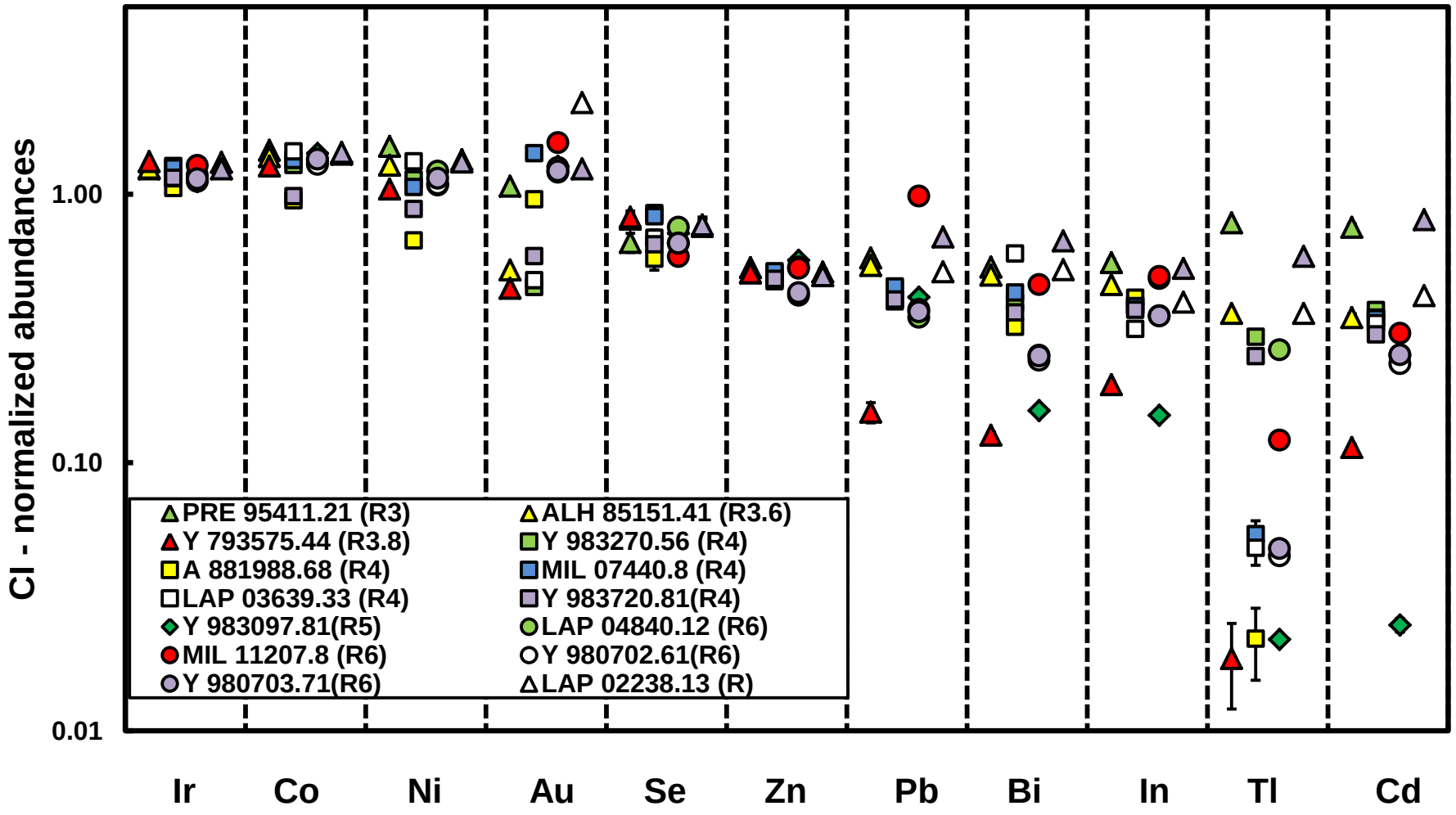


**Fig. 4.8** CI-normalized abundances of Ir, Co, Ni, Se, Zn, Pb, In, Bi, Cd and Tl in a petrologic suite of R chondrites. Triangles represent R3 – R3.8, squares represent R4, diamond represents R5 and circles represent R6 R chondrites.

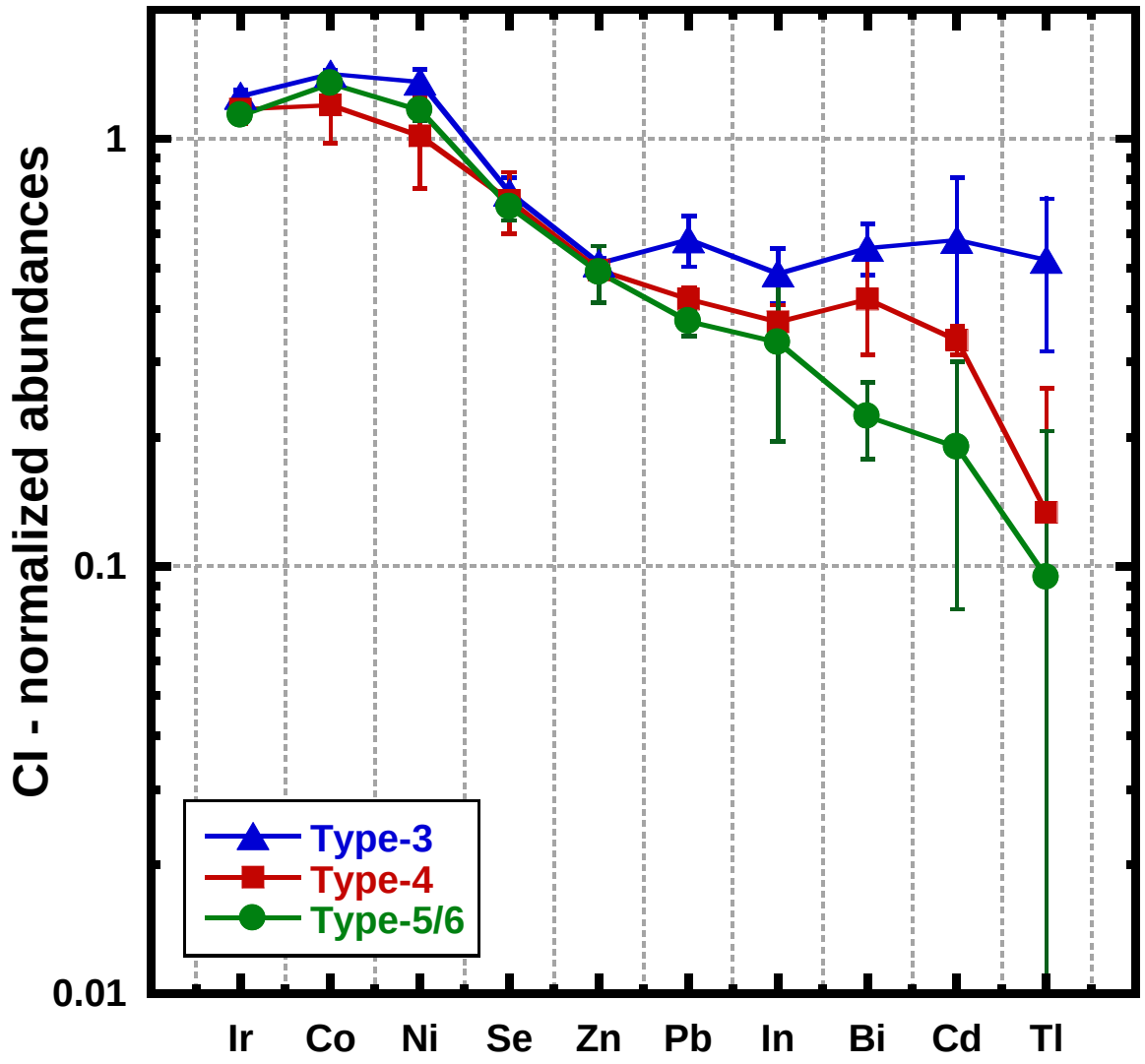


**Fig. 4.9** CI-normalized abundances of Ir, Co, Ni, Se, Zn, Pb, In, Bi, Cd and Tl in a petrologic suite of R chondrites. Type-3 is represented by blue triangles and is the average of PRE 95411.21, ALH 85151.41, LAP 02238.13 and PCA 91002.64. Type 4 is represented by red squares and is the average of Y 983270.56, A 881988.68, MIL 07440.8, LAP 03639.33 and Y 983720.81. Type 5/6 is represented by green circles and is the average of Y 983097.81, LAP 04840.12, Y 980702.61 and Y 980703.71. Error bars are due the standard deviation of corresponding R chondrites. Refractory siderophiles (Ir, Co, Ni) and moderately volatiles (Se, Zn) do not show any fractionation within the petrologic type 3 to 6. But highly volatile elements (Pb, Bi, In, Tl, Cd) show fractionation within the petrologic type.

### 4.4.1 Volatile elements abundances in R chondrites: Comparison with Ordinary chondrites

From the INAA data of this study as well as from literature data (e.g., Kallemyn et al. 1996; Isa et al., 2014 etc.), it is quite noticeable that in R chondrites, lithophile elements abundances are comparable to those of ordinary chondrites, siderophile elements abundances are intermediate between H and L chondrites and only volatile elements (Zn and Se) showed significant enrichment compared with those of ordinary chondrites (Fig. 3.1). Bulk chemical compositions of R chondrites obtained from INAA experiment do not show any systematic variation with the petrologic types. But in this study, volatile elements (Pb, Bi, Tl, In and Cd) in R chondrites show a systematic variation with the petrologic types (section 4.3). Tandon and Wasson (1967) also found a systematic variation of In content in a petrologic suite of L chondrites. According to the previous studies (e.g., Greenwood et al., 2000), there is some linkage among the R chondrites and ordinary chondrites. So, the volatile elements abundances (Bi, Tl, In and Cd) of R chondrites are compared with those of ordinary chondrites in Fig. 4.10. Previously volatile elements in chondrites have been studied by RNAA mostly by Anders and Lipschutz and their co-workers (e.g., Keays et al., 1971, Laul et al., 1973, Takahashi et al., 1978 and Kaczaral et al., 1989). So, Pb data were not available from their study. In Fig 4.10a, 4.10b, 4.10c and 4.10d CI-normalized Bi, Tl, In and Cd abundances are plotted, respectively to compare the R chondrites abundances with those of ordinary chondrites. In our sample list, we have only one R chondrite of petrologic type 5.

In Fig. 4.10, for unequilibrated chondrites, CI-normalized Bi, Tl, In and Cd abundances in R chondrites are within the range of ordinary chondrites. But in higher metamorphic grade, CI normalized Bi, Tl, In and Cd abundances in R chondrites are generally higher than those of H, L and LL chondrites with few exception. The higher abundances of volatile elements in equilibrated R chondrites are more prominent for Bi, In and Cd. For Tl, the trend of higher volatile elements abundances in R chondrites is also noticeable (especially for petrologic type 6), but somehow less conspicuous than Bi, In and Cd. References of literature data for H, L and LL chondrites are given in corresponding figure captions.

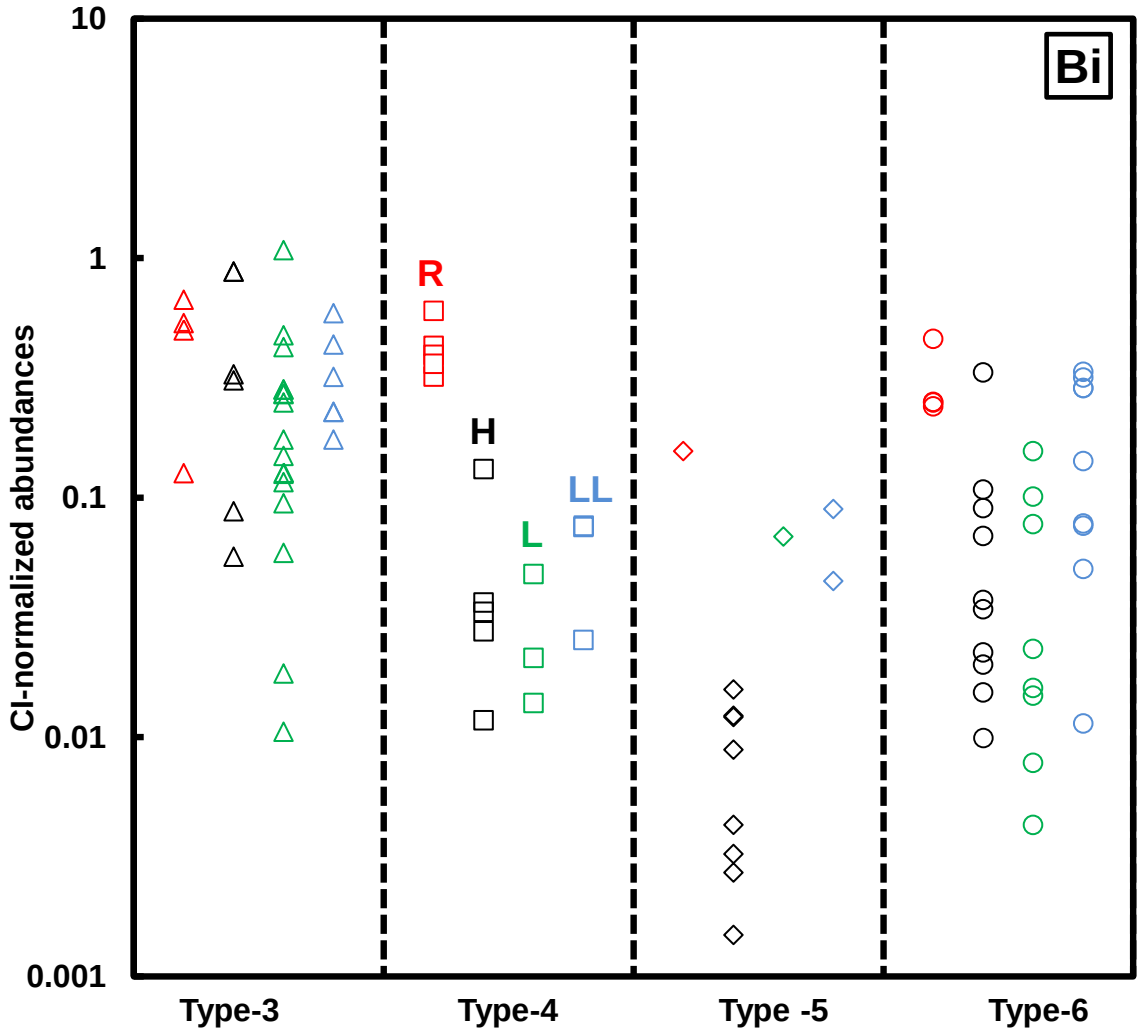


**Fig. 4.10a** CI-normalized abundances of Bi in R chondrites (of this study) are compared with those of H, L and LL chondrites according to their petrologic types. Triangles, squares, diamond and circles represent the petrologic type 3, 4, 5 and 6, respectively. Red, black, green and blue colors represent the R, H, L and LL chondrites, respectively. For H, L and LL chondrites literature values are used from Laul et al., 1973; Wang et al., 2007; Dennison et al., 1987; Laul et al., 1970a and Friedrich et al., 2003.

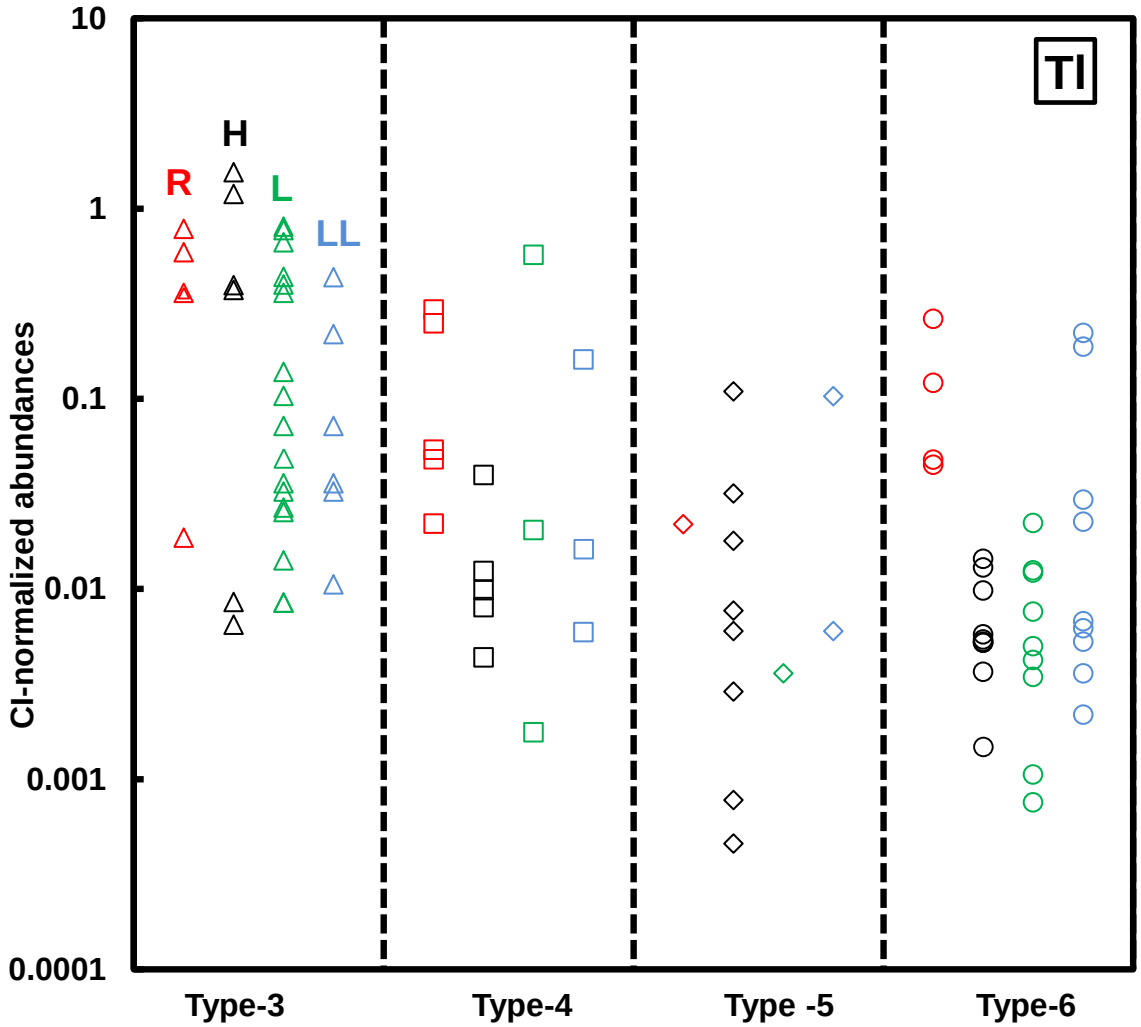


**Fig. 4.10b** CI-normalized abundances of Tl in R chondrites (of this study) are compared with those of H, L and LL chondrites according to their petrologic types. Triangles, squares, diamond and circles represent the petrologic type 3, 4, 5 and 6, respectively. Red, black, green and blue colors represent the R, H, L and LL chondrites, respectively. For H, L and LL chondrites literature values are used from Laul et al., 1973; Wang et al., 2007; Dennison et al., 1987; Laul et al., 1970b and Friedrich et al., 2003.

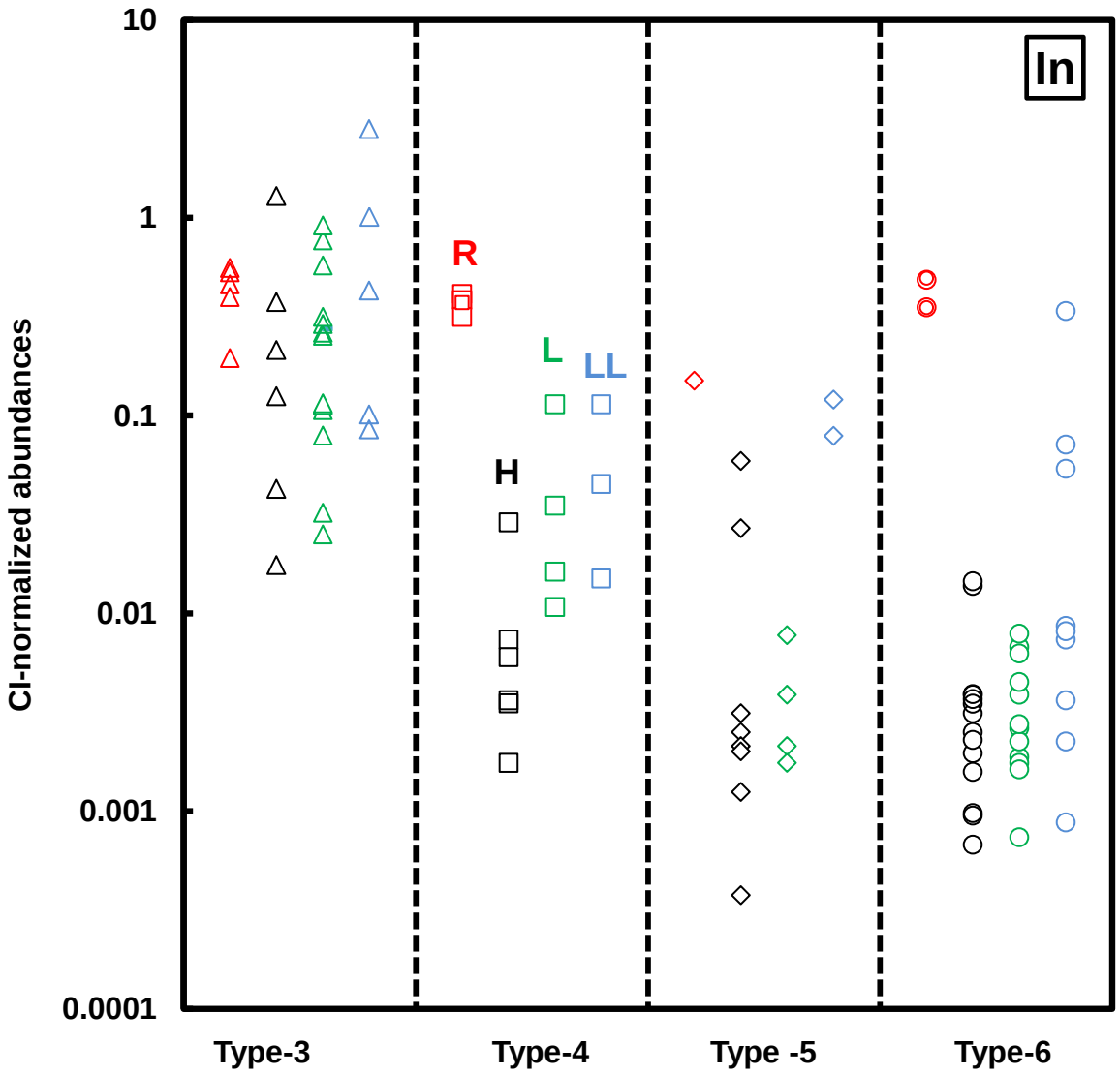


**Fig. 4.10c** CI-normalized abundances of In in R chondrites (of this study) are compared with those of H, L and LL chondrites according to their petrologic types. Triangles, squares, diamond and circles represent the petrologic type 3, 4, 5 and 6, respectively. Red, black, green and blue colors represent the R, H, L and LL chondrites, respectively. For H, L and LL chondrites literature values are used from Laul et al., 1973; Wang et al., 2007; Dennison et al., 1987; Tandon and Wasson, 1967 and Friedrich et al., 2003.

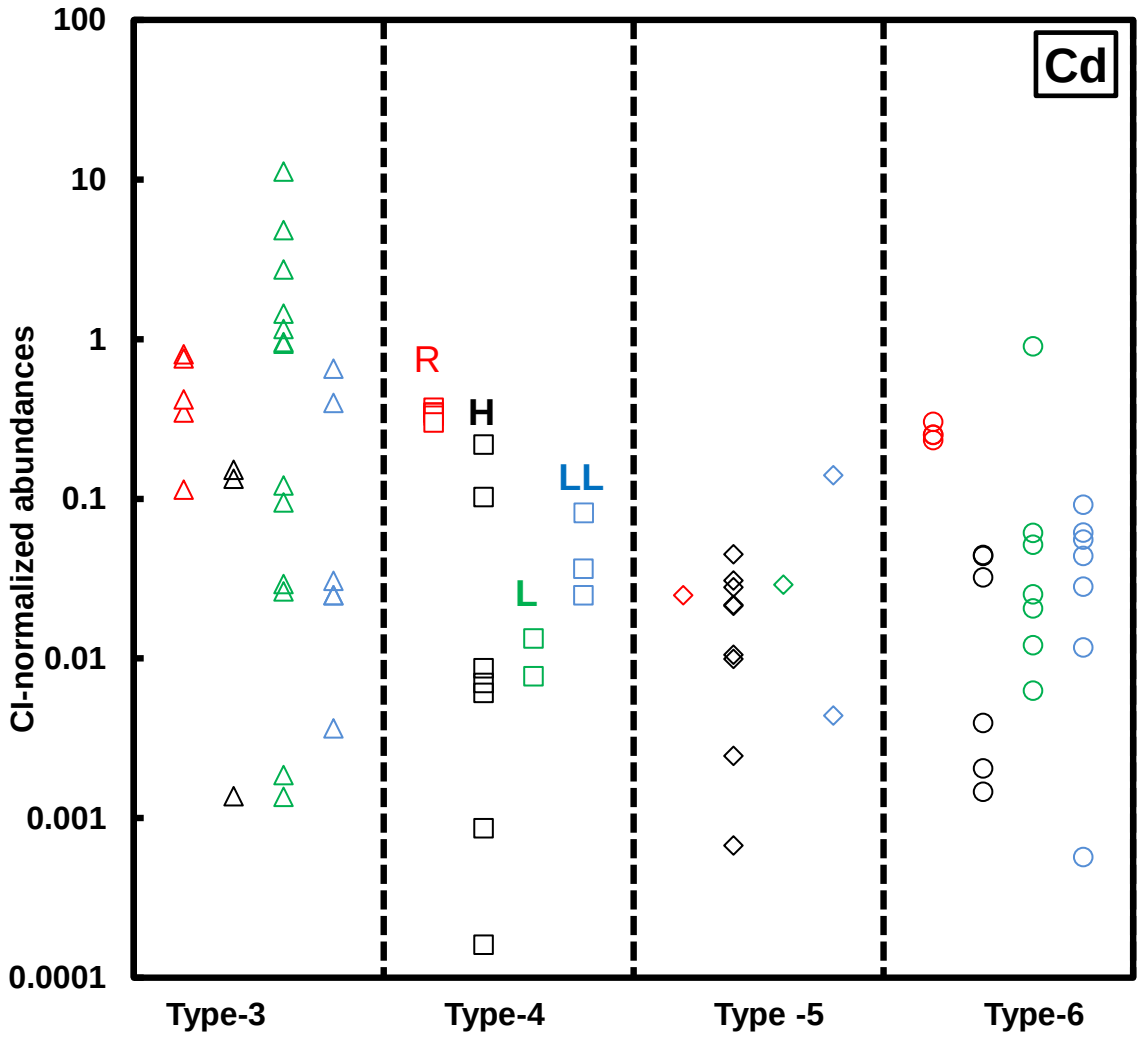


**Fig. 4.10d** CI-normalized abundances of Cd in R chondrites (of this study) are compared with those of H, L and LL chondrites according to their petrologic types. Triangles, squares, diamond and circles represent the petrologic type 3, 4, 5 and 6, respectively. Red, black, green and blue colors represent the R, H, L and LL chondrites, respectively. For H, L and LL chondrites literature values are used from Laul et al., 1973; Wang et al., 2007; Lingner et al., 1987; Dennison and Lipschutz, 1987 and Friedrich et al., 2003.

### 4.4.2 Condensation model

R chondrites and ordinary chondrites show systematic variation of volatile elements abundances with the petrologic types. In contrast to R chondrites and ordinary chondrites, carbonaceous chondrites do not show such variation. Among the carbonaceous chondrites, only CK chondrites are metamorphosed and possessing all petrologic types (CK3 to CK6). Even in CK chondrites no systematic variation of volatile elements abundances were observed with the petrologic types (Isa et al. 2011). Instead of showing systematic variation with petrologic types, carbonaceous chondrites show depletion with constant factor compared with CI meteorite (Larimer and Anders, 1967). To explain the elemental abundance pattern in chondritic meteorites, Anders and Larimer (Anders, 1964; Larimer and Anders, 1967) proposed two component nebular condensation model. According to the two-component model, the elemental abundance pattern was established during accretion from the solar nebula and the condensation was followed by a simultaneous accretion. In a regime of falling temperatures, elements would condense in succession on the fine-grained dust (fraction A), but not on the coarse-grained chondrules-plus-metal (fraction B). The composition of fraction A (low temperature condensate: matrix) would thus vary with temperature, while that of fraction B (high temperature condensate) remains essentially fixed. Meteorites last to accrete would therefore be richest in volatiles. Being situated in the outermost layers of the parent body, they would also be least metamorphosed. Thus a strict, yet non-causal correlation between trace element depletion and metamorphism would result.

To explain the systematic variation of In contents in a petrologic suite of L chondrites, Tandon and Wasson (1968) proposed three component condensation model. In this model elemental abundance pattern was established during accretion, as in the two component model. However, strongly depleted elements were brought in mainly by a third component (fraction C), strongly enriched in all volatile elements. All three components are assumed to have fixed composition. Now we need to evaluate the validity of nebular condensation models for R chondrites:

According to the condensation calculation of Keays et al. (1971) for two component model, the theoretical condensation curve for Tl and Bi has a slope near 1 for low degree of condensation. But once the solubility limit of Bi is reached the curve changes its slope and flattens abruptly then rises very sharply with a slope of 90°. Assuming a three component model, Tl and Bi correlation curve should have 45°. In Fig. 4.11a, observed trend of Tl and

Bi is shown with an arbitrary drawn correlation line of 45° slope. The data points in Fig. 4.11a, seems to be fit for both two and three component model.

From the prediction of three component model, In-Bi curve should have a slope 45°. But in the observed slope of In-Bi curve (Fig. 4.11b) for R chondrites is fairly less than 45°. An even better test is provided by linear three element plots (e.g., X/Z vs. Y/Z), as are commonly used to resolve isotopic components of noble gases. It is a property of such a plot that all compositions obtained by mixing two components of fixed composition lie along a straight line joining the two components. Inasmuch as the volatiles in the three component model are contributed only by fractions A and C, both of fixed composition, three element plots should yield straight lines. But the observe trend (Fig. 4.11c) of Bi/In and Tl/In ratios do not fall on a straight line.

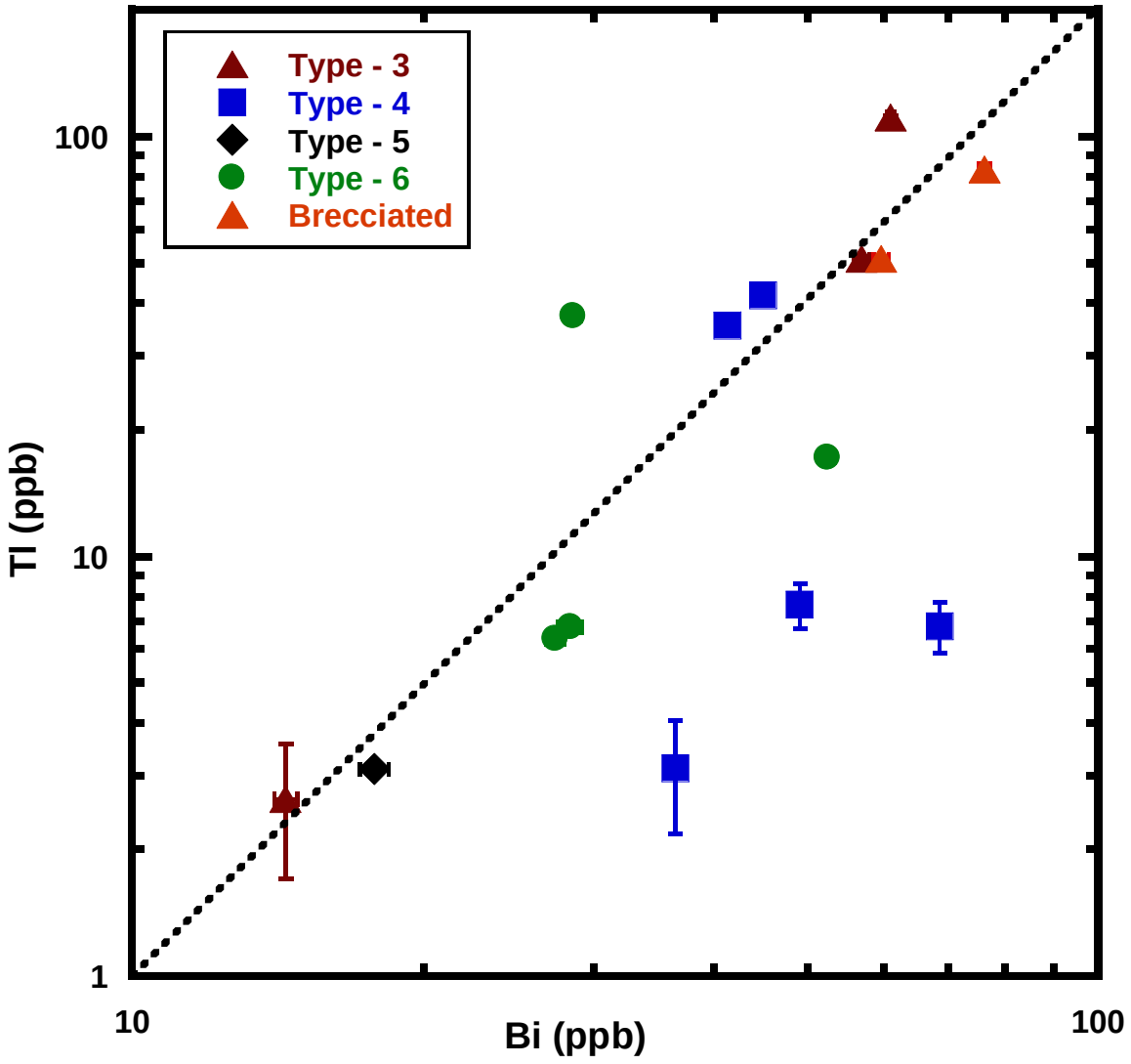


**Fig. 4.11a** Observed trend of Tl and Bi data. Only an arbitrary correlation line (dashed line) is drawn. Brown triangles, blue squares, black diamond, green circles and red triangles represent petrologic types 3, 4, 5, 6 and brecciated R chondrites, respectively.

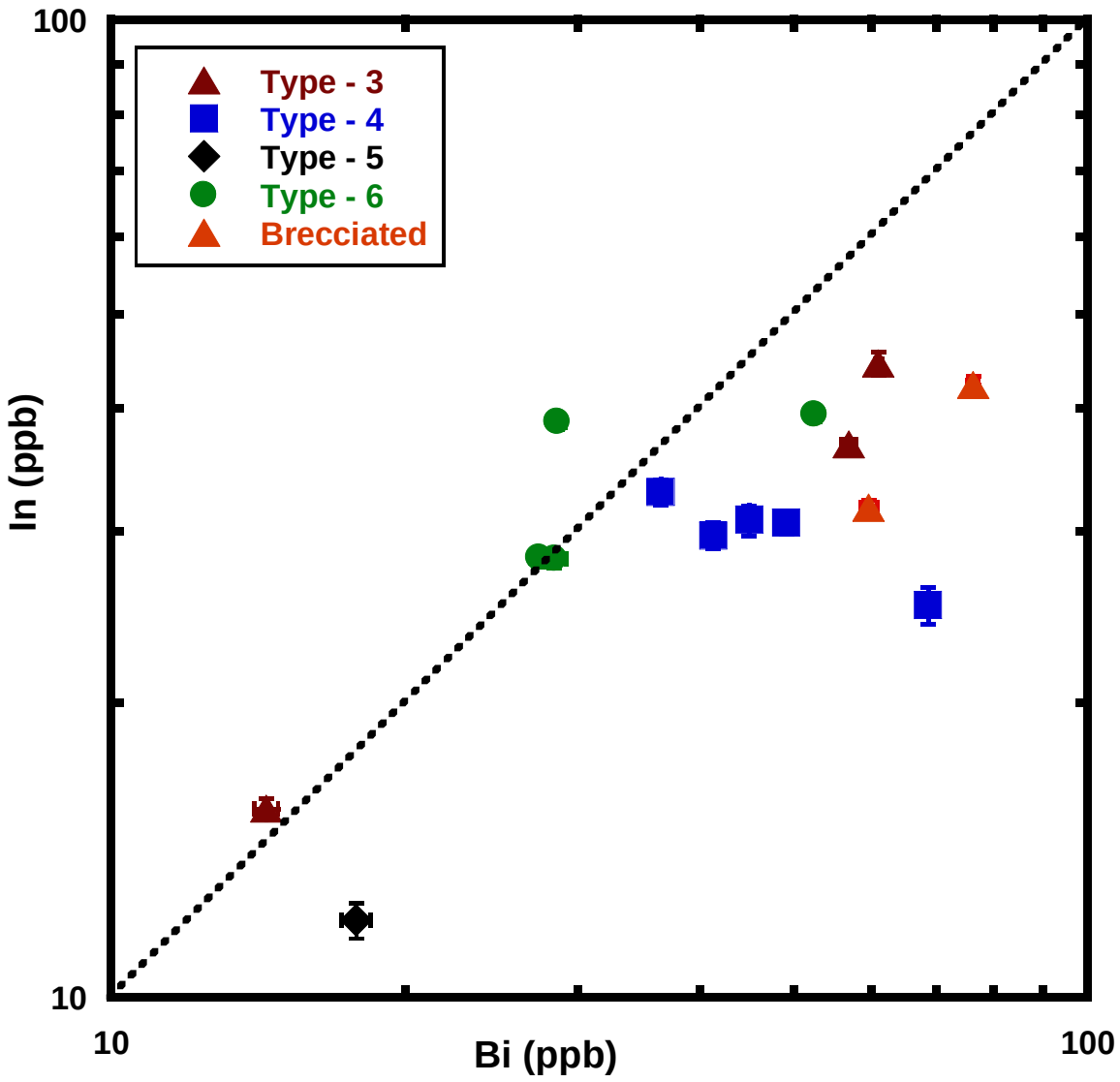


**Fig. 4.11b** Observed trend of In and Bi data. Only a correlation line (dashed line) of slope 45° is drawn arbitrary. Brown triangles, blue squares, black diamond, green circles and red triangles represent petrologic types 3, 4, 5, 6 and brecciated R chondrites, respectively.

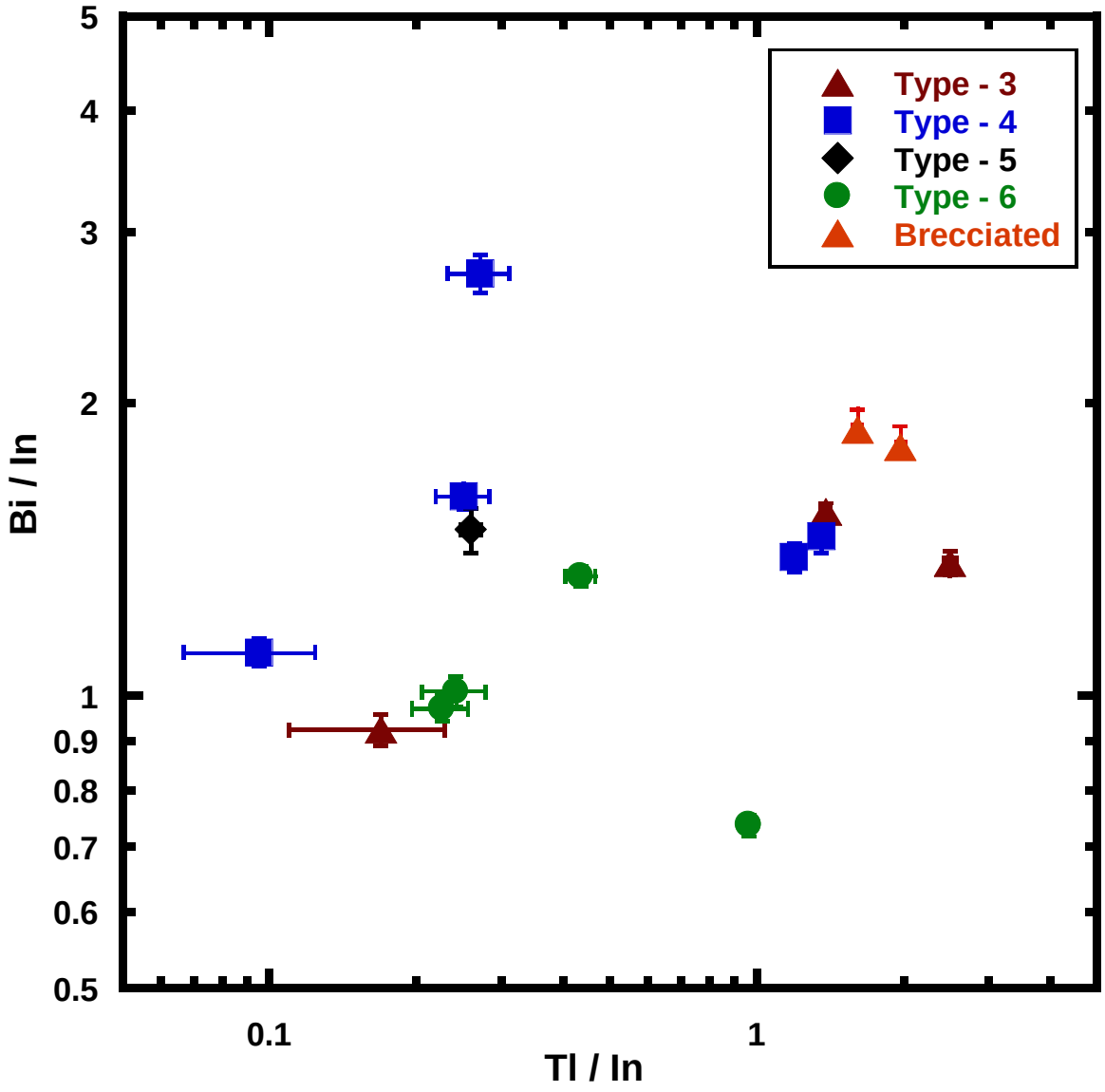


**Fig. 4.11c** Observed trend of Bi/In and Tl/In data. No linear correlation is observed as expected by three component model.

According to the two component model, volatile elements abundances depend on the modal abundance of matrix (fraction A). The modal abundances of matrix are 90%, 70% and 40% in CI, CM and CV chondrites, respectively (Scott and Krot, 2005), which are nearly closer to the two component prediction. In the case of ordinary chondrites, volatile elements are not depleted by a constant factor. So the prediction of 25% modal abundance of matrix component (Larimer and Anders, 1967) is not concomitant with the observed depletion of volatile elements in ordinary chondrites. The modal abundances of matrix are 10-15% and 35% for ordinary and R chondrites, respectively (Scott and Krot, 2005). Two component model is thus an idealized model that can be applicable to carbonaceous chondrites, most efficiently.

### 4.4.3 Metamorphic model

Similar to the ordinary chondrites, volatile elements are not depleted by a constant factor in R chondrites. R chondrites/CI ratios for highly volatile elements (Pb, Bi, Tl, In and Cd) appear to be randomly distributed over the range 0.81 – 0.02. To explain the depletion pattern for ordinary chondrites metamorphism model was proposed (Wood, 1967 and Dodd, 1969). According to this model, all ordinary chondrites initially had the composition and mineralogy of petrologic type 3. The depletion pattern was established during metamorphism, with the most intensely metamorphosed meteorites losing the greatest proportion of volatiles. Later on, Lipschutz and co-workers (e. g., Ikramuddin and Lipschutz, 1975; Ikramuddin et al., 1976, 1977) presented their heating experiments and supported the metamorphism model along with the condensation model. To explain the volatile elements depletion pattern by condensation model followed by metamorphism, a layered parent body with an internal heat source is needed. Based on the experimental observations, Wood (2003) and Trieloff et al. (2003) demonstrated the onion-shell model for H chondrites, where low petrologic type chondrites reside at the outer surface of the parent body while higher petrologic types gradually positioned into the inner portion of the parent body (Fig. 4.12). In the onion-shell model, decay of $^{26}$Al was advocated as the most probable heat source. The signature of $^{26}$Al was proved by the presence of its decay product (excess $^{26}$Mg) in refractory inclusions and chondrules (Russell et al., 1996; Kita et al., 1998). Depending on the model calculation, Miyamoto et al. (1981) drew the same conclusion as Wood (2003) did.

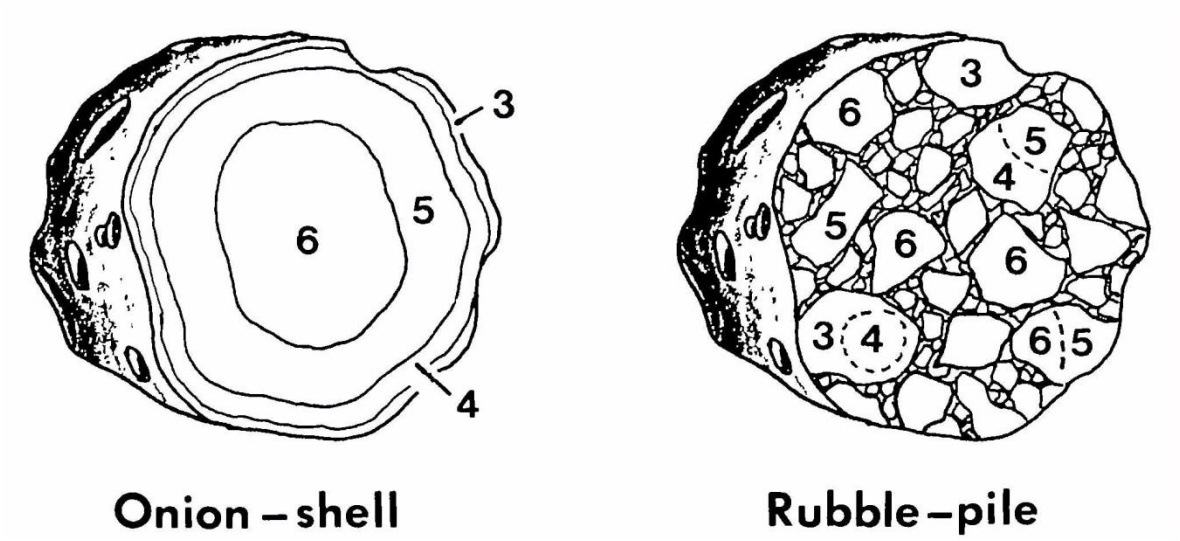


**Fig. 4.12** Sketches of onion-shell and rubble-pile configurations for ordinary chondrite parent bodies. Numbers identified regions of different petrologic type (this figure is taken from McSween and Patchen, (1989) after the permission of Harry Y. McSween)

So, the condensation model followed by thermal metamorphism can be invoked to explain the systematic variation of highly volatile elements in a petrologic suite of R chondrites. Up to this point, there are close similarities between the parent body formation of R chondrites and ordinary chondrites.

CI-normalized volatile elements abundances in unequilibrated R chondrites are comparable with those of unequilibrated ordinary chondrites but with the higher degree of metamorphism, volatile elements abundances are getting higher value compared with those of corresponding metamorphic grade of ordinary chondrites (Fig. 4.10). Two reasonable assumptions can be made at this stage: (1) The agglomeration temperature for R chondrites was lower than ordinary chondrites or, (2) Internal heating for metamorphic recrystallization was somehow lower for R chondrites than the ordinary chondrites.

A serious problem with associating the volatile loss with metamorphism is that heating only causes the elements to enter the local gas phase, but no net loss occurs if this gas remains in local voids until the asteroid cools down below the evaporation temperature (Wasson, 2005).

### 4.4.4 Impact and the parent body of R chondrites

Rubin (2004) examined a detailed mineralogical study in several equilibrated ordinary chondrites to study the thermal and shock histories of chondritic asteroids and concluded that collisional events caused all equilibrated ordinary chondrites to reach shock stages S3-S6. Equilibrated ordinary chondrites which are now classified as S1 or S3, underwent the postshock annealing. $^{39}$Ar-$^{40}$Ar isotopic age is one of the meteoritic chronometer that was reset due to impact heating (Bogard, 1995). So, Rubin (2004) argued for the impact history for petrologic type-6 ordinary chondrites. According to Rubin (2004), $^{39}$Ar-$^{40}$Ar isotopic age ranges from 4.44 - 4.45 Ga when impacts were prevalent and most ordinary chondrites were thermally metamorphosed.

Dixon et al., (2003) determined the $^{39}$Ar-$^{40}$Ar ages for the whole-rock of Carlisle Lakes, Rumuruti, Acfer 2017 and PCA 91002 which were breccias except for Carlisle Lakes. Noticing a complicated age spectra due to recoil of $^{39}$Ar and diffusive loss of radiogenic $^{40}$Ar to various extent, they reported the peak $^{39}$Ar-$^{40}$Ar ages: ≥4.35 Ga (Carlisle Lakes), ~4.47±0.02 Ga (Rumuruti), 4.30±0.07 Ga (Acfer 217) and ≥4.37 Ga (PCA 91002). R chondrites have relatively old $^{39}$Ar-$^{40}$Ar ages that overlap those of the oldest L and LL chondrites (Dixon et al., 2003 and references therein). Following Rubin's (2004) arguments for ordinary chondrites, we can assume that impacts were prevalent for R chondrites as well. Asteroid growth involved random collisions that randomly mixed early-condensed and late condensed objects (Wasson, 2005). Apparently, early condensed objects were depleted in volatile elements and are more thermally metamorphosed compared with those of late condensed objects. For this we need to consider rubble-pile structure instead of onion-shell model (Fig. 4.12). In rubble-pile structure, objects with different metamorphic grades are assembled together without following any sequence.

# Chapter-5

## Conclusion

In our INAA study, CI, Cr-normalized lithophile abundance pattern in R chondrites are almost flat and are comparable with those of ordinary chondrites. Mean CI-normalized Na and Mn abundances are 1.32 ± 0.07 and 1.21 ± 0.04, respectively, which are comparable with those of ordinary chondrites but higher than those of carbonaceous and enstatite chondrites. However, CI, Cr-normalized siderophile abundance pattern in R chondrites are intermediate between H and L chondrites. A mean iron content in R chondrites is 24.6 ± 0.7 (%, 1σ, n=15, this study) whereas the mean iron contents in H, L and LL are 27.1 ± 0.7 (%, 1σ, n=22), 21.6 ± 0.5 (%, 1σ, n=20) and 18.4 ± 0.4 (%, 1σ, n=16), respectively. Bulk Ir contents in R chondrites also show the same trend as iron. CI-normalized Ni/Co ratios (~0.9) in R chondrites are comparable with those of ordinary chondrites. Moderately volatile elements, Zn and Se in R chondrites are more abundant than those in ordinary chondrites. Selenium is a chalcophile and mostly partitioned into the sulfide while Zn is found in almost all sorts of mineralogical phases in meteorites. Both of them share the same nebular condensation temperature, but they are fractionated. Enstatite chondrites are the most reduced chondritic meteorites whose Se abundances are comparable with those in R chondrite. But Zn abundances in R chondrite are remarkably higher than those in EL chondrite and comparable with CM chondrite abundances. Higher stability of ZnO in oxidized condition can be a plausible explanation for this Zn enrichment.

In CI-normalized REE, Th and U abundance patterns, heavy rare earth elements (HREE) are faintly enriched compared with those of light rare earth elements (LREE). CI-normalized Nd/Yb and Pr/Tm ratios for R chondrites are systematically lower than CI values. Apparently, HREEs (represented by Tm and Yb) are enriched compared with LREEs (represented by Pr and Nd). In our ICP-MS experiment, we have corrected the interferences from LREE (oxides and hydroxides) and Ba on HREE determination, although in most cases such interference is less than 1%. Nebular process can be responsible for such small HREE-LREE fractionation in R chondrites. To explain the nebular process in R chondrites, an analogically well explained fractionated pattern of REEs, Th and U abundances in Allende meteorite can be considered. In Allende, HREEs are depleted compared with LREEs. According to condensation calculation, high temperature early condensates (e.g., perovskite, hibonite, corundum etc.) enriched in refractory HREEs could have been removed from the nebular gas, making the remaining gas enriched in less refractory LREEs. It is likely that the Allende parent body formed from such later condensates of the remaining gas. In R chondrites, the inclination of CI-

normalized REE pattern is opposite to the Allende pattern (except positive Tm anomaly). A simple interpretation is that R chondrites formed in the nebula where early condensates were relatively abundant. Unlike the REE fractionation pattern, Th-U fractionation patterns are the same both in R chondrites and in Allende. In the seven replicate measurements of Allende powder, Th/U ratio is 4.10 ± 0.20, whereas in R chondrites, Th/U ratio is 3.81 ± 0.13. A subtle positive Ce anomaly (5.4 ± 1.5 %) is observed in CI-normalized REE abundance pattern of R chondrites.

Highly volatile elements abundances in R chondrites show a systematic variation with the petrologic types, except for MIL 11207.8 and Y 793575.44. In higher metamorphic grade, volatile elements abundances are lower compared with those of lower metamorphic grade. Following the condensational accretion as in two component model, early condensates were depleted in volatile elements and placed in the inner portion of chondritic parent body. On the other hand, later condensates were comparatively enriched in volatile elements than those of early condensates and placed in the outer layer of the parent body. Thus, the higher metamorphic R chondrites are the inner portion of the parent body and the lower R chondrites are the outer portion if we consider the onion-shell model for R chondrites. However, chondritic materials faced a random impact during accretion. So the early condensates and the later condensates were mixed together without following a sequence and resulting a rubble-pile type parent body.

**References**


Acken D. V., Brandon A. D. and Humayun M. (2011) High-precision osmium isotopes in enstatite and Rumuruti chondrites. *Geochim. Cosmochim Acta.* **75**, 4020 - 4036.

Allègre C. J., Manhès G. and Göpel C. (1995) The age of the earth. *Geochim. Cosmochim. Acta.* **59**, 1445-1456.

Allen Jr. R. O. and Mason B. (1973) Minor and trace elements in some meteoritic minerals. *Geochim. Cosmochim Acta.* **37**, 1435 - 1456.

Anders E. (1964) Origin, Age and composition of meteorites. *Space Sci. Rev.* **3**, 583-714.

Anders E. and Ebihara M. (1982) Solar-system abundances of the elements. *Geochim. Cosmochim. Acta.* **11**, 2363-2380.

Anders E. and Grevesse N. (1989) Abundances of the elements: Meteoritic and solar. *Geochim. Cosmochim. Acta.* **53**, 197-214.

Baker J., Peate D., Waight T. and Meyzen C. (2004) Pb isotopic analysis of standards and samples using a 207Pb-204Pb double spike and thallium to correct for mass bias with a double-focusing MC-ICP-MS. *Chem. Geol.* **211**, 275-303.

Barrat J. A., Zanda B., Moynier F., Bollinger C., Liorzou C. and Bayon G. (2012) Geochemistry of CI chondrites: Major and trace elements and Cu and Zn isotopes. *Geochim. Cosmochim. Acta.* **83**, 79-92.

Berglund M. and Wieser M. E. (2011) Isotopic compositions of the elements 2009 (IUPAC Technical Reports). *Pure Appl. Chem.* **83(2)**, 397-410.

Binns R.A. and Poolley G.D. (1979) Carlisle Lakes (a): A unique oxidized chondrite (abstr.). *Meteoritics* **14**, 349 – 350.

Binz C. M., Ikramuddin M., Rey P. and Lipschutz M. E. (1976) Trace elements in primitive meteorites – VI. Abundance patterns of thirteen trace elements and inter-element relationships in unequilibrated ordinary chondrites. *Geochim. Cosmochim. Acta.* **40**, 59–71.

Bischoff A. and Keil K. (1983) Ca, Al-rich chondrules and inclusions in ordinary chondrites. *Nature* **303**, 588-592.

Bischoff A. and Keil K. (1984) Al-rich objects in ordinary chondrites: Related origin of carbonaceous and ordinary chondrites and their constituents. *Geochim. Cosmochim. Acta.* **48**, 693-709.

Bischoff A., Keil K. and Stöffler D. (1985) Perovskite-hibonite-spinel-bearing inclusions and Al-rich chondrules and fragments in enstatite chondrites. *Chmie der Erde* **44**, 97-106.

Bischoff A., Geiger T., Palme H., Spettel B., Schultz L., Scherer P., Loeken T., Bland P., Clayton R. N., Mayeda T. K., Herpers U., Meltzow B., Michel R., Dittrich-Hannen B.

(1994) Acfer 217 – A new member of the Rumuruti chondrite group (R). *Meteoritics* **29**, 264-274.

Bischoff A. (2000) Mineralogical characterization of primitive, type 3 lithologies in Rumuruti chondrites. *Meteorit. Planet. Sci.* **35**, 699-706.

Bischoff A., Sokol A., Palme H., Schultz L., Weber H. W. and Wolf D. (2001) Mineralogy, chemistry and noble gases of the unpaired Rumuruti-chondrites NWA 753 and NWA 755. *Meteorit. Planet. Sci.* **36**, A21.

Bischoff A., Vogel N. and Roszjar J. (2011) The Rumuruti chondrite group. *Chemie der Erde* **71**, 101-133.

Bland P., Hutchison R., Pillinger C. T. and Bischoff A. (1992) A unique type 4 chondrite from the Sahara – Acfer 217 (abstract). *Meteoritics* **27**, 204 – 205.

Blander M. and Abdel-Gawad M. (1969) The origin of meteorites and the constrained equilibrium condensation theory. *Geochim. Cosmochim. Acta.* **33**, 701-716.

Bogard D. D. (1995) Impact ages of meteorites: A synthesis. *Meteoritics* **30**, 244-268.

Boynton W. V. (1975) Fractionation in the solar nebula: condensation of yttrium and the rare earth elements. *Geochim. Cosmochim Acta.* **39**, 569-584.

Boynton W. V. (1978) Fractionation in solar nebula, II. Condensation of Th, U, Pu and Cm. *Earth Planet. Sci. Lett.* **40**, 63 - 70.

Bouvier A., Blichert-Toft J., Moynier F., Vervoort J.D. and Albarède F. (2007) Pb-Pb dating constraints on the accretion and cooling history of chondrites. *Geochim. Cosmochim Acta.* **71**, 1583-1604.

Buikin A. I., Trieloff M., Korochantseva E. V., Hopp J., Berlin J. and Stöffler D. (2006) High precision $^{39}$Ar-$^{40}$Ar dating of different Rumuruti lithologies. *Meteorit. Planet. Sci.* **51**, A30.

Caporali S., Pratesi G., Moggi-Cecchi V., Franchi I. A. and Greenwood R. C. (2009) NWA 4419: A new R chondrite from Northwest Africa. *Lunar Planet. Sci.* **40**, (abstract # 2488).

Case D. R., Laul J. C., Pelly I. Z., Wechter M. A., Schmidt-Bleek F. and Lipschutz M. E. (1973) Abundance patterns of thirteen trace elements in primitive carbonaceous and unequilibrated ordinary chondrites. *Geochim. Cosmochim. Acta.* **37**, 19–23.

Cassidy W. A. (1980) In Meteoritical Bulletin No. 57, edited by Graham A. L. *Meteoritics* **15**, 93-94.

Chai J., Oura Y. and Ebihara M. (2003) Comparison of RNAA and ICP-MS for the determination of ultra-trace of Th and U in geological and cosmochemical samples. *J. Radioanal. Nucl. Chem.* **255**, 471-475.

Clayton R. N. (2004) Oxygen isotopes in meteorites. In *Treatise on Geochemistry, Volume 1: Meteorites, Cometes, and Planets*, ed. Davis A. M. Oxford: Elsevier, pp. 129-142.

Connolly Jr. H. C., Smith C., Benedix G., Folco L., Righter K., Zipfel J., Yamaguchi A. and Chennaouiaoudjehane H. The meteoritical bulletin, No. 92, 2007 September. *Meteorit. Planet. Sci.* **42**, 1647-1694.

Dauphas N. and Pourmand A. (2011) Hf-W-Th evidence for rapid growth of Mars and its status as a planetary embryo. *Nature* **473**, 489-492.

Davis A. M. and Grossman L. (1979) Condensation and fractionation of rare earths in solar nebula. *Geochim. Cosmochim. Acta.* **43**, 1611–1632.

Davis A. M. (2005) Volatile evolution and loss. In *Meteorites and the early solar system II* (eds. Lauretta D.S. and McSween H.Y) 295-307, Tucson, AZ: University of Arizona press.

Dennison J. E. and Lipschutz M. E. (1987) Chemical studies of H chondrites. II: Weathering effects in the Victoria Land, Antarctic population and comparison of two Antarctic populations with non-Antarctic falls. *Geochim. Cosmochim. Acta.* **51**, 741–754.

Dreibus G., Palme H., Spettel B., Zipfel J. and Wanke H. (1995) Sulfur and selenium in chondritic meteorites. *Meteoritics* **30**, 439 - 445.

Dixon E. T., Bogard D. D. and Garrison D. H. (2003) $^{39}$Ar-$^{40}$Ar chronology of R chondrites. *Meteorit. Planet. Sci.* **38**, 341-355.

Dodd R. T. (1969) Metamorphism of the ordinary chondrites: A review. *Geochim. Cosmochim. Acta.* **33**, 161-203.

Endo T., Sawada Y., Nishido H., Ninagawa K., Kusakabe M., Nagao K., Dettmann E. L., Sampei Y., Ahn I. and Lee J. L. (2010) A new R chondrite (NWA 6236) from Fezzou, Morocco. *Meteorit. Planet. Sci.* **45**, A51.

Friedrich J. M., Wang M. S. and Lipschutz M. E. (2003) Chemical studies of L chondrites. V: Compositional patterns for 49 trace elements in 14 L4-6 and LL4-6 falls. *Geochim. Cosmochim. Acta.* **67**, 2467–2479.

Gooding J. L. and Keil K. (1981) Relative abundances of chondrule primary textural types in ordinary chondrites and their bearing on conditions of chondrule formation. *Meteoritics* **16**, 17 – 43.

Goreva J. S. and Burnett D. S. (2001) Phosphate control on the thorium/uranium variations in ordinary chondrites: Improving solar system abundances. *Meteorit. Planet. Sci.* **36**, 63 - 74.

Grady M.M. (2000) *Catalogue of Meteorites*. Cambridge University Press. Cambridge, England, 689.

Greenwood J. P., Rubin A. E. and Wasson J. T. (2000) Oxygen isotopes in R-chondrite magnetite and olivine: Links between R chondrites and ordinary chondrites. *Geochim. Cosmochim. Acta.* **64**, 3897-3911.

Grossman J. N. (1994) The meteoritical bulletin, No. 76, 1994 January. *Meteoritics* **29**, 100-143.

Grossman J. N. (1998) The meteoritical bulletin, No. 82, 1998 July. *Meteorit. Planet. Sci.* **33**, A221-A239.

Heumann K. G., Gallus S. M., Rädlinger G. and Vogl J. (1998) Precision and accuracy in isotope ratio measurements by plasma source mass spectrometry. *J. Anal. At. Spectrom.*, **13**, 1001-1008.

Ikramuddin M. and Lipschutz M. E. (1975) Thermal metamorphism of primitive meteorites – I. Variation of six trace elements in Allende carbonaceous chondrite heated at 400-1000°C. *Geochim. Cosmochim. Acta.* **39**, 363-375.

Ikramuddin M., Binz C. M. and Lipschutz M. E. (1976) Thermal metamorphism of primitive meteorites – II. Ten trace elements in Abee enstatite chondrite heated at 400-1000°C. *Geochim. Cosmochim. Acta.* **40**, 133-142.

Ikramuddin M., Binz C. M. and Lipschutz M. E. (1977) Thermal metamorphism of primitive meteorites – III. Ten trace elements in Krymka L3 chondrite heated at 400-1000°C. *Geochim. Cosmochim. Acta.* **41**, 393-401.

Isa J., Rubin A. E. and Wasson J. T. (2014) R-chondrite bulk-chemical composition and diverse oxides: Implication for parent-body processes. *Geochim. Cosmochim. Acta.* **124**, 131 - 151.

Isa M., Shirai N., Ebihara M., Kubuki S. and Yamaguchi A. (2011) Chemical characteristics for CK carbonaceous chondrite (abstract). *Lunar Planet. Sci.* **42**, 1876pdf.

Jäckel A., Bischoff A., Clayton R. N. and Mayeda T. K. (1996) Dar al Gani 013 – A new Saharan rumuruti-chondrite (R3-6) with highly unequilibrated (type 3) fragments. *Lunar Planet. Sci.* **27**, 595-596.

Jarosewich E., Clarke R. S. J. and Barrows J. N. E. (1987) The allende meteorite reference sample. *Smithson. Contrib. Earth Sci.* **27** (1).

Jochum K.P. and Jenner G. (1994) Trace element analysis of Geological Survey of Japan silicate reference materials: Comparison of SSMS with ICP-MS data and a critical discussion of compiled values. *Fresenius J. Anal. Chem.* **350**, 310-318.

Kaczaral W. P., Dodd R. T and Lipschutz M. E. (1989) Chemical studies of L chondrites: IV. Antarctic/non-Antarctic comparisons. *Geochim. Cosmochim. Acta.* **53**, 491-501.

Kallemeyn G. W. and Wasson J. T. (1981) The compositional classification of chondrites – I. The carbonaceous chondrite group. *Geochim. Cosmochim. Acta.* **45**, 1217-1230.

Kallemeyn G. W. and Wasson J. T. (1986) Compositions of enstatite (EH3, EH4,5 and EL6) chondrites: Implication regarding their formation. *Geochim. Cosmochim. Acta.* **50**, 2153-2164.

Kallemeyn G. W., Rubin A. E., Wang D. and Wasson J. T. (1989) Ordinary chondrites: Bulk compositions, classification, lithophile-element fractionations, and composition-petrographic type relationships. *Geochim. Cosmochim. Acta.* **53**, 2747-2767.

Kallemeyn G. W., Rubin A. E. and Wasson J. T. (1991) The compositional classification of chondrites: V. The Karoonda (CK) group of carbonaceous chondrites. *Geochim. Cosmochim. Acta.* **55**, 881-892.

Kallemeyn G. W., Rubin A. E. and Wasson J. T. (1996) The compositional classification of chondrites: VII. The R chondrite group. *Geochim. Cosmochim. Acta.* **60**, 2243-2256.

Keays R. R., Ganapathy R. and Anders E. (1971) Chemical fractionations in meteorites – IV: Abundances of fourteen trace elements in L-chondrites; implications for cosmothermometry. *Geochim. Cosmochim. Acta.* **35**, 337-363.

Kita N. T., Nagahara H., Togashi S. and Morishita Y. (1998) New evidence of aluminum-26 from a ferrous-oxide-rich chondrule in Semarkona (LL 3.0). *Meteorit. Planet. Sci.* **33**, A83-A84 (abstract).

Kojima H., Imae N. and Yamaguchi A (2009) Meteoritic Newsletter: Japanese collection of Antarctic meteorites. **18**, 1-33.

Krot A. N., Keil K., Goodrich C. A., Scott E. R. D. and Weisberg M. K. (2005) Classification of meteorites. 83-128. In *Meteorites, Comets, an Planets* (ed. A. M. Davis) **Vol. 1** *Treaties on Geochemistry* (eds. H. D. Holland and K.K. Turekian), Elsevier-Pergamon, Oxford.

Larimer J. W. and Anders E. (1967) Chemical fractionations in meteorites – II. Abundance patterns and their interpretation. *Geochim. Cosmochim. Acta.* **31**, 1239-1270.

Laul J. C., Case D. R., Schmidt-Bleek E. and Lipschutz M. E. (1970a) Bismuth contents of chondrites. *Geochim. Cosmochim. Acta.* **34**, 89-108.

Laul J. C., Pelly I. and Lipschutz M. E. (1970b) Thallium contents of chondrites. *Geochim. Cosmochim. Acta.* **34**, 909-920.

Laul J. C., Ganapathy R. Anders E. and Morgan J. W. (1973) Chemical fractionations in meteorites – VI. Accretion temperatures of H-, LL-, and E-chondrites, from abundance of volatile trace elements. *Geochim. Cosmochim. Acta.* **36**, 329-357.

Lingner D. W., Huston T. J., Hutson M. and Lipschutz M. E. (1987) Chemical studies of H chondrites. I: Mobile trace elements and gas retention ages. *Geochim. Cosmochim. Acta.* **51**, 727–739.

Lipschutz M. E. (1997) Nebular and parent body processes in chondrites: Labile trace elements as indicators and thermometers. *Workshop on parent-body and nebular modification of chondritic materials*, Proceedings of a conference held 17-19 july, 1997 in Maui, Hawai`I. Edited by M. E. Zolensky, A. N. Krot and E. R. D. Scott. LPI technical report, LPITR 97-02. Houston, TX: Lunar and Planetary Institute, 1997. P.38.

Lodders K. (2003) Solar system abundances and condensation temperatures of the elements. *Astrophys. J.* **591**, 1220-1247.

Lodders K., Palme H. and Gail H. P. (2009) In: Trümper J. E. (ed.), *Abundances of the elements in the solar system*, in Landolt-Börnstein, New series, Vol. VI/4B, Chap. 4.4, Springer-verlag, Berlin, Heidelberg, New York, pp. 560-598.

MacPherson G. N. and Huss G. R. (2005) Petrogenesis of Al-rich chondrules: Evidence from bulk compositions and phase equilibria. *Geochim. Cosmochim. Acta.* **69**, 3099-3127.

McCanta M. C., Treiman A. H., Dyar M. D., Alexander C. M. O`d., Rumble III. D. and Essene E. J. (2008) The LaPaz Icefield 04840 meteorite: Mineralogy, metamorphism and origin of an amphibole- and biotite-bearing R chondrite. *Geochim. Cosmochim. Acta.* **72**, 5757-5780.

Marlow R. and Mason B. (1992) Description of PCA 91002. *Antarc. Meteorite Newslet.* **15**, 30-31.

McSween Jr. H. Y. and Patchen A. D. (1989) Pyroxene thermobarometry in LL-group chondrites and implications for parent body metamorphism. *Meteoritics* **24**, 219-226.

McSween H. Y (1979) Are carbonaceous chondrites primitive or processed? A review. *Reviews of Geophyphysics and Space Physics*, **17**, 1059-1078.

McSween Jr. H. Y. and Huss G. R. (2010) Meteorites: a record of nebular and planetary processes. *Cosmochemistry*, Cambridge Univ. Press, 157-191.

Makishima A. and Nakamura E. (1997) Suppression of matrix effects in ICP-MS by high power operation of ICP: Application to precise determination of Rb, Sr, Y, Cs, Ba, REE, Pb, Th and U at ηg g-1 level in milligram silicate samples. *Geostandards Newsletter: The Journal of Geostandards and Geoanalysis* **21**, 307-319.

Makishima A. and Nakamura E. (2006) Determination of major, minor and trace elements in silicate samples by ICP-QMS and ICP-SFMS applying isotope dilution-internal standardization (ID-IS) and multi-stage internal standardization. *Geostand. Geoanal. Res.* **30**, 245-271.

Makishima A., Yamakawa A., Yamashita K. and Nakamura E. (2010) Precise determination of Cr, Mn, Fe, Co and Ni concentration by an isotope dilution-internal standardization method employing high resolution MC-ICP-MS. *Chem. Geol.* **274**, 82-86.

Miyamoto M., Fujii N. and Takeda H. (1981) Ordinary chondrite parent body: An internal heating model. *Proc. Lunar Planet. Sci.* **12B**, 1145-1152.

Nakaruma N. (1974) Determination of REE, Ba, Fe, Mg, Na and K in carbonaceous and ordinary chondrites. *Geochim. Cosmochim. Acta* **38**, 757-775.

Nakamura T., Tomeoka K. and Takeda H. (1993) Mineralogy and petrology of the CK chondrites Yamato-82104, -693 and a Carlisle Lakes-type choncrite Yamato-82002. *Proc. NIPR Symp. Ant. Met.* **6**, 171-185.

Nakamura N., Sawada S., Tamaki M., Kondorosi G., Imae N., Kojima H., Clayton R. N. and Mayeda T. K. (1999) Consortium studies of five Antarctic Rumuruti-group chondrites: A progress report. *Antarctic Meteorite* **24**, 121-122.

Ozaki H., Shinotsuka K., Kallemeyn G.W. and Ebihara M. (1998) Chemical composition of Asuka-881988, Yamato-75302 and Ymato-791827, Antarctic R chondrites. *Antarctic Meteorite* **23**, 123-125.

Palme H. Weckwerth G. and Wolf D. (1996) The composition of a new R-chondrite and the classification of chondritic meteorites. *Lunar. Planet. Sci. Conf.* **27**, 991-992.

Palme H. and Jones A. (2003) Solar system abundances of the elements. *In Treatise of Geochemistry, Vol. 1: Meteorites, Comets and Planets* (ed. Davis M. A.) 41-61. Elsevier, Oxford.

Paul R. L. and Lipschutz M. E. (1990) Chemical studies of differentiated meteorites: I. Labile trace elements in Antarctic and non-Antarctic eucrites. *Geochim. Cosmochim. Acta.* **54**, 3185-3196.

Pourmand A., Dauphas N. and Ireland T. J. (2012) A novel extraction chromatography and MC-ICP-MS technique for rapid analysis of REE, Sc and Y: Revising CI-chondrite and Post-Archean Australian Shale (PAAS) abundances. *Chem Geol.* **291**, 38-54.

Prinz M., Weisberg M. K. and Clayton R. N. and Mayeda T. K. (1993) Ordinary and Carlisle Lakes-like chondrite clasts in the Weatherford chondrite breccia (abstract). *Meteorites* **28**, 419 – 420.

Righter K. (2011) *Antarctic meteoritic newsletter* **34**, 1-29.

Righter K. (2012) *Antarctic meteoritic newsletter* **35**, 1-25.

Rout S. S. and Bischoff A. (2008) Ca, Al-rich inclusions in Rumuruti (R) chondrites. *Meteorit. Planet. Sci.* **43**, 1439-1464.

Rout S. S., Keil K. and Bischoff A. (2010) Bulk chemical compositions of Al-rich objects from Rumuruti (R) chondrites: Implications for their origin. *Chmie der Erde* **70**, 35-53.

Rubin A. E. and Kallemeyn G. W. (1989) Carlisle Lakes and Allan Hills 85151: Members of a new chondrite grouplet. *Geochim. Cosmochim. Acta.* **53**, 3035-1232.

Rubin A. E. (1990) Kamacite and olivine in ordinary chondrites: Intergroup and intragroup relationships. *Geochim. Cosmochim. Acta.* **54**, 1271-3044.

Rubin A. E. and Kallemeyn G. W. (1993) Carlisle Lakes chondrites: Relationship to other chondrite groups. *Meteoritics* **28**, 424-425.

Rubin A. E. and Kallemeyn G. W. (1994) Pecora Escarpment 91002: A member of new Rumuruti (R) chondrite. *Meteoritics* **29**, 255-264.

Rubin A. E., Scott E. R. D. and Keil K. (1997) Shock metamorphism of enstatite chondrites. *Geochim. Cosmochim. Acta.* **61**, 847-858.

Rubin A. E. (2004) Postshock annealing and postannealing shock in equilibrated ordinary chondrites: Implications for the thermal and shock histories of chondritic asteroids. *Geochim. Cosmochim. Acta.* **68**, 673-689.

Rubin A. E. and Huber H. (2005) A weathering index for CK and R chondrites. *Meteorit. Planet. Sci.* **40**, 1123-1130.

Rubin A. E. (2011) Origin of the differences in refractory-lithophile-elements abundances among chondrite groups. *Icarus* **213**, 547-558.

Russell S. S., Srinivasan G., Huss G. R., Wasserburg G. J. and MacPherson G. J. (1996) Evidence for widespread $^{26}$Al in the solar nebula and constraints for nebula time scale. *Science* **273**, 757-762.

Russell S. S., Folco L., Grady M. M. Zolensky M. E. Jones R., Righter K., Zipfel J., Grossman J. N. (2004) The meteoritical bulletin, No. 88, 2004 July. *Meteorit. Planet. Sci.* **39**, A215-A272.

Schulze H., Bischoff A., Palme H., Spettel B., Dreibus G. and Otto J. (1994) Mineralogy and chemistry of Rumuruti: The first meteorite fall of the new R chondrite group. *Meteoritics* **29**, 275-286.

Scott E. R. D., Keil K. and Stöffler D. (1992) Shock metamorphism of carbonaceous chondrites. *Geochim. Cosmochim. Acta.* **56**, 4281-4293.

Scott E. R. D. and Krot A. N. (2005) Chondrites and their components, pp. 143 – 200. In *Meteorites, Comets and Planets* (ed. A. M. Davis) Vol. **1** *Treatise on Geochemistry* (eds. H. D. Holland and K. K. Turekian), Elsevier-Pergamon, Oxford.

Sears D. W. G., Grossman J. T., Melcher C. L., Ross L. M. and Mills A. A. (1980) Measuring the metamorphic history of unequilibrated ordinary chondrites. *Nature*, **287**, 791-795.

Shinotsuka K., Hidaka H. and Ebihara M. (1995) Detailed abundances of rare earth elements, thorium and uranium in chondritic meteorites: An ICP-MS study. *Meteoritics* **30**, 694-699.

Shinotsuka K. and Ebihara M. (1997) Precise determination of rare earth elements, thorium and uranium in chondritic meteorite by inductively coupled plasma mass spectrometry – a comparative study with radiochemical neutron activation analysis. *Anal. Chim. Acta* **338**, 237-246.

Stracke A., Palme H., Gellissen M., Münker C., Kleine T., Birbaum K., Günther D., Bourdon B. and Zipfel J. (2012) Refractory element fractionation in the Allende meteorite: Implications for solar nebula condensation and the chondritic composition of planetary bodies. *Geochim. Cosmochim. Acta.* **85**, 114-141.

Stöffler D., Keil K. and Scott E. R. D. (1991) Shock metamorphism of ordinary chondrits. *Geochim. Cosmochim. Acta.* **55**, 3845-3867.

Takahashi H., Gros J., Higuchi H., Morgan J. W. and Anders E. (1978) Volatile elements in chondrites: metamorphism or nebular fractionation? *Geochim. Cosmochim. Acta.* **42**, 1859-1869.

Tandon S. N. and Wasson J. T. (1967) Indium variation in a petrologic suite of L-group chondrites. *Science* **158**, 259-261.

Tandon S. N. and Wasson J. T. (1968) Gallium, germanium, indium and iridium variations in a suite of L-group chondrites. *Geochim. Cosmochim. Acta.* **32**, 1087-1109.

Tatsumoto M., Knight J. and Allègre C. J. (1973) Time differences in the formation of meteorites as determined from the ratio of lead-207 to lead-206. *Science* **180**, 1279-1283.

Trieloff M., Jessberger E. K., Herrwerth I., Hopp J., Fieni C., Ghelis M., Bourot-Denise M. and Pellas P. (2003) Structure and thermal history of the H-chondrite parent asteroid revealed by thermochronometry, *Nature*, **422**, 502 – 506.

Trieloff M., Nakashima D. and Ott U. (2007) Nobel gas chronology of rumuruti. *Meteorit. Planet. Sci.* **42**, A151.

Auke A. van Heuzen, Tjeerd Hoekstra and Bob van Wingerden (1989) Precision and accuracy attainable with isotope dilution analysis applied to inductively coupled plasma mass spectrometry: theory and experiments. *J. Anal. At. Spectrom.*, ,4, 483-489

Van Schmus W. R. and Wood J. A. (1967) A chemical-petrologic classification for the chondritic meteorites. *Geochim. Cosmochim. Acta*. **31**, 747-765.

Van Schmus W. R. (1969) The minerology and petrology of chondritic meteorites. *Earth Sci. Rev.* **5**, 145-184.

Wakita H. and Schmitt R. A. (1970) Rare earth and other elemental abundances in the Allende meteorite. *Nature* **227**, 478-479.

Wasson J. T. (1985) Meteorites: Their Record of Early Solar System History. W. H. Freeman, New York.

Wasson J. T. and Kallemeyn G. W. (1988) Composition of chondrites. *Phil. Trans. R. Soc. Lond. A* **325**, 535-544.

Wasson J. T. (2005) Loss of highly volatile elements from ordinary chondrites during impact heating. *Meteorit. Planet. Sci.* **40**, A166.

Wasson J. T., Isa J. and Rubin A. E. (2013) Compositional and petrographic similarities of CV and CK chondrites: A single group with variations in texture and volatile concentrations attributable to impact heating, crushing and oxidation. *Geochim. Cosmochim. Acta.* **108**, 45-62.

Watters Jr. R. L., Eherhardt K. R., Beary E. S. and Fassett J.D. (1997) Protocol for isotope dilution using inductively coupled plasma-mass spectrometry (ICP-MS) for the determination of inorganic elements. *Metrologia.* **34**, 87-96.

Weber H. W. and Schultz L. (2001) Nobel gases in five new Rumuruti chondrites. *Lunar Planet. Sci.* **32**, (abstract # 1500).

Weisberg M. K., Prinz M., Kojima H., Yanai K., Clayton R. N. and Mayeda T. K. (1992) The Carlisle Lakes-type chondrites: a new grouplet with high $\Delta^{17}O$ and evidence for nebular oxidation. *Geochim. Cosmochim. Acta.* **55**, 2657-2669.

Weisberg M. K., McCoy T. J. and Krot A. N. (2006) Systematics and evaluation of meteorite classification. In *Meteorites and the Early Solar System II*, eds. Lauretta D.S and McSween H. Y. Jr. Tucson: University of Arizona Press, pp. 19-52.

Wang M. S. and Lipschutz M. E. (2007) Trace elements in primitive meteorites – VII Antarctic unequilibrated ordinary chondrites. *Geochim. Cosmochim. Acta.* **71**, 1062-1073.

Wlotzka F. (1993) The Meteoritical Bulletin, No. 75, 1993 December. *Meteoritics* **28**, 692 – 703.

Wlotzka F. (1993a) A weathering scale for the ordinary chondrites. *Meteoritics* **28**, 460.

Willbold M., Jochum K. P., Raczek I., Amini M. N., Stoll B. and Hofmann A. W. (2003) Validation of multi-element isotope dilution ICPMS for the analysis of basalts. *Anal Bioanal Chem.* **377**, 117-125.

Wolf D. and Palme H. (2001) The solar system abundances of phosphorus and titanium and the nebular volatility of phosphorus. *Meteorit. Planet. Sci.* **36**, 559-571.

Wood J. A. (1967) Chondrites: Their metallic minerals, thermal histories and parent planets. *Icarus* **6**, 1-49.

Wood J. A (2003) Of asteroids and onions, *Nature*, **422**, 479 – 480.

Yamaguchi A., Imae N., Kimura M. and Kojima H. (2012) Meteoritic Newsletter: Japanese collection of Antarctic meteorites. **21**, 1-33.

Yanai K. (1992) Bulk composition of Yamato-793575 classified as Carlisle Lakes-type chondrite. *Lunar Planet. Sci.* **23**, (abstract#1559).

Yokoyama T., Makishima A. and Nakamura E. (1999) Evaluation of the coprecipitation of incompatible trace elements with fluoride during silicate rock dissolution by acid digestion. *Chem. Geol.* **157**, 175-187.

Xiao X. and Lipschutz M. E. (1992) Labile trace elements in carbonaceous chondrites: A survey. *J. Geophys. Res.* **97**, 10199-10211.